PhD-FSTC-2015-54
The Faculty of Sciences, Technology and Communication

DISSERTATION

Defense held on 27/11/2015 in Luxembourg

to obtain the degree of

DOCTEUR DE L'UNIVERSITÉ DU LUXEMBOURG

EN SCIENCES DE L'INGÉNIEUR

by

Amirhoushang Mahmoudi
Born on 23 September 1983 in Sabzevar (Iran)

PREDICTION OF HEAT-UP, DRYING AND GASIFICATION OF FIXED AND MOVING BEDS BY THE DISCRETE PARTICLE METHOD (DPM)

Dissertation defense committee

Dr.-Ing. Bernhard Peters, dissertation supervisor
Professor, Université du Luxembourg

Dr.-Ing. Manfred Greger, Chairman
Professor, Université du Luxembourg

Dr.-Ing. Thomas Nussbaumer, Vice-chairman
Professor, Lucerne school of engineering and architecture

Dr.-Ing. Viktor Scherer
Professor, Ruhr-Universität Bochum

Dr. Algis Dziugys
Lithuanian Energy Institute

Summary

Increasing concern about environmental problems of using fossil fuels from one side, and longevity of fossil fuel resources from the other side, demand for some alternative resources with less or even non unpleasant impact on the environment. Biomass as a renewable source of energy is almost accessible everywhere and it is possible to either convert it to other forms of fuel or burn it directly for heat generation. Moreover biomass is considered as a CO_2 neutral source of energy. These advantages have attracted many attention in studying biomass conversion during the last decades in both academia and industry.

Understanding the details of the conversion process helps to improve reactor efficiency of furnaces. However, the entire process is of very complex nature due to many involved physical and chemical phenomena such as gas flow through the void space in the bed, heat and mass transfer between two phases, drying of the wet fuel, devolatilization, heterogeneous and homogeneous reactions, motion of the solid fuels either by the movement of the grate or due to solid shrinkage.

The main objective of this thesis is to propose a numerical model to describe the gasification/combustion of biomass in a fixed-bed and moving bed in detail. This will help to understand deeply the process of biomass conversion and provides insights into how to improve the efficiency of a boiler and how to control the product composition. For this purposes, a CFD-DEM approach is developed, in which the fluid phase is a continuous phase while each biomass particle is tracked with a Lagrangian approach. Within the present model a packed bed is considered as an ensemble of a finite number of particles. Heat-up, drying, pyrolysis, gasification and combustion process of each particle is described by one-dimensional and transient conservation equations for mass and energy. Applying this model to all particles of a packed bed forms the entire packed bed process as a sum of the individual particle processes. The gas flow through the void space between particles is modeled as a flow passing through a porous media, while the interaction between the solid and the gaseous phase by heat and mass transfer is taken into account.

This thesis starts with an introduction about the biomass technology and is followed with four chapters describing details of numerical modeling and two chapters on parametric studies. First, drying, pyrolysis and combustion of biomass in a fixed-bed are studied and the process is discussed and analysed in full detail. Subsequently, the proposed model is extended by considering the motion of solid particles in the bed to investigate the combustion of biomass on a forward acting grate. In chapter 6 the influence of particle size and packing configuration in a fixed bed on the pyrolysis products is discussed.

Self-ignition may occur as a favorable or an unfavorable process. Therefore it is important to study this phenomenon to avoid a serious and unforeseen risk or use it for a particular

purpose. This phenomenon can be controlled by managing some parameters such as gas velocity and temperature. The effect of these parameters together with some other such as moisture content and particle size on self-ignition will be investigated in chapter 7.

A novel semi-resolved coupled model is presented in the last chapter that addresses many practical applications.

The numerical model is compared with experimental data for each main process step of biomass conversion (drying, pyrolysis, combustion) separately. However, validation of combustion/gasification of biomass in the fixed-bed contains all the involved phenomena in biomass conversion. These series of validations prove the reliability of the proposed numerical model.

Acknowledgements

Here, I would like to express my gratitude to all people who had significant role during the past four years, working as a PhD fellow at University of Luxembourg. First of all, I would like to thank my supervisor Prof. Bernhard Peters, for his continuous support and supervision throughout the whole period of my PhD study. He accompanied me step by step in this project, giving me interesting ideas and remarks which always helped me deal with problems and find my way. I am also grateful to Dr. Florian Hoffman for fruitful discussion and comments. His support, guidance, and advice throughout the research project, and writing papers, are greatly appreciated.

I also would like to thank Prof. Thomas Nussbaumer and his team (Martin Kiener and Dr. Gabriel Barroso) in Lucerne University, for their support. I am also grateful to Prof. Viktore Scherer for the valuable discussions we had during our meeting. I would also like to thank Prof. Manfered Greger for reviewing this thesis and for being a part of the PhD review committee. My sincere thanks also goes to Dr. Algis Dziugys for being a member of my defense jury and for his very interesting comments on my work.

I had great time in and out of the group, during the coffee breaks and social events. Thanks also to my great colleagues: Kasra Samiei, Suresh Kumar Kannan, Mark Michael, Florian Hoffmann, Xavier Besseron, Alvaro Estupinan, Andrew Ignatenko, Mohammad Mohseni, Anas Obeidat, Maryam Baniasadi, Yu Chung Liao, Gabriele Pozzetti, Mehdi Baniasadi, Edder Rabadan, Pascal Loew and Alina Gritecnko.

I would like to thank my private translator, Mr. Alvaro, who could also read any handwriting. Thanks to Xavier who proved everything is possible to do in the computer! Special thanks to Mohammad who always amused me by telling his stories with professional guys. Thanks to Mehdi and Maryam, the main board of coffee breaks, for their special Kermani´s Coffee. Special thanks to my former officemate for the wide range of discussion we had and for all of his supports. I appreciate Gabrieles endless effort to explain me the difference between Pasta, Makaroni, Spageti and Noodles. Tanks to Yu (not you) for a great time we had during our breaks.

I am grateful to my parents for giving me their deep love, sacrifice, encouragement and unconditional support during my whole life. And finally, I would like to thank my beloved wife, Mina, who was always supportive when I needed.

Contents

List of Tables

List of Figures

Chapter 1

Introduction

1.1 Importance of the renewable energy

During the last decades, an interest has grown to substitute an alternative energy source for fossil fuels. This is due to many reasons including environmental, technical and political issues.

The concern about the security of the energy supply is caused by the concentration of the production of oil in a small number of countries with large reserves. This situation has resulted in supply disruptions by geopolitical events and increasing oil prices. Because of this issue, a secure energy supply is required which is placed at the top of the international political agenda. On the other hand, another serious issue that we are facing is uncertainties over longevity of fossil fuels.

Combustion of fossil fuels releases CO_2 into the atmosphere which is the main greenhouse gas. Scientists believe that CO_2 emission is the primary cause of the global warming that has occurred in recent decades. Because the effects of carbon dioxide result in more than just rising temperature, scientists prefer the phrase climate change, which helps convey that other changes are taking place as well.

A statistic survey has been conducted based on data released by the Energy Information Administration (EIA) [9] to identify the CO_2 emissions as a results of fossil fuels (coal, oil and natural gas) consumption in the world during the first decade of the 21^{th} century. Fig 1.1.1 depicts that CO_2 emissions have increased in the world about 27% in 10 years.

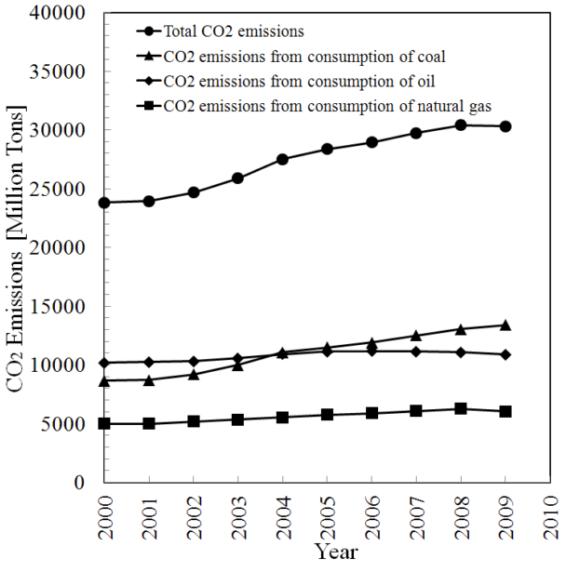

Figure 1.1.1: History of the CO_2 emissions from the consumption of fossil fuels during the first decade of the 21^{th} century

These reasons lead us to arrive at the conclusion that the dependency on fossil fuels will have serious consequences in the near future. Therefore it should be looked for alternative, renewable and environmental friendly fuels. Among the alternative fuels, biomass is one of the most attractive energy sources because of several important advantages:

- unlike solar, wind and geothermal energies that are available only in certain regions of the world, biomass is accessible in many parts of the globe.
- unlike wind or solar energies, the supply of biomass is less dependent on external influences. In case of wind energy, the varying wind force strongly affects the energy yield of wind farms, while in case of solar energy cloudiness can reduce temporarily the energy yield.
- biomass can be easily stored, which is not the case for the wind and solar energies.
- biomass can be used for domestic or industrial purposes even with a quite simple technology.

1.2 Biomass

Biomass is biological material derived from living, or recently living organisms. In the context of biomass for energy, this is often used for plant based material, however, biomass can equally apply to both animal and vegetable derived materials. Biomass is formed as soon as a seed sprouts or an organism is born. Unlike fossil fuel, biomass does not take millions of years to develop. Every year, a vast amount of biomass grows through photosynthesis by absorbing CO_2 from the atmosphere. When it burns it releases CO_2 that the plants had absorbed from the atmosphere only recently (a few years to a few hours). Therefore, any burning of biomass does not add additional CO_2 to the atmosphere. For this reason biomass is considered a "canbon-nutural" fuel.

Biomass can be used directly for heat generation (e.g. combusting in the furnace of a power plant for the electricity generation). However, the bulky and inconvenient form of biomass makes it difficult to transport compared to the oil and the gas. Moreover, using solid fuels in many industrial applications that have been designed for gas or liquid fuels, requires a major redesign. These disadvantages become the motivation for the conversion of solid biomass into liquid and gaseous fuels. Among different ways of biomass conversion, the thermochemical conversion (pyrolysis, gasification) is one of the most promising and efficient ways.

Pyrolysis is a thermal decomposition of the biomass into gas, liquid and solid. In the pyrolysis large hydrocarbon molecules of biomass are broken down into smaller hydrocarbon molecules. Fast pyrolysis produces mainly liquid fuel, while slow pyrolysis produces more solid charcoal. This will be explained in more details in chapter 3

Gasification is the conversion of solid or liquid feedstock into useful and convenient gaseous fuel that can be burned to release energy. Gasification and combustion are two closely related thermochemical processes, but there is an important difference between them. Gasification packs energy into chemical bonds in the product gas; combustion breaks those bonds to release the energy [4]. This will be explained more in chapter 4

1.3 Gasifier/Combustor

The two most common types of boilers for biomass combustion are grate-firing systems and fluidized bed combustors. Grate-firing is the first combustion system used for solid fuels; it can be classified into stationary sloping grates, traveling grates, reciprocating grates, and vibrating grates [10]. In the stationary sloping grates, the grate does not move while fuel burns and slides down under gravity. In traveling grates, the fuel is fed from one side and is burned while the grate transports it to the ash pit. Due to the thin layer of fuel on the grate on traveling grates, it has better fuel burnout effectively compared to the stationary grates. In the reciprocating grates, the fuel is transported by reciprocating (forward or reverse) movements of the grate bars while it is burned. Higher fuel burnout efficiency is achieved in reciprocating grates than traveling grates. This is due to the better mixing of the fuel on the grate in the case of reciprocating grates. Less moving parts are used in the vibrating grates compared to two other moving grates, in which the fuel is spread evenly by shaking the bed.

Based of the position of the inlet gas and product gas, gasifiers can be classified into three groups: updraft (countercurrent), downdraft (cocurrent) and crossdraft.

Updraft gasifier is one of the oldest and simplest designs. In this type of gasifier, the hot gas (air, oxygen or steam) travels upward and leaves from top while the bed of fuel moves downward. Then the gas and solids are in countercurrent mode (fig 1.3.1). In updraft gasifier, the gas enters to the bed through a grate or a distributor, where it meets with the hot bed of ash. The oxygen is consumed at the grate, essentially through the partial combustion of char. The resulting hot gases cause char gasification and biomass pyrolysis. However, further above the grate where pyrolysis is taking place, due to the relatively low temperature and the absence of oxygen, large amounts of tar are produced. High tar production in the updraft gasifier, makes it unsuitable for high-volatility fuels.

However, it is suitable for high-ash, high-moisture biomass. Furthermore, it has high cold-gas efficiency (cold-gas efficiency is the ratio between the heat value of gas products at ambient temperature to heat value of input fuel) hence, it is suitable for direct firing.

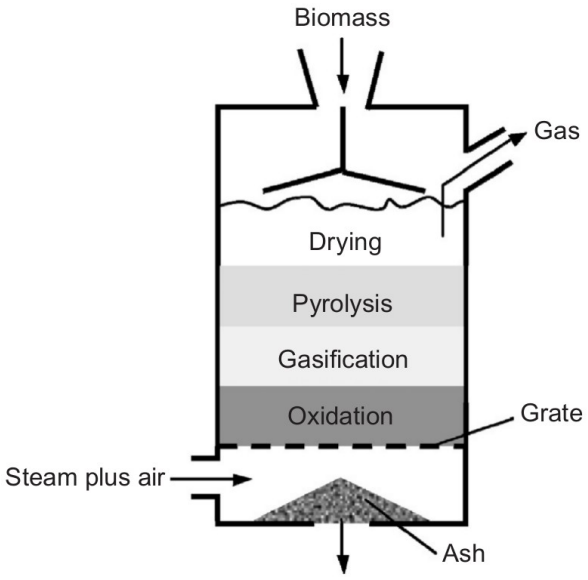

Figure 1.3.1: Schematic of an updraft gasifier [4].

A downdraft gasifier is a co-counter reactor where air enters the gasifier at a certain height below the top (in some types, it enters from the top). The product gas flows downward and leaves the reactor from the bottom, as it can be seen in fig 1.3.2. After entering air into the bed, it flows downward and meets the pyrolyzed char particles, developing a combustion zone. The gas descends further through the bed of hot char particles, gasifying them. Tar in the gas product, on the way out, passes through the high temperature zone (gasification zone and hot ash bed). Since high temperature is favorable for tar cracking, tar can be decomposed to other gas species. For this reason, a downdraft gasifier, of all type, has the lowest tar production.

In a crossdraft gasifier the fuel is fed from the top and air is injected through a nozzle from the side. The product gas leaves the reactor from the side wall opposite to the entry point of the air (fig 1.3.3). Part of the char in front of the nozzle is burned, creating high temperature, while the remaining char is gasified to CO downstream. Heat from the combustion zone is conducted around, which results in drying and pyrolysis of the raw wood in the furnace. This type of gasifier is generally used in small-scale biomass units. One of its important features is a relatively small reaction zone with a low thermal capacity, which gives a faster response time than any other type. Moreover, startup time is much shorter than in the downdraft and updraft units. However, the crossdraft design is less suitable for high-ash or high-tar fuels. Although tar in the gas product passes through the hot zone, similar to the downdraft gasifier, it has less residence time to crack

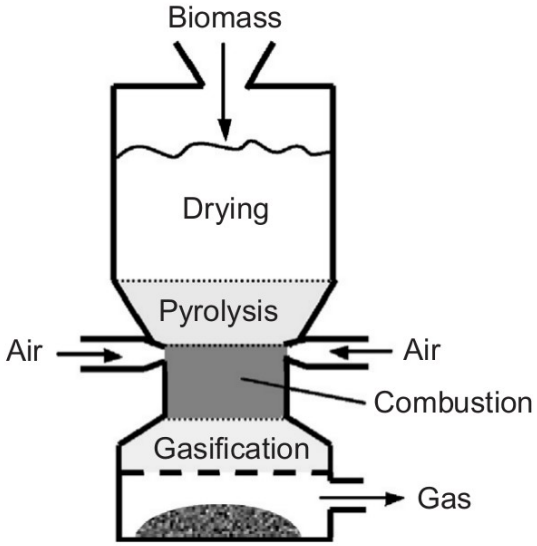

Figure 1.3.2: Schematic of a downdraft gasifier [4].

due to the small size of the reactor and high air velocity.

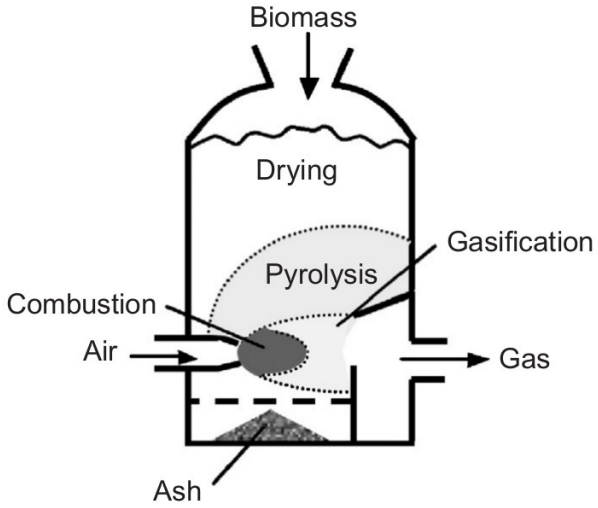

Figure 1.3.3: Schematic of a crossdraft gasifier [4].

1.4 Modeling background

Experimental investigations into packed bed processes are usually difficult to carry out due to a limited access inside the packed bed and therefore, demand a cost-intensive set-up. However, to be able to fully understand the characteristics of biomass conversion, numerical modeling studies have proven to be convenient means to get a deeper insight into the various physiochemical processes involved in biomass combustion in a packed-bed.

One of the most common ways of modeling of a packed bed is 1D-1D or so called representative model [11, 12]. This model includes one-dimensional model for the gas phase and one-dimensional model for the representative particle. In this model the interaction between the particles (conduction and radiation) is not taken into account precisely.

Euler-Lagrange models can provide more details in a bed [13, 14, 15]. Normally in this type of model, the fluid phase is a continuous phase but each particle is tracked with a Lagrangian approach. In many studies, intra partial gradient is neglected. However, this assumption is just valid in a specific condition (when *Biot* number is very large).

Modeling of combustion and gasification of solid fuel on a moving grate is much more complex than a fixed-bed due to motion of solid fuels in the bed. Many authors used a batch-type fixed bed reactor to describe the entire process in a moving grate furnace [16, 17, 11, 18, 19]. The main assumption in these studies is that the gradients of temperature and concentrations of chemical species in the direction of the movement of the bed are negligible compared to those in the direction of gas flow. Therefore, a vertical slice of the bed is modeled and followed along the grate. However, by comparing the real plants and fixed bed model [20], it can be concluded that a fixed bed cannot explain quantitatively as well as qualitatively observed phenomena in a moving grate. Few works have been reported in literature that used either Euler-Euler approach [21] or Euler-Lagrange approach [22, 23] to model motion and conversion of solid fuel together. However, more investigations and more precise models are needed to better understand the detailed information about the whole process in a boiler.

1.5 Objective

The main objective of this thesis is to propose a numerical model to describe the detailed information of many involved phenomena in gasification/combustion of biomass in a fixed-bed and moving bed. This will help us to understand deeply the process of biomass conversion and give us the knowledge how to improve the efficiency of a boiler and how to control the product composition. For this purposes, a CFD-DEM solver is developed, where the fluid phase is a continuous phase but each particle is tracked with a Lagrangian approach. Within the present model a packed bed is considered as an ensemble of a finite number of particles. Heat-up, drying, pyrolysis, gasification and combustion process of each particle is described by one-dimensional and transient conservation equations for mass and energy. Applying this model to all particles of a packed bed forms the entire packed bed process as a sum of the individual particle processes. The flow through the void space in the bed is modeled as a flow passing through a porous media, while the interaction between the solid and the gaseous phase by heat and mass transfer is taken

into account. Furthermore, using the proposed model, different parameters are studied to determine their effects on the operation of a boiler.

1.6 Thesis outline

The introduction chapter, will be followed with eight chapters. Given information in the chapter 2 to 7 can be divided as:

- Detailed modeling study and validation (chapters 2, 3,4 and 5)
- parameter study (chapters 6 and 7)

In the chapter 2, governing equations, coupling between two phases, the details of the numerical model and the concept of XDEM are explained. The main goal of this chapter is to describe drying of wet particles in a packed-bed. The predicted results are compared with the measurements taken from the literature.

The model to describe pyrolysis of wood particles in a fixed-bed is developed in chapter 3. Two models have been used to represent the devolatilization of wood particles (single step reaction and three parallel reactions). The results are compared with several series of measurements in both particle and bed scale provided by different research groups .

Chapter 4 explains the details of the combustion and the gasification modeling of biomass in a fixed-bed. Here, homogeneous reaction in the gas phase is taken into account. The results are explained for both solid and gas phases. The numerical model is validated with the measurements done at university of Twente.

The developed model in the previous chapter is further extended, in chapter 5, by considering the motion of solid particles. This allows simulating combustion and gasification of biomass in a forward acting grate.

Applying the proposed model in chapter 3, the effect of different packing on drying and pyrolysis product are studied in chapter 6. Self-ignition as a favorable and unfavorable phenomena is studied in chapter 7. The effect of different operating conditions on self-ignition characteristics are investigated and the results are presented in details.

In the chapter 8, a new approach (semi-resolved) of coupling between fluid and solid phases is presented. In the previous approach (standard approach), the solid phase is fully resolved while fluid phase is resolved with low degree. Althoguh, the standard approach can address many applications, when the ratio between partial size and reactor

is not small enough, it cannot describe the local flow condition in a inhomogeneous bed. While in semi-resolved approach, fluid phase will be calculated more precisely as smaller CFD cell size compared to the size of particles can be considered.

Finally, the main conclusion from this thesis will be given in chapter 9.

Chapter 2

Modeling of drying in a fixed-bed

A majority of solid fuels especially biomass contains moisture, which may amount up to the mass of the dry particles. Thus it is important to determine the details of drying when considering biomass as a fuel. Therefore, the objective of this chapter is to introduce a numerical model to predict drying of wet biomass particles within a packed bed reactor. [1]

[1] This chapter is written based on the following published article:
Amir Houshang Mahmoudi, Florian Hoffmann, Bernhard Peters, Application of XDEM as a novel approach to predict drying of a packed bed, **International Journal of Thermal Sciences**. 75 (2013) 65-75.

2.1 Introduction

During the recent years the use of biomass in energy production is the center of attentions in both academic and industry, since it is expected to play an important role as an energy source in the future. But improving the efficiency of the power plants using biomass is one of the biggest issues. Hence it is necessary to determine the details of various processes taking place in the combustion/gasification of biomass. A majority of solid fuels especially biomass contains moisture, which may amount up to the mass of the dry particles. Thus water is an important parameter when considering biomass as a fuel. With wet fuel, some heat of combustion is used to evaporate the water inside the solid fuel. Moreover during combustion of biomass the presence of steam increases the volume of the gases in the combustion chamber, deteriorates the quality of the product gas, and decreases the gas mixture temperature and the combustion rate. Reduction in combustion temperature below the optimum may result in incomplete combustion and leads to higher carbon monoxide levels leaving the boiler. Thus, the thermal output of the boiler and overall performance of the whole system are reduced [24, 25]. Therefore, drying may be of crucial importance to the combustion process in terms of both time and energy. Liang et al. [24] studied experimentally the effect of moisture content on combustion characteristics of municipal solid wastes. They found drying of material ended much later and the ignition front temperatures, ignition front velocity and overall burning rate were reduced for higher moisture content. Their results showed the average concentration of CO and CO_2 from the bed was inversely proportional to the moisture level, and average concentration of NO decreased with increasing moisture content. Brammer et al. [25] studied the influence of feedstock moisture content both before and after drying on the performance and cost of a biomass gasifier-engine system for combined heat and power at a given scale and feedstock cost. An initial review in various technological schemes for wood drying in combination with combustion/gasification may be found in the study by Svoboda et al. [26].

Experimental investigations into packed bed processes usually are difficult to carry out due to a limited access inside the packed bed and therefore, demand a cost-intensive set-up. Numerical models appear as a complimentary method to gain deeper knowledge of the processes in a packed bed. A comprehensive review on numerical approaches to model heat transfer in granular material may be found in Peters et al.[27] and [1].

Water in wood is present in three physical states: liquid water, also called free water, bound water and water vapor. Liquid water is similar to pure liquid water that flows in the pores of the wood and bound water is adsorbed in the cell wall [28]. Natural drying occurs by diffusion of the water vapor out of the particle. There is a thermodynamic equilibrium between the water vapor and the free water. Part of the free water evaporates to

compensate the loss of water vapor. When the liquid water is exhausted, the bound water starts to evaporate. More details about theory and physics of drying is explained by Bellais [28]. The most important part of a drying model is calculating the evaporation rate. Several models have been reported in the literature that either come from experimental correlations or theory and physics of evaporation.

Izadifar et al. [29] studied drying of paddy rice using local volume averaging approach and compared with experimental data. The evaporation rate has been used in their drying model was a function of both temperature and relative humidity which was recommended by ASAE (2001) for a plant-based product. They attributed the deviation from the experimental data to the local thermal equilibrium assumption. Since this assumption leads the gradient of moisture content and temperature inside particles to be negligible. In the same way Assari et al. [30] ignored the temperature and moisture gradient inside the particle and predicted drying in a fluidized bed. They calculated the evaporation rate as a function of temperature and moisture content of the particle. The comparison with measurements showed, that there was a considerable difference in moisture content of solid particles, although the solid temperature was very close to the experiment data. Mabrouk et al. [31] have used an experimental correlation for the drying rate under certain condition for a thin layer of particles. Saastamoinen [32] also presented a model for moving bed dryer based on thin layer drying rate equation and compared the drying rate in parallel and counterflow. Picado and Martinez [33] considered analytically vibrating fluidized bed dryer for grain. They calculated the vapor molar fraction at a gas-solid interface using the ratio between the partial pressure of water vapor and the total pressure, where the partial pressure of water vapor is calculated using an experimental correlation.

Generally the most common drying models are categorized as follows: heat sink model [1, 28, 13, 34, 35], first order kinetic evaporation rate[36, 37] and equilibrium model [11]. A *heat sink model* (or constant evaporation model) is based on the assumption that drying occurs at fixed boiling temperature. For this approach, heat available above the boiling temperature is consumed by evaporation without distinguishing between bound and free water. In this model there is no resistance to mass transfer so the water vapor instantaneously leaves the particle. A *first order of kinetic model* is a heterogeneous reaction according to the Arrhenius equation for free and bound water. In this approach water evaporates below the evaporation temperature. Moreover it is difficult to apply the given kinetics to conditions different to these under which the data has been derived. An *equilibrium model* is based on the hypothesis that water vapor is in equilibrium with the liquid and the bound water. Therefore the partial pressure of water vapor is fixed by the saturation pressure [28].

Collazo et al. [13] used a heat sink model but the temperature of a particle is allowed

increasing above the drying limit during a time step, and afterward part of its overheating is used to evaporate local moisture. So during the drying in each time step, portion of the receiving heat flux is used for evaporation of water inside a particle and the rest increases the temperature of a particle. This ratio can be changed for cases of thicker or thinner particles.

The objective of this chapter is to present a comprehensive numerical model for heat and mass transfer of granular material in a packed bed in order to describe a high level of detailed information about drying, heat and mass transfer of biomass materials in a packed bed. Within the present model a packed bed is considered as an ensemble of a finite number of particles. The heat-up and drying process of each particle is described by one-dimensional and transient conservation equations for mass and energy. Applying this model to all particles of a packed bed forms the entire packed bed process as a sum of individual particle processes. The arrangement of particles within the bed defines a solid phase and a void space between the particles. The flow through the void space of a packed bed is modeled as a flow through a porous media taking into account interaction between the solid and the gaseous phase by heat and mass transfer.

2.2 eXtended Discrete Element Method (XDEM)

The extended discrete element method is an advanced multiphysics and numerical simulation framework in which the dynamics of granular material or particles described by the classical discrete element method (DEM) (Cundall [38] and Allen [39]) is extended by additional properties such as the thermodynamic state, stress/strain or electro-magnetic field for each particle. In addition, the XDEM concept covers the coupling between discrete and continuous phases simultaneously. Thus, within this framework, continuous numerical approaches such as CFD (Computational Fluids Dynamics) and/or Finite Element Analysis (FEA) are coupled to discrete approaches such as Discrete Particle Method (DPM) in order to address numerous challenges in engineering e.g. drug production, agriculture food and processing industry, mining, construction and agricultural machinery, metals manufacturing, energy production and systems biology. In this method continuous fields are described by solving the respective differential conservation equations. Properties of individual particles such as temperature are also resolved by conserving energy that yields both a spatial and temporal internal distribution of temperature.

The proposed bed model for this study, schematically represented on Fig. 2.2.1, solves heat and mass transfer in a packed bed. This means that the solid feedstock consists of individual particles. They undergo conversion as well as granular flow. At the same time

interaction with and through the surrounding gas phase is accounted by CFD. Problem-relevant processes are predicted for each particle by efficient and fast numerical techniques. Hence the sum of all particle processes represents the entire process like of a moving or fixed bed. In a nutshell, this may be summarized with the following symbolic formula

$$\text{Entire Process} = \sum \text{Particle Processes} + \text{CFD}$$

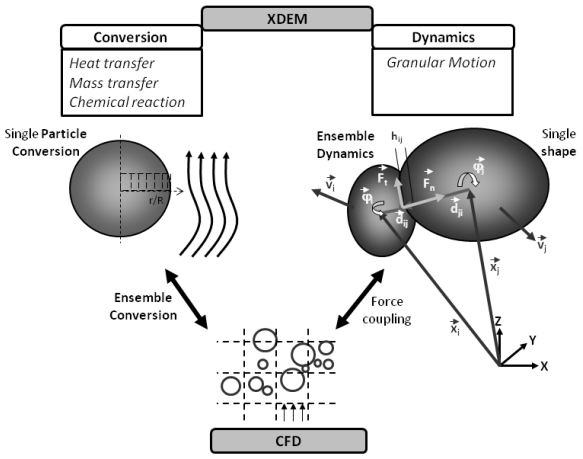

Figure 2.2.1: XDEM and its different interaction

2.2.1 Discrete Particle Method

The Discrete Particle Method, developed by Peters [15], is a numerical tool dealing with both motion and chemical conversion of particulate material. However, predictions of solely motion or conversion in a de-coupled mode are also applicable [40]. In contrast to a continuum approach that averages over an ensemble of particles in space, DPM considers a solid particle as an individual entity with the above-mentioned conversion and motion attached to it.

DPM offers a high level of details information and, therefore, is assumed to omit empirical correlations, which makes it independent of particular experimental conditions [15]. Particles may be of different shapes such as sphere, barrel, block, cone, cube, cylinder, disc, ellipsoid, tetrahedron and other complex shapes. Thus DPM can be seen as one of the most flexible and accurate approach among the heterogeneous models. A full description of DPM is presented by Peters in [15, 40, 41]. In DPM a discrete particle may be considered to consist of different phases: Solid, liquid, gas or inert material. Since particles may be considered as porous, gas diffusion within the pore volume is accounted for. Subject to the boundary conditions specified by its surrounding gas, a particle is allowed to exchange heat and mass with its environment. The distribution of temperature

and species are accounted for by system of one-dimensional and transient conservation equations [15, 42].

Conservation of mass for gas within the pore volume of a porous particle writes as follows:

$$\frac{\partial}{\partial t}\left(\epsilon_f \langle \rho_f \rangle^f\right) + \vec{\nabla} \cdot \left(\epsilon_f \langle \rho_f \rangle^f \langle \vec{v}_f \rangle^f\right) = \dot{m}'''_{s,f} \tag{2.2.1}$$

where the term on the right hand side accounts for mass transfer between the fluid within the pore of the particle or the solid phase with gas as a result of water evaporation or chemical reactions. ϵ_f denotes particle porosity, ρ_f gas phase density and $\vec{v_f}$ advective velocity. The gas density (ρ_f) is given by the sum of partial densities of species present in the gas phase as

$$\rho_f = \sum_{i=1} \rho_i \tag{2.2.2}$$

Transport of gaseous species within the pore space of the particle is considered to obey Darcy's law. Thus, for momentum conservation it states:

$$-\frac{\partial(\epsilon_f p)}{\partial x} = \frac{\mu_f \epsilon_f}{K} \langle v_f \rangle \tag{2.2.3}$$

Since Darcy's law is derived for a certain flow regime, the Reynolds number can be used to verify its applicability. In the present context the Reynolds number does not exceed a value of 5 based on the order of the relevant quantities: $\mu = \mathcal{O}(1 \times e^{-5})\ kg/ms$, $\rho = \mathcal{O}(1)\ kg/m^3$, $\langle v_f \rangle = \mathcal{O}(1 \times e^{-3})\ m/s$, $l_g = \mathcal{O}(1 \times e^{-3})\ m$, $d_P = O(1 \times e^{-6})\ m$.

For the energy balance of a particle local thermal equilibrium between phases of a particle (gas phase, the liquid and the porous solid) is assumed. This may be justified by the negligible thermal mass (ρc_p) of the gas phase compared to the solid and fluid phase, so that heat transported through bulk motion or diffusion of gaseous species within the pore space is neglected. Hence, the energy equation is based on the homogeneous model for a porous medium as described by Faghri [43] and writes as:

$$\frac{\partial \langle \rho c_p T \rangle}{\partial t} = \frac{1}{r^n}\frac{\partial}{\partial r}\left(r^n \lambda_{\text{eff}} \frac{\partial \langle T \rangle}{\partial r}\right) + \sum_{k=1}^{l} \dot{\omega}_k H_k \tag{2.2.4}$$

where λ_{eff} is the effective thermal conductivity. The source term on the right hand side represents release or consumption of heat due to chemical reactions where H_k is the enthalpy of reaction k. This formulation allows the geometry of the domain to be one of the following: infinite plate $n = 0$, infinite cylinder $n = 1$ or a sphere $n = 2$.

Assuming thermodynamic equilibrium within the intra-particle fluid and considering it as a perfect gas the equations of state in terms of the two state variables temperature T

and gas density ρ are:

$$p = \rho R_v T \tag{2.2.5}$$
$$h = c_p T \tag{2.2.6}$$

Taking into account mass fractions and molecular weights of individual gaseous species the density of the gas phase can be calculated with the following equation:

$$\rho_f = \frac{p_f}{\mathcal{R} T \sum_i \frac{\xi_i}{M_i}} \tag{2.2.7}$$

Peters et al. [1] compared the *Heat sink model* (constant evaporation model) versus *first order kinetic evaporation rate* and concluded that heat sink model has a better agreement with experiment. So in this study heat sink model is chosen for calculating the drying rate as defined in Eq. (2.2.8).

$$\dot{w}_{H_2O} = \begin{cases} \frac{(T - Tevap)\rho\, c_p}{H_{evap}\, \delta t} & \text{if} \quad T \geq T_{evap} \\ 0 & \text{if} \quad T \leq T_{evap} \end{cases} \tag{2.2.8}$$

For this approach, heat available above the evaporation temperature T_{evap} is consumed by evaporation without distinguishing between bound and free water. Here ρ, c_p and H_{evap} are the density and thermal capacity of dry wood and its evaporation enthalpy. It is worth to mention in the present model the water vapor inside the particle does not leave the particle instantaneously. Here the vapor transfer from particle to ambient is limited by the difference in vapor concentration inside the particle and ambient.

To complete the mathematical model for a single particle, boundary conditions must be provided. Since geometries are considered to be either sphere, infinite cylinder or infinite plate, a symmetric boundary condition is applied for the particle center:

$$-\lambda_{\text{eff}} \frac{\partial \langle T \rangle}{\partial r}\bigg|_{r=0} = 0 \tag{2.2.9}$$

The following boundary conditions for mass and heat transfer were chosen for the particle surface:

$$-D_{\text{i,eff}} \frac{\partial \langle \rho_i \rangle}{\partial r}\bigg|_{r=R} = \beta_i(\rho_{i,R} - \rho_{i,\infty}) \tag{2.2.10}$$

$$-\lambda_{\text{eff}} \frac{\partial \langle T \rangle}{\partial r}\bigg|_{r=R} = \alpha(T_R - T_\infty) + \dot{q}''_{\text{rad}} + \dot{q}''_{\text{cond}} \tag{2.2.11}$$

where T_∞ and $\rho_{i\infty}$ denote ambient gas temperature and ambient density of gas specie i,

respectively. The heat fluxes on the right hand side of Eq. (2.2.11) account for potential radiative heat exchange with the surroundings or conductive heat transport through physical contact with other objects. Concerning transfer coefficients, a range of experimental work has already been carried out by numerous authors (for a summary see [33, 44, 45]) to establish appropriate laws for different geometries and flow conditions at the particle surface. Different regimes can be distinguished by using dimensionless numbers such as Nusselt, Sherwood, Reynolds, Schmidt and Prandtl.

2.2.2 Coupling between DPM and CFD

In the present coupling model the heat interaction between particles (conduction, radiation) and also heat and mass transfer between particles and their environment (conduction, convection) is resolved with the above mentioned XDEM, whereas the continuous phases are solved with a CFD tool. Thermal energy and mass are transferred from fluid to particles and/or particles to fluid as heat source and mass source respectively. Hence depending on the particles properties within each specific CFD cell, the heat source and mass source values are calculated. The gas phase is modeled in an Eulerian approach with a variant of Navier Stokes equations for compressible fluid in porous media implemented in OpenFoam.

CFD model Packed beds can be characterized as a type of porous media in which fluid flow behaves more like an external flow. The flow may be accurately described for a continuum approach by averaging relevant variables and parameters on a coarser level. Hence, although the solid particles are considered as a separate phase, fluid flow in the bed is treated as one homogeneous continuum. For this reason macroscopic governing equations are obtained from the corresponding microscopic equations through an averaging process over a representative elementary volume (REV) [46, 47, 48]. For a given system three characteristic length scales are introduced: For the global system under study there exists a macroscopic length scale L. The choice of a REV introduces a length scale l_{REV} related to the dimension of this volume and the third one is a microscopic scale l_g representative of the pore space. For any real porous flow it holds $l_g << l_{\mathrm{REV}} << L$ and in that case the medium is considered homogeneous within one REV [46, 47]. Hence this approach for multiphase systems will be extended to obtain the formulation for porous media:

Continuity equation The continuity equation of the fluid phase f writes as:

$$\frac{\partial}{\partial t}\left(\epsilon_f \langle\rho_f\rangle^f\right) + \vec{\nabla}\cdot\left(\epsilon_f \langle\rho_f\rangle^f \langle\vec{v}_f\rangle^f\right) = \dot{m}'''_{s,f} \tag{2.2.12}$$

Momentum Equation Gas flow within a porous media like a packed bed of particles is modelled using the Brinkmann or Forchheimer relations [45, 43].

$$\begin{aligned}&\tfrac{\partial}{\partial t}\left(\epsilon_f \langle\rho_f\rangle^k \langle\vec{v}_f\rangle^f\right) + \vec{\nabla}\cdot\left(\epsilon_f \langle\rho_f\rangle^f \langle\vec{v}_f\vec{v}_f\rangle^f\right)\\ &= \vec{\nabla}\cdot\left(\epsilon_f \left\langle\vec{\tau}'_f\right\rangle^f\right) - \tfrac{\mu_f}{K}\epsilon_f^2 \langle\vec{v}_f\rangle^f - C\langle\rho_f\rangle^f \epsilon_f^3 |\langle\vec{v}_f\rangle^f| \langle\vec{v}_f\rangle^f\end{aligned} \tag{2.2.13}$$

where K is the permeability of the bed and C the dimensionless drag coefficient. Both parameters can be obtained from empirical relations which are tabulated for various of types packed bed [43]. The latter with a voidage ϵ_f consisting of spherical particles having diameter D_P the following relations hold [43, 15]:

$$K = \tfrac{D_P^2 \epsilon_f^3}{150(1-\epsilon_f)^2} \tag{2.2.14}$$

$$C = \tfrac{1.75(1-\epsilon_f)}{D_P \epsilon_f^3} \tag{2.2.15}$$

Energy equation Conservation of energy in a porous medium consisting of a gas and a solid phase is accounted for by volume-averaging the corresponding energy equation of multiphase systems. The intensity of heat exchange between solid-fluid phases ($q'''_{s,f}$) is subjected to the thermal boundary conditions at the interface

$$\vec{q_p}'' = -\vec{q_f}'' \tag{2.2.16}$$

$$S_p \alpha (T_p - T_f) = q'''_{s,f} V_{\mathrm{REV}} \tag{2.2.17}$$

leading to the following formulation:

$$\begin{aligned}&\tfrac{\partial}{\partial t}\left(\epsilon_f \langle\rho_f\rangle^f \langle h_f\rangle^f\right) + \left(\epsilon_f \langle\rho_f\rangle^f \langle\vec{v}_f h_f\rangle^f\right)\\ &= \tfrac{\partial\langle p_f\rangle}{\partial t} + \epsilon_f \cdot \langle\vec{v}_f\rangle^f \cdot \vec{\nabla}\langle p_f\rangle + \sum_{i=1}^{M}\left\langle \tfrac{S_p}{V_{\mathrm{REV}}}\alpha(\Delta T_i)\right\rangle\end{aligned} \tag{2.2.18}$$

where the last term of the right hand side of Eq. (2.2.18) refers to the before cited heat source term. This term is reflecting the coupling between DPM and CFD for heat transfer simulations. Thus the mesh-based Eulerian fields and the particle-based Lagrangian quantities are linked.

Species equation Like the energy equation, the intensity of mass exchange between solid-fluid phases ($m'''_{s,f}$) is related to boundary conditions at the interface

$$S_p \beta_i \left(\rho_{p,i} - \rho_{f,i}\right) + S_p \cdot \epsilon_{f,p} \langle \rho_{p,i} \rangle^f \langle V_{f,p} \rangle^f = m'''_{s,f,i} V_{\mathrm{REV}} \tag{2.2.19}$$

where $\epsilon_{f,p}$ is the porosity of single particle and $V_{f,p}$ is the outlet or inlet velocity at the surface of the particle. Hence, the species equation is:

$$\frac{\partial}{\partial t}\left(\epsilon_f \langle \rho_{f,i} \rangle^f\right) + \nabla \cdot \left(\epsilon_f \langle \rho_{f,i} \rangle^f \cdot \langle V_f \rangle^f\right) = \sum_{i=1}^{M} m'''_{s,f,i} \tag{2.2.20}$$

2.2.3 Characteristics of flow in packed beds

Packed bed reactors have a wide range of engineering applications of which a biomass gasifier is an example. Common to all these devices is heat and mass transfer between the solid particles and the gas flow streaming through the void space between the particles. Hence, the gas phase is coupled to the particle surfaces by heat and mass transfer. For a classical continuous representation of the particulate phase either experimental data or empirical correlations have to be employed that determine both total surface area of the particles and the distribution of void space between them. However, these disadvantages are omitted by the current approach that allows evaluating the available surface for heat transfer and void space affecting the flow distribution. Both particle surface area and void space distribution are inherently determined by filling a reactor vessel with spherical particles. The final random arrangement of particles is shown in fig. 2.2.2. Therefore the position of each particle in a packed bed is determined so that the predicted conditions of the gas flow in the vicinity of the particles are identifiable in order to assess local heat and mass transfer. Among these parameters, the local velocity significantly influences the heat transfer. Distribution of flow in the void space of the packed bed depends on the distribution of the void space i.e. porosity in a packed bed (fig. 2.2.3). With known positions and size of particles the porosity distribution is readily determined. Therefore the mass source and heat source in the gas phase, that are as a result of heat and mass transfer with solid phase, are determined at each point within the bed.

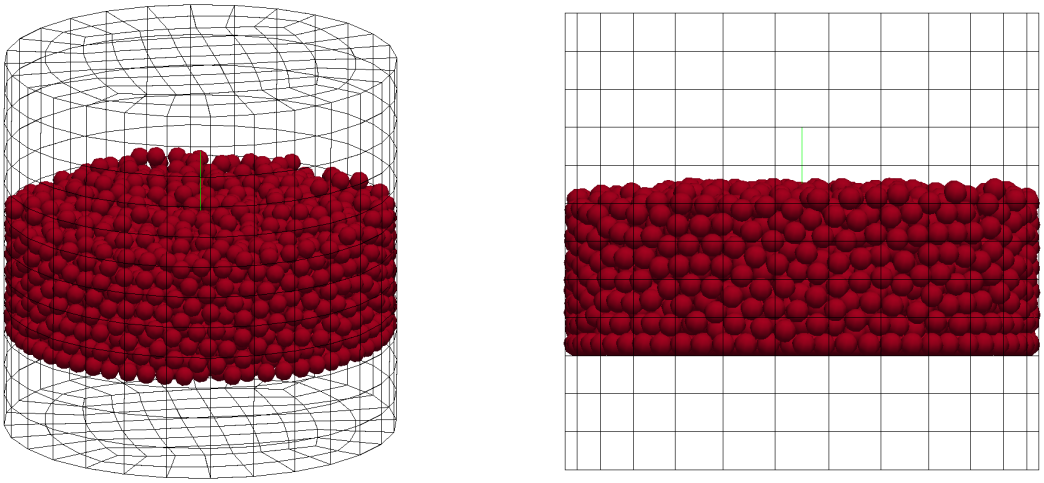

Figure 2.2.2: Problem geometry

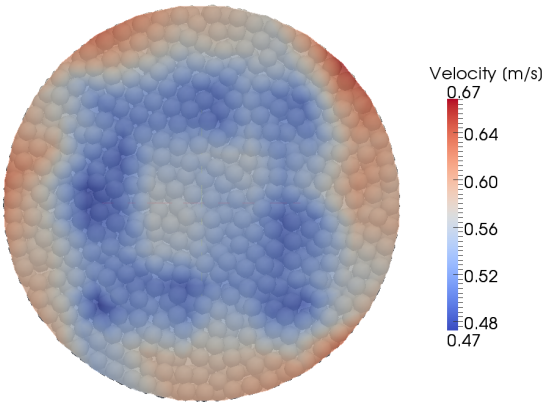

Figure 2.2.3: intrinsic velocity contour in the bed

2.3 Predicted Results

The experimental data used for validation was obtained by Peters et al. [1] at the test reactor Pantha. The reactor was set-up to investigate heating up, drying and pyrolysis of particles in packed beds. The experimental reactor shown in Fig. 2.3.1 consists of an outer steel cylinder designed for a maximum temperature of $T = 800\ ^oC$ and a maximum pressure of p = 2 bar. The containment is electrically heated and thermally insulated at its cylindrical wall and the bottom to compensate heat losses. The top of the reactor

is insulated, but not heated. The packed bed is filled into a cylindrical basket, which is positioned in the interior of the reactor. The fuel bed is 250 mm in diameter and 190 mm in height. A rod connects the basket containing the packed bed to a load cell. The load cell is located in a cold instrumentation compartment at the top of the containment. While the fuel bed is heated, the reaction chamber rests on a metal seat. In order to record mass losses due to evaporation and pyrolysis, the gas flow is turned off and the reaction tube is lifted via an electrical motor, which is connected with the load cell. Afterwards the reaction tube is reinstalled in its previous position and the gas flow is turned on again. By adjusting the intervals of the weight measurements appropriately, a mass loss history for the packed bed due to evaporation is produced. The bed is heated by a flow of hot gas entering from top of the container and passed through the reaction tube from top to bottom. More details about the experimental setup is given in [3]. The drying experiments were carried out with 2 kg of air-dried cube of beach wood $10 \times 10 \times 10\ mm^3$ in size. The moisture content of particles is approximately 10% of dry mass. The relevant properties of the beach wood are listed in Table. 2.3.1 [3]. When the reaction tube has

Table 2.3.1: Beech wood properties [1].

Particle radius R (mm)	6.2
Density ρ (kg/ m^3)	750
Porosity ϵ	0.64
Permeability K	0.02
Pore diameter (m)	50.0×10.0^{-6}
Tortuosity	1.0
Specific heat c_p (J/kg K)	2551.3
Conductivity λ (W/m K)	0.47

been filled with the particles, the steel containment is closed and the bed is preheated by the circumferential electric heater to appropriately $T = 90\ ^oC$. A flux of heated nitrogen ($\dot{m}_{N_2} = 16\ kg\ h^{-1}$) as an inert gas streamed through the packed bed to dry it. Due to the thermal capacity of the test facility the temperature of incoming gas stream approaches its steady state value after a certain period, whereby the evolution of the temperature follows an exponential relation of following form:

$$T_{in} = T_{dry} - \Delta T e^{\gamma t} \tag{2.3.1}$$

where T_{dry}, ΔT, γ and t stand for the steady state drying temperature, the relevant temperature difference, the time constant and time, respectively. The value for the two drying temperature are given in Table. 2.3.2.

According to the experimental setup, the simulation model is prepared as shown in Fig. 2.2.2. In the simulation instead of using cube particles, the spherical particles with

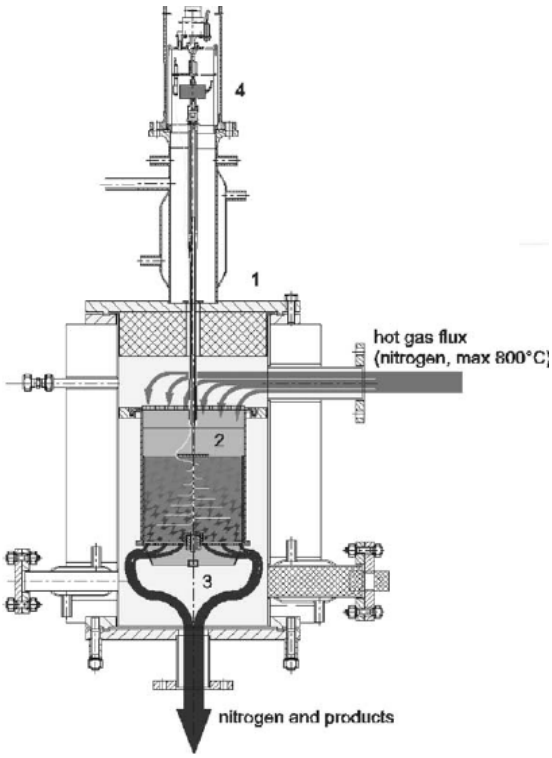

Figure 2.3.1: Schematic sketch of experimental set-up

Table 2.3.2: Specification of inlet temperature [1].

Drying temperature (°C)	ΔT (°C)	γ (1 s^{-1})
135	115	-0.001
150	126	-0.001

equal volume are used. Thus the container is filled with 2667 particles randomly and the height of bed reaches to about 100 mm, similar to experiment. It should be noted, as shown in Fig. 2.2.2 at the top and bottom of the container the simulation domain is stretched for 8 and 6 cm respectively, which there are not any particle in these space.

Fig. 2.3.2 presents dimensionless the loss of moisture for both simulation and experiment for two different inlet temperatures. Good agreement between simulation and measurements for each cases has been achieved, so the drying model for a random packed bed works well.

Fig. 2.3.3 depicts the mean temperature of particles and fig. 2.3.4 illustrates the gas temperature and the dimensionless water of particles at different height when inlet temperature is set to 403 K. As explained above, at the beginning the inlet temperature is lower than initial temperature of particles in the container, as can be seen at $t = 100\ s$ and $t = 400\ s$ the mean temperature of particles decreases from top to bottom. The mean temperature at $t = 800\ s$ shows heating up the particles has been started so that the uppermost layer of particles are warmer than others. At $t = 1000\ s$ the temperature of

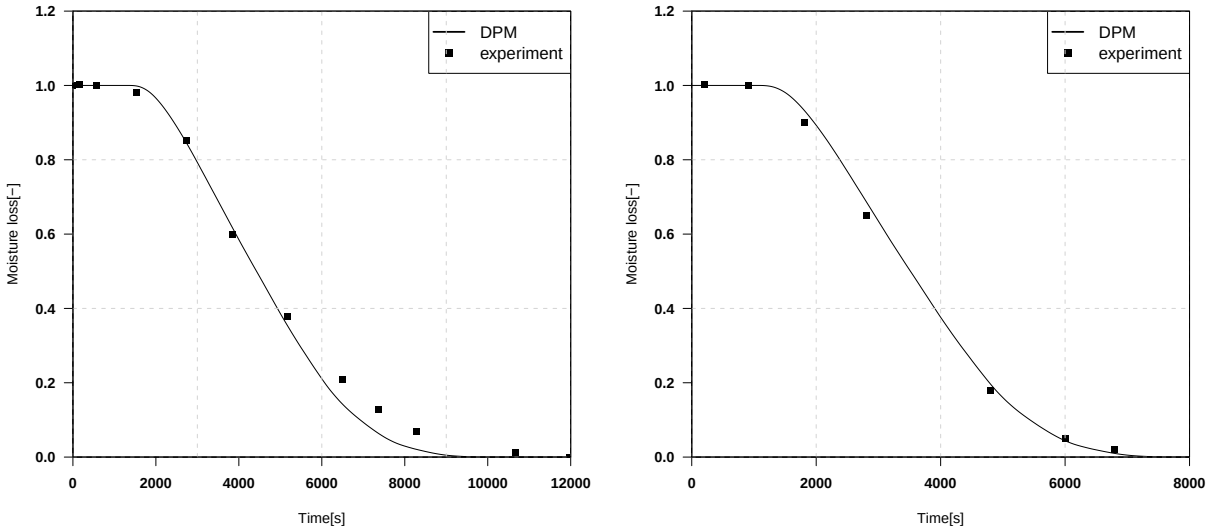

(a) **(b)**

Figure 2.3.2: comparison with experiment data a) inlet temperature equal to 408 K b) inlet temperature equal to 423 K

particles is still lower than the evaporation temperature, so that, no evaporation occurred as shown in Fig. 2.3.4. At $t = 2000\ s$ the fist layer of particles, except some particles that already lost their whole water content, is in middle of drying process so that the mean temperature is approximately 373 K, after a further period of 1000 seconds they lose their whole water content, and their mean temperature increase as shown in fig. 2.3.3. This behavior can be seen for lower layers in next times. Fig. 2.3.3 and 2.3.4 show that up to $t = 4000\ s$ the inlet gas loses its whole thermal energy, as a result of contact with particles, and leaves the container almost at lowest particles temperature (bottom layer). But at $t = 5000\ s$ it is observed that the difference between outlet gas temperature and lowest particle temperature increases so that at $t = 8000\ s$ it reaches to 25 K. This is due to the fact, that after 4000 s many of particles in upper layers have lost their whole water content and their temperature exceeds the boiling temperature, so that they are almost at the same inlet gas temperature. Thus they use less gas thermal energy and result in less reduction in gas temperature. The results in Fig. 2.3.3 and 2.3.4 at $t = 8000\ s$ indicate, although there is not water in the particles, but there are some particles which are still heating up. Thus the system has not reached to the steady state condition and hence the outlet gas temperature is lower than inlet temperature.

In order to understand better heat transfer between gas and particles, the gas temperature at the center line and different heights of container is presented in fig. 2.3.5. The temperature reduction during the first minutes as explained before, is because of lower inlet gas temperature than initial bed temperature. At $z = 160\ mm$, approximately from

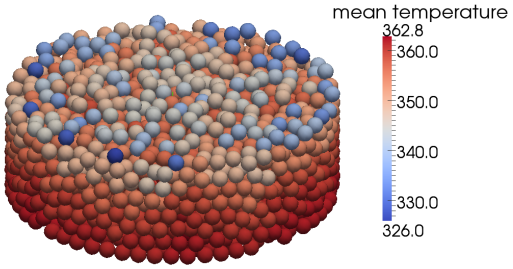

(a) t=100s

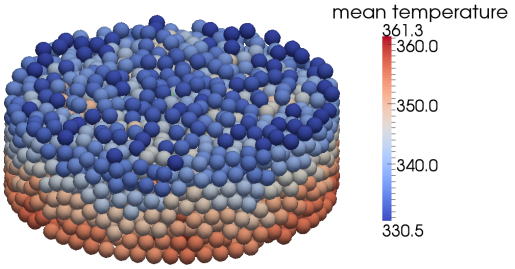

(b) t=400s

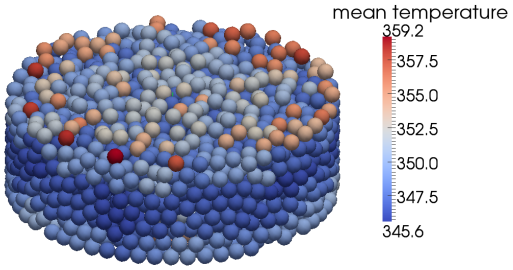

(c) t=800s

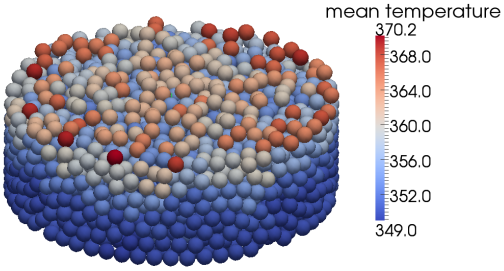

(d) t=1000s

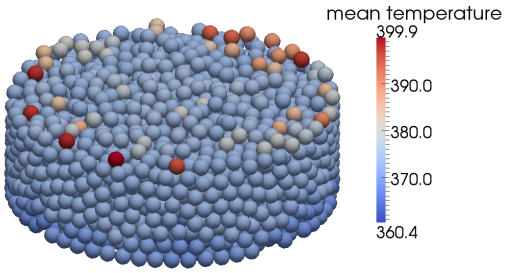

(e) t=2000s

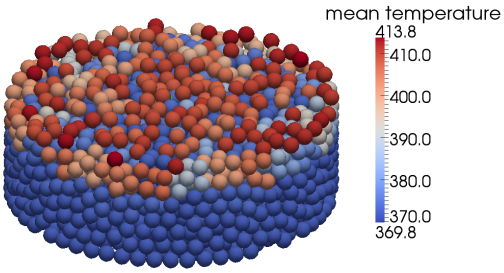

(f) t=3000s

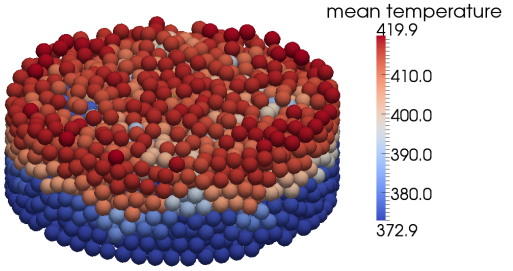

(g) t=4000s

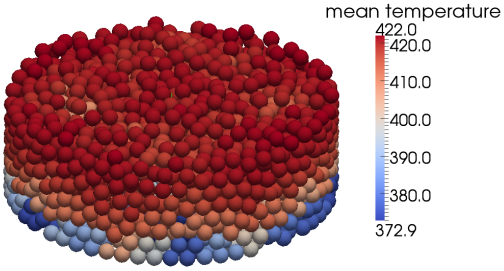

(h) t=5000s

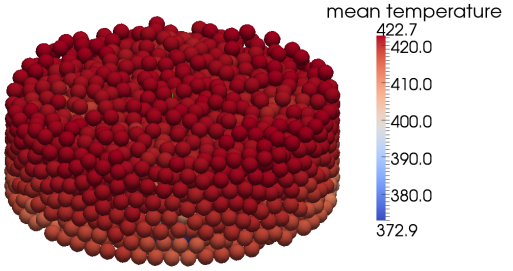

(i) t=6000s

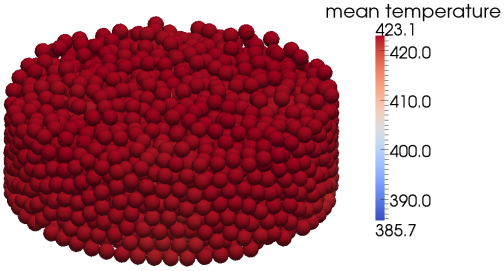

(j) t=8000s

Figure 2.3.3: Mean temperature of particles at different times when $T_{in} = 423\ K$

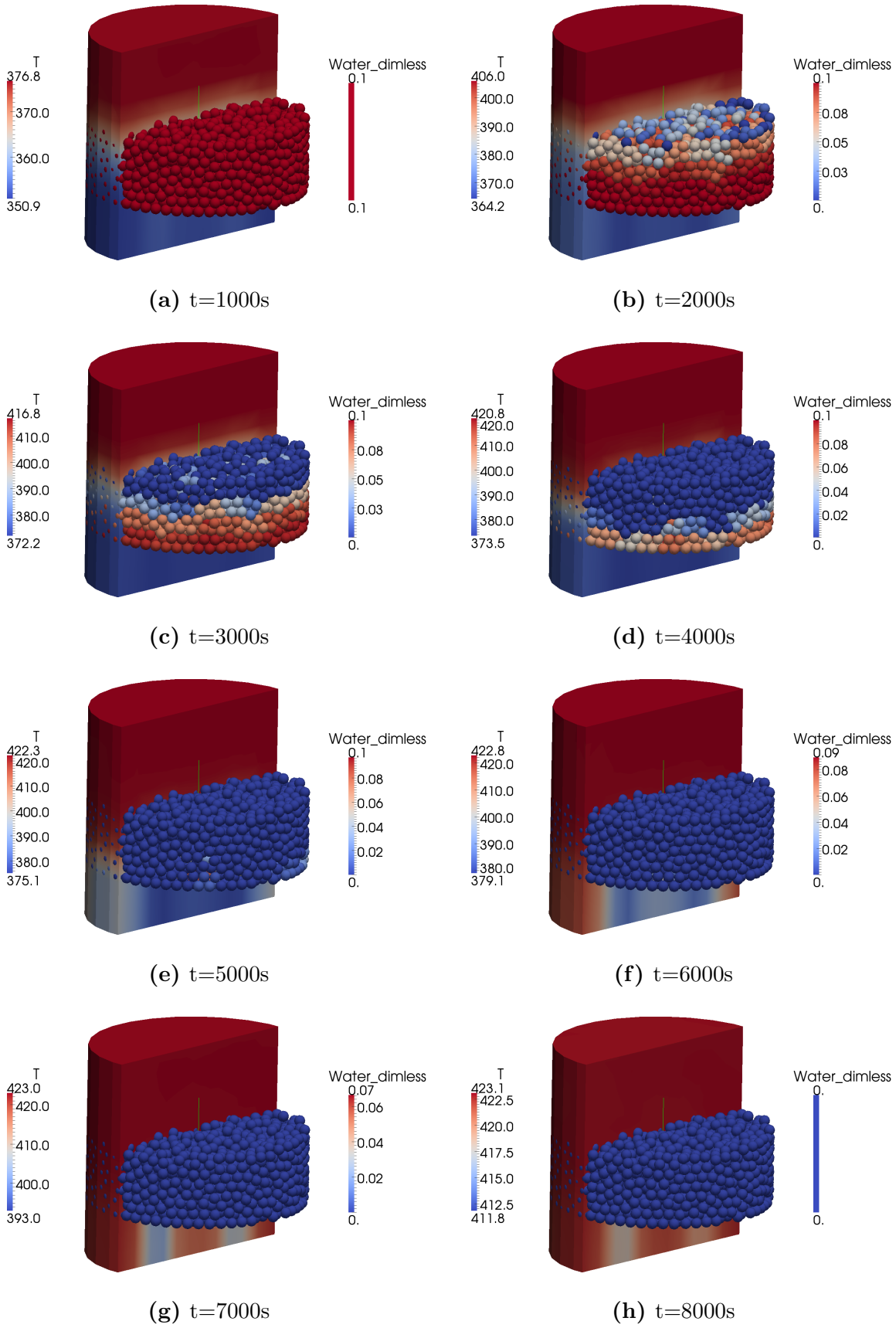

(a) t=1000s **(b)** t=2000s

(c) t=3000s **(d)** t=4000s

(e) t=5000s **(f)** t=6000s

(g) t=7000s **(h)** t=8000s

Figure 2.3.4: Gas temperature and dimensionless water content in the particles

$t = 1200\ s$ until around $t = 2200\ s$ the obtained temperature profile deviates from the expected exponential profile. Instead an almost straight line with a smaller slope is observed. This deformation occurs during the evaporation phase of particles around that point ($z = 160\ mm$). This is due to the fact that during heating up of the particles, the temperature difference between a particle and surrounding gas decreases with time, which is accompanied by a reduction of the heat sink for hot gas flow. But during the drying period, since the temperature of particle is constant, so there is larger difference between particle and ambient gas temperature than before drying. This results in a larger heat sink for gas phase and hence, increase of gas temperature is slower. When water content of particles in that location finished, the gas temperature increases and its profile return again to exponential form. This behavior can be seen in other locations but with multi step. For example at $z = 140\ mm$, evaporation starts approximately from $t = 1500\ s$ so the temperature profile change to straight line, but around $t = 2200\ s$ the temperature jump up and again fallows the straight line until about $t = 3200\ s$, which drying of particles in that area has finished, and then increases and changes to the exponential form until the end of simulation. The jump at the middle of the straight part is due to finishing of the evaporation in particles at upper layers, that result in an increase of gas temperature. The same behavior was observed for other points but the slope of the first straight line is lower due to the use of gas energy by upper particle layers.

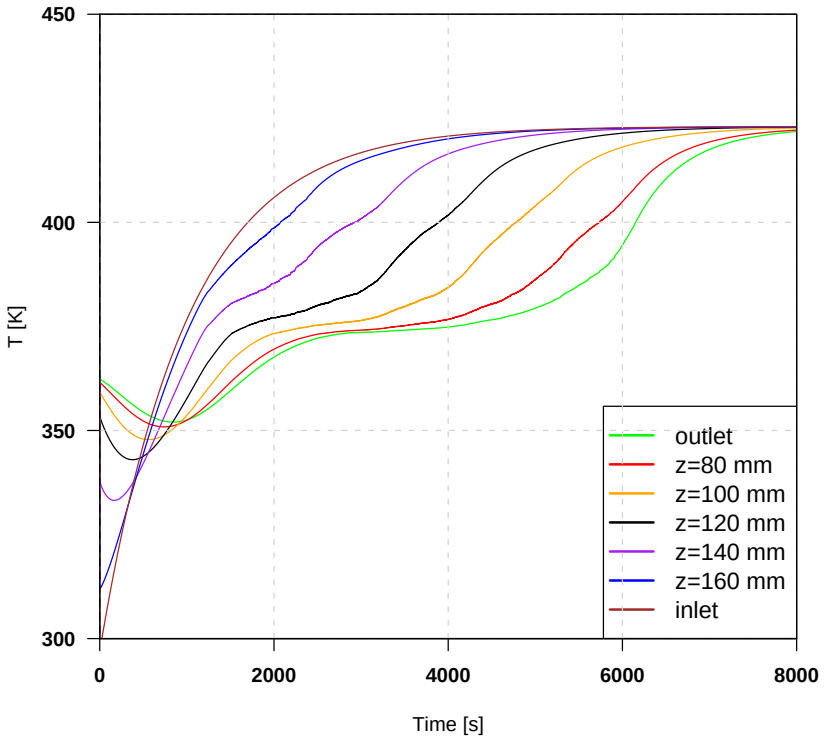

Figure 2.3.5: Gas temperature at different height in container.

In order to add more details about a single particle in a packed bed, fig. 2.3.6, 2.3.7 and 2.3.8 present mean temperature, dimensionless water and vapor mass fractions respectively for three particles at bottom, middle and top of the bed. Similar to fig. 2.3.5, the temperature of particles decreases during the first minutes. This reduction is most intense in the upper particle layer because the incoming gas flow with a temperature of app. 300 K cools the particles. Fig. 2.3.6 shows clearly that a particle experiences a period of constant temperature of 373 K that represents the evaporation of moisture. When the whole water within the particle is evaporated, the temperature approaches the inlet gas temperature. Loss of water for the above mentioned particles is presented in fig. 2.3.7. At the end of drying period, some small jumps are observed. This is due to the fact that layers near to the surface of the particle have lost their stored water and the temperature in those layers rises, which in tern increases the mean temperature. Fig. 2.3.6 shows the drying process for particles is longer if they are far from the inlet port. This can be explained by the fact that the hot inlet gas loses a large amount of its thermal energy during the contact with upper particle layers. Thus when it advances toward the bottom of the reactor, there is no more available energy for heating up of those layers

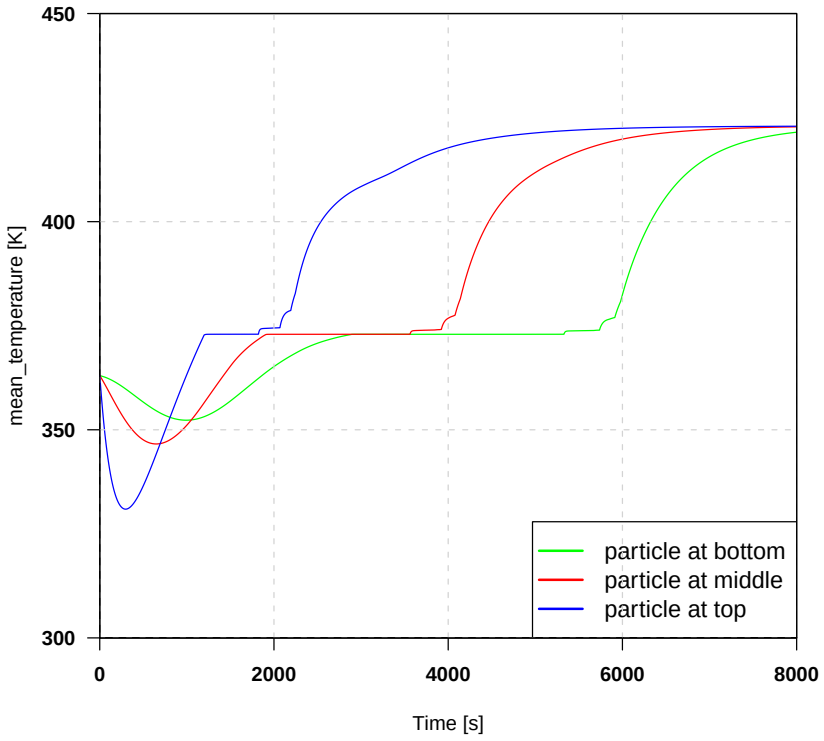

Figure 2.3.6: Mean temperature of particles at different heights.

Fig. 2.3.8 shows vapor mass fraction inside three particles at different heights. As described above the evaporation of the bed starts at approximately 1200 s which is accom-

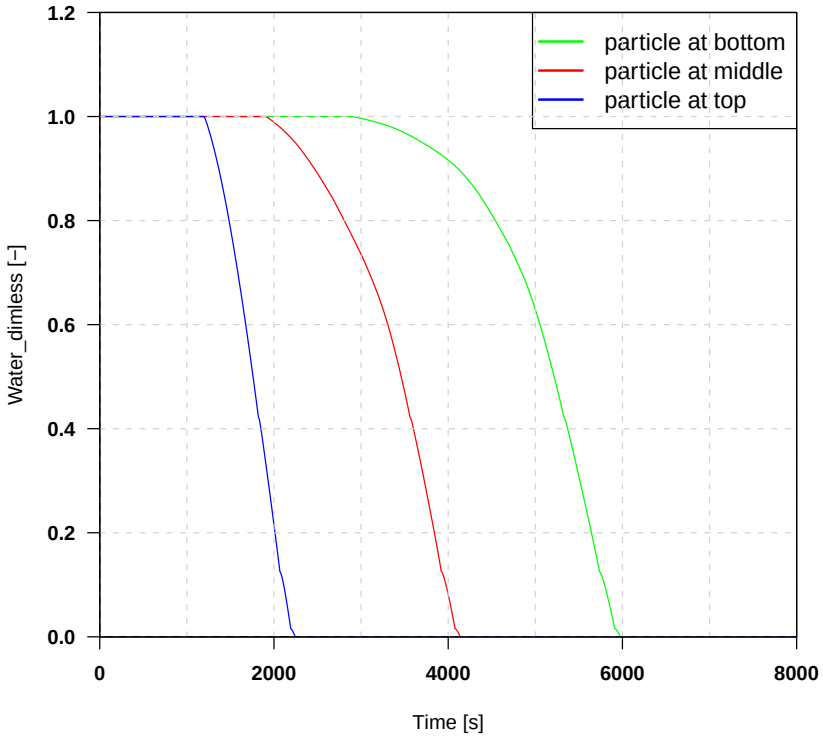

Figure 2.3.7: Dimensionless water inside the particles at different heights

panied by a rapid increase in vapor mass fraction in the top particle. For particles in lower layers a moderate increase in vapor mass fraction can also be observed. Nevertheless, this rise in vapor content in these lower particles is mainly due to mass transfer from the layers above. Vapor released within top layers of the bed is transported downstream by the drying gas and is absorbed by particles in lower layers. From this it can be explained that at the same point in time these lower particles are exposed to an ambient gas that has a much higher vapor content than the gas surrounding the top of the bed. Consequently, for the lower part of the bed there is a much smaller gradient between the particles and the ambient vapor concentration. This also is another reason for the slower drying process of particles located downstream.

2.4 Conclusions

A comprehensive numerical model for heat and mass transfer of granular material was presented in order to predict drying of biomass materials in a packed bed. Within the presented model a packed bed was considered as an ensemble of a finite number of particles. One-dimensional and transient conservation equations for mass and energy were solved

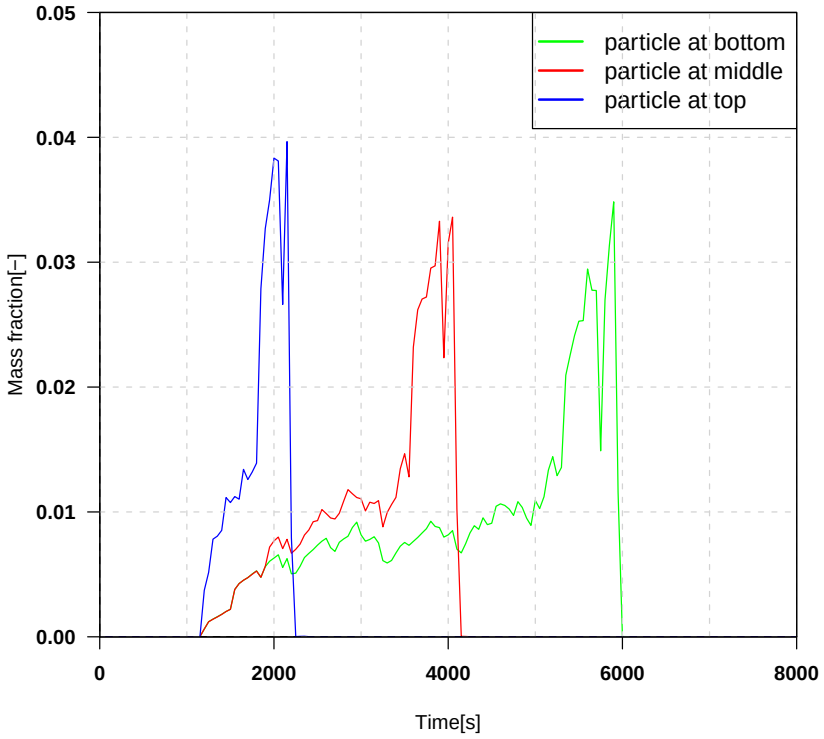

Figure 2.3.8: Vapor mass fraction in the particles at different heights

for each particle. Using this model for all particles within the bed in combination with an appropriate continuous model for the surrounding gas, enables prediction of a process for an entire packed bed by summation of individual particle processes. The flow through the packed bed was modeled as a flow through a porous medium which thermochemically interacts with the solid phase by heat and mass transfer. Characteristic properties of the porous medium such as void space were calculated based on the position and size of each particle. Drying rate was calculated using heat sink model, in which heat available above the evaporation temperature is consumed by evaporation of water within the particle. The predicted results were compared with experimental data that was obtained by Peters et al. [1] at the test reactor Pantha. Good agreement between simulation and measurements for two different inlet temperature has been achieved. The results showed the ability of the model to present the details of drying for a random packed bed of biomass.

Chapter 3

Modeling of pyrolysis in a fixed-bed

Pyrolysis is one of the unavoidable steps in combustion/gasification that must be investigated carefully. Apart from that, pyrolysis itself can be considered as an independent process to produce a useful form of energy from biomass. The main aim of this chapter is to introduce a numerical model that describes pyrolysis of biomass in a packed bed. [1]

[1] This chapter is written based on the following articles:
Amir Houshang Mahmoudi, Florian Hoffmann, Bernhard Peters, Detailed numerical modeling of pyrolysis in a heterogeneous packed bed using XDEM, **Journal of Analytical and Applied Pyrolysis** 106 (2014) 9-20.
Amir Houshang Mahmoudi, Florian Hoffmann, Bernhard Peters, Xavier Besseron, A study of size distribution of particles in a backed bed on pyrolysis products using XDEM, accepted on September 2015 to be published in "**International communications in heat and mass transfer**".

3.1 Introduction

Biomass as a solid particle with considerable amount of moisture and non-homogeneous properties, is difficult to be used in many applications. Thus it is more useful to convert it into a more convenient form of energy. Gasification and pyrolysis are the most promising ways. Combustion and gasification of biomass particles are very complex phenomena because of the involved physical and chemical processes including heating up, drying, pyrolysis, oxidation of pyrolysis product, char oxidation and gasification.

Pyrolysis/devolatilization is also one of the unavoidable steps in combustion/gasification that must be investigated carefully. Apart from the important role of pyrolysis in the combustion/gasification of biomass, pyrolysis itself can be considered as an independent process to produce a useful form of energy from biomass. According to Gronli et al. [5] pyrolysis is the thermal degradation (devolatilization) of a feedstock in the absence of an oxidizing agent (like O_2), leading to the formation of a mixture of liquid (tarry composition), gases, and a highly reactive carbonaceous char, of which the relative proportions depend on the method used. Each of the pyrolysis products can be the main aim of the pyrolysis. For example char can be used as a reducing agent in the metallurgical industry, as a domestic cooking fuel. Pyrolysis gas can be used for power generation, heating, or synthesized to produce methanol or ammonia, whereas the tarry liquid (pyrolysis oil or bio-oil) can be used for combustion engines. It can be also used directly for power generation or heat [5].

A literature survey indicates that several kinetic models for pyrolysis of wood particles have been proposed by different authors; comprehensive review are given by Di Blasi [49] and Peters et al.[50]. Generally they can be categorized in three groups: one step global reaction [51], three parallel reactions [37, 52, 53] and devolatilization model of three main biomass components (cellulose, hemicellulose, and lignin) [54]. The latest is very accurate and considers many complex reactions and products however it is very expensive from numerical point of view. The one step global reaction model is simpler which considers decomposition of biomass into char, gas and tar. This model neglects all the intermediate reactions but it can still predict the process very well as it has been reported by many researchers [51, 55, 36].

Heat of pyrolysis, due to difficulty in measuring, is one of the challenging topics in modeling of pyrolysis [56, 57, 58, 59]. Literature review indicates that this term is usually used as an adjustable parameter [57]. For example Gronli et al. [5] and Blasi [60] assumed 150 kJ/kg and 418 kJ/kg as an endothermic heat of reaction respectively, while Wurzenberger et al. [11] neglected the heat of pyrolysis in their simulation. Haseli et al. [57] considered the temperature dependency of pyrolysis heat. They could capture higher particle

inner temperature than particle surface temperature which was confirmed in experiment by Koufopanos et al. [61]. Strom and Thunman [58] also described heat of pyrolysis as a linear function of temperature. They determined the coefficients of this linear function by fitting the model predictions to the experimental data. In another work Haseli et al. [59] similar to Rath et al. [56] included the char yield into the formulation of the heat of pyrolysis.

Particles shape/size and heating condition have considerable effect on the pyrolysis products and reaction rate, hence it is another challenge in modeling of pyrolysis. Blasi [60] developed a numerical model to investigate the coupled effects of particle size and heating conditions (reactor heating rate and final temperature) on pyrolysis of cellulose. She presented a map of particle size as a function of reactor temperature to identify the transition from a kinetically to a heat transfer controlled conversion and from fast to slow pyrolysis. The results show that larger tar yields can be obtained from smaller particles since the thermally thin and the kinetic regimes are approached. Lu et al. [62] showed both particle shape and size can affect the product yield of biomass devolatilization. They found that almost spherical particles exhibit lower volatile and higher tar yield relative to ideally spherical particles with the same mass. Their results also indicate that for each particle shape, volatile yields decrease with increasing particle size.

In order to optimize the whole reactor, a good knowledge of all the chemical and physical phenomena inside the bed is necessary. Unlike single particle models, just few models of fixed-bed pyrolysis have been reported in literature [36, 13, 12, 63].

Wurzenberger et al. [11] have proposed a bed model using representative particle in each CFD cell. This model includes one-dimensional model for the gas phase and one-dimensional model for the representative particle. No comparison with experiment has been reported in this work, however Anca-Couce et al. [12] have later used this method for simulation of pyrolysis in a packed bed, which was showing promising result compared to the experiments. The main purpose of using this model was to have faster solver compared to other more accurate models like DPM [15]. Mandl et al. [36] also used this one-dimensional approach for modeling of an updraft fixed-bed gasifier. Since shrinkage of particle due to char oxidation is not negligible, they have considered movement of particles within the bed as well. Umeki et al. [63] used a one-dimensional model in the same way and considered uniform porosity along the bed to simulate an updraft biomass gasifier with high temperature steam.

A literature review indicates that in many of the packed bed studies, one-dimensional (1D-1D) or representative approaches have been used. Although it is a viable model especially from CPU time point of view, it cannot describe the interaction between the particles well. The latter will affect the overall accuracy of simulation, which could be a possible reason

of diverging from experiment. The objective of this chapter is to develop the proposed model in previous chapter by considering devolatilization of biomass material in a packed bed

3.2 Mathematical model

A wet wood particle in a packed bed which is subjected to a hot inlet inert gas (for example N2) experiences heat up, drying and pyrolysis. The most important part of a drying model is calculating the evaporation rate. Several models have been reported in the literature that either come from experimental correlations or theory and physics of evaporation. More common drying models are categorized as follows: heat sink model [1, 13], first order kinetic evaporation rate [36] and equilibrium model [11]. A *heat sink model* (or constant evaporation model) is based on the assumption that drying occurs at fixed boiling temperature. For this approach, heat available above the boiling temperature is consumed by evaporation without distinguishing between bound and free water. A *first order of kinetic model* is a heterogeneous reaction according to the Arrhenius equation for free and bounded water. In this approach water evaporates below the evaporation temperature. An *equilibrium model* is based on the hypothesis that water vapor is in equilibrium with the liquid and the bound water. Therefore the partial pressure of water vapor is fixed by the saturation pressure [28]. In this work heat sink model is chosen to calculate the drying rate as defined in Eq. (3.2.1).

$$\dot{w}_{H_2O} = \begin{cases} \frac{(T - Tevap)\rho\, c_p}{H_{evap}\, \delta t} & \text{if} \quad T \geq T_{evap} \\ 0 & \text{if} \quad T \leq T_{evap} \end{cases} \tag{3.2.1}$$

Devolatilization or pyrolysis occurs during heating up of raw biomass in absence of an oxidizer up to a certain temperature. This leads to decomposition of the biomass into char and volatiles. The latter escapes from the particle by advection and diffusion. Two models are used in this work to describe the devolatilization of wood particles, *one step global model* and *three parallel reactions*.

One step global model is given in Eq (3.2.2); and the reaction rates are formulated in terms of an Arrhenius type equation, Eq (3.2.3).

$$\begin{aligned} Wood \rightarrow \nu_c\, Char + \nu_t\, Tar + \nu_{CO}\, CO + \nu_{CO_2}\, CO_2 + \nu_{H_2O}\, H_2O \\ + \nu_{H_2}\, H_2 + \nu_{CH_4}\, CH_4 \end{aligned} \tag{3.2.2}$$

$$\dot{w}_{wood} = k_0 e^{\frac{-E_a}{RT}} \rho_{wood} \tag{3.2.3}$$

Where ν_i are the mass fractions for the above reaction ($i = CO$, CO_2, CH_4, H_2, H_2O, Tar, $Char$) and are taken from Blasi [2] and listed in Table 3.2.1. Peters et al. [28] showed that for a global reaction model, the kinetic data taken from Balci et al. [64] would allow an more accurate prediction of the particles decomposition rate compared to other existing models in the literature. The value for K_0 and E_a are $1.35 \times 10^9\ s^{-1}$ and 123100 J/mol taken from Balci et al. [64]. In this model, pyrolysis is considered as an endothermic process and the heat of reaction is taken from Blasi [60] with $\triangle h = 418\ kJ/kg$. Tar cracking is neglected in pyrolysis modeling because of low temperature gradient within the particle, which is shown in the result section.

Table 3.2.1: Product mass fraction (wt%, d.b) of the pyrolysis reaction [2].

Char	Tar	CO	CO2	H2O	H2	CH4
0.255	0.48	0.045	0.1	0.115	0.002	0.003

In **three parallel reactions model**, the pyrolysis is described with three independent reactions expressing decomposition of wood to its main products (char, tar and gas), as given in Eq (3.2.4, 3.2.5, 3.2.6).

$$Wood \rightarrow Char \tag{3.2.4}$$

$$Wood \rightarrow Tar \tag{3.2.5}$$

$$Wood \rightarrow \nu_{CO}\, CO + \nu_{CO_2}\, CO_2 + \nu_{H_2O}\, H_2O + \nu_{H_2}\, H_2 + \nu_{CH_4}\, CH_4 \tag{3.2.6}$$

Where ν_i are the mass fractions for the above reactions ($i = CO$, CO_2, CH_4, H_2, H_2O), taken from [65] which are listed in Table 3.2.2.

Table 3.2.2: Product mass fraction of the pyrolysis reactions.

	CO	CO2	H2O	H2	CH4
ν_i [65]	0.156	0.271	0.521	0.021	0.031

During conversion of the biomass, wood particles experience both slow and fast pyrolysis. For example particles close to the inlet port of the hot gas experience high rate of heat input, therefore fast pyrolysis occurs for these particles. However inlet gas reaches with the lower temperature to the particles far away in downstream, thus less heat input causes slow pyrolysis. Therefore a particle may experience both fast and slow pyrolysis during one experiment. Hence, in order to have precise prediction, kinetic data should be able to

describe both fast and slow pyrolysis. Haseli et al. [59] showed the kinetic data presented by Blasi and Branca [53], allows accurate prediction in fast pyrolysis. Therefore in the present work, the kinetic data of Blasi is used for the fast pyrolysis and the kinetic data proposed by Chan et al. [37] is used for the slow pyrolysis. The rate expression and the kinetic data of these reactions are listed in Table 3.2.3 and 3.2.4 respectively.

Table 3.2.3: Rate expressions

reaction number	rate expression
	$K_i = A_i exp(Ei/RT)$
3.2.4	$\frac{\partial \rho_B}{\partial t} = K_{3.2.4}\rho_B$
3.2.5	$\frac{\partial \rho_B}{\partial t} = K_{3.2.5}\rho_B$
3.2.6	$\frac{\partial \rho_B}{\partial t} = K_{3.2.6}\rho_B$

Table 3.2.4: Kinetic data

reaction number	A $(1/s)$	E (kJ/mol)	ref
3.2.4	3.27×10^6	111.7	[53]
	1.08×10^7	121	[37]
3.2.5	1.08×10^{10}	148	[53]
	2×10^8	133	[37]
3.2.6	4.38×10^9	152.7	[53]
	1.3×10^8	140	[37]

A literature survey indicates, most of the conducted researches assumed pyrolysis to be an endothermic reaction, as it was already mentioned in introduction. In contrast some other researcher assumed it as an exothermic process. Rath et al. [56] reported the heat of pyrolysis versus final char yield. The results indicated the strong dependency of the heat of pyrolysis on the final char yield. The possible explanation for this behavior is an exothermic char formation and endothermic volatile formation [56]. Therefore, the amount of char formation determines the total heat of pyrolysis. Different values for heat of formation of char and volatiles are reported by Milosavljevic et al. [66], Mok et al. [67] and Rath et al. [56]. The mentioned studies indicate the dependency of heat of pyrolysis on the wood properties and the conditions used in the measurements. Therefore in this model the value of the heat of reaction for char and volatiles formation are selected in the same order of magnitude as reported in the literature, in a way to get the best agreement with several measurements of different researchers. Hence $-1800\ kJ/kg$ and $842\ kJ/kg$ are used as heat of formation of char and volatiles, respectively.

For modeling of solid particles the following assumptions have been made:

- Gas phase species are ideal gas

- Particles are assumed as isotropic material and the properties change along the radius (for sphere particles)
- Solid and gas (inside the particle) are in local thermal equilibrium

The distribution of temperature and species within the particles are accounted for by a system of one-dimensional and transient conservation equations [15, 42]. Model equations are listed in Table 3.2.5.

Table 3.2.5: Particle equations

- Mass conservation

$$\frac{\partial}{\partial t}\left(\epsilon_f \langle\rho_f\rangle^f\right) + \vec{\nabla}\cdot\left(\epsilon_f \langle\rho_f\rangle^f \langle\vec{v}_f\rangle^f\right) = \dot{m}'''_{s,f} \tag{3.2.7}$$

- Momentum conservation

$$-\frac{\partial(\epsilon_f p)}{\partial x} = \frac{\mu_f \epsilon_f}{K^*}\langle\vec{v}_f\rangle \tag{3.2.8}$$

- Energy equation

$$\frac{\partial \langle\rho c_p T\rangle}{\partial t} = \frac{1}{r^n}\frac{\partial}{\partial r}\left(r^n \lambda_{\text{eff}}\frac{\partial \langle T\rangle}{\partial r}\right) + \sum_{k=1}^{l}\dot{\omega}_k H_k \tag{3.2.9}$$

- Species equation

$$\frac{\partial}{\partial t}\left(\epsilon_f\langle\rho_{f,i}\rangle^f\right) + \nabla\cdot\left(\epsilon_f\langle\rho_{f,i}\rangle^f\cdot\langle\vec{v}_f\rangle^f\right) = \frac{1}{r^n}\frac{\partial}{\partial r}\left(r^n\epsilon_f D\frac{\partial\langle\rho_{f,i}\rangle}{\partial r}\right) + \dot{m}'''_{s,f,i} \tag{3.2.10}$$

- Boundary condition

$$-\lambda_{\text{eff}}\frac{\partial\langle T\rangle}{\partial r}\bigg|_{r=0} = 0 \tag{3.2.11}$$

$$-\lambda_{\text{eff}}\frac{\partial\langle T\rangle}{\partial r}\bigg|_{r=R} = \alpha(T_R - T_\infty) + \dot{q}''_{\text{rad}} + \dot{q}''_{\text{cond}} \tag{3.2.12}$$

$$-D_{\text{i,eff}}\frac{\partial\langle\rho_i\rangle}{\partial r}\bigg|_{r=R} = \beta_i(\rho_{i,R} - \rho_{i,\infty}) \tag{3.2.13}$$

In the present coupling model the heat interaction between particles (conduction, radiation) and also heat and mass transfer between particles and their environment (con-

duction, convection) is resolved with above mentioned XDEM, whereas the continuous phases are solved with a CFD tool. Thermal energy and mass are transferred from fluid to particles and/or particles to fluid as heat source and mass source respectively. The heat source and mass source values are evaluated according to the particle properties within a specific CFD cell.

Packed beds may be treated as a porous media in which fluid flow behaves like an external flow. The flow may be accurately described for a continuum approach by averaging relevant variables and parameters on a coarser level. Although the solid particles are considered as a separate phase, fluid flow in the bed is treated as one homogeneous continuum. For this reason macroscopic governing equations are obtained from the corresponding microscopic equations through an averaging process over a representative elementary volume (REV) [47, 48]. These equations are listed in Table 3.2.6. The gas phase is modeled in an Eulerian approach with a variant of Navier Stokes equations for compressible fluid in porous media and implemented in OpenFoam.

Table 3.2.6: Coupling equations

- Continuity equation

$$\frac{\partial}{\partial t}\left(\epsilon_f \langle\rho_f\rangle^f\right) + \vec{\nabla}\cdot\left(\epsilon_f \langle\rho_f\rangle^f \langle\vec{v}_f\rangle^f\right) = \dot{m}'''_{s,f} \tag{3.2.14}$$

- Momentum Equation

$$\frac{\partial}{\partial t}\left(\epsilon_f \langle\rho_f\rangle^f \langle\vec{v}_f\rangle^f\right) + \vec{\nabla}\cdot\left(\epsilon_f \langle\rho_f\rangle^f \langle\vec{v}_f\vec{v}_f\rangle^f\right) = \vec{\nabla}\cdot\left(\epsilon_f \langle\vec{\tau}'_f\rangle^f\right) - \frac{\mu_f}{K}\epsilon_f^2 \langle\vec{v}_f\rangle^f - C\langle\rho_f\rangle^f \epsilon_f^3 |\langle\vec{v}_f\rangle^f| \langle\vec{v}_f\rangle^f \tag{3.2.15}$$

$$K = \frac{D_P^2 \epsilon_f^3}{150(1-\epsilon_f)^2} \tag{3.2.16}$$

$$C = \frac{1.75(1-\epsilon_f)}{D_P \epsilon_f^3} \tag{3.2.17}$$

- Energy equation

$$\frac{\partial}{\partial t}\left(\epsilon_f \langle\rho_f\rangle^f \langle h_f\rangle^f\right) + \left(\epsilon_f \langle\rho_f\rangle^f \langle\vec{v}_f h_f\rangle^f\right) = \frac{\partial\langle p_f\rangle}{\partial t} + \epsilon_f \cdot \langle\vec{v}_f\rangle^f \cdot \vec{\nabla}\langle p_f\rangle + q'''_{s,f} \tag{3.2.18}$$

- Species equation

$$\frac{\partial}{\partial t}\left(\epsilon_f \langle\rho_{f,i}\rangle^f\right) + \nabla\cdot\left(\epsilon_f \langle\rho_{f,i}\rangle^f \cdot \langle V_f\rangle^f\right) = \sum_{i=1}^{M} m'''_{s,f,i} \tag{3.2.19}$$

3.3 Validation

In order to validate the numerical model, the prediction results are compared with several experimental data for both the single particle and the packed bed. It should be noted that in single particle validation only the second pyrolysis model (three parallel reactions) is used, while in the packed bed validation both pyrolysis models are used and the results are presented and discussed in the results section.

3.3.1 Single particle validation

Gronli et al. [5] used a cylindrical spruce particle ($D = 20\ mm$, $L = 30\ mm$) which absorbs heat flux from the top surface. Temperature at different depth of the particle was measured for two different heat fluxes (80 kW/m^2 and 130 kW/m^2). Figure 3.3.1 shows the comparison of the particle temperature at different depths between measurements and predictions. As it can be seen in fig 3.3.1, in order to indicate the reproducibility of the experiments, the temperature at each position has been presented as an area (the area between upper and lower value). Good agreements between measurements and predicted results are observed for both high and low heat fluxes.

Lu et al. [6] did series of experiments on devolatilization of poplar particles for two regular shapes; near-sphere ($D = 9.5\ mm$) and cylinder ($D = 9.5\ mm$ and $L/D = 4$). Gas temperature around the particle and the average wall temperature of the reactor have the measured value of 1050 K and 1276 K which were assumed to be constant during the experiment. The experiments have been done for two initial moisture contents (6.0 wt% and 40.0 wt%), while in each case the mass loss, the surface and the center temperature of the particle have been measured. The comparison between predicted results and measurements are presented in fig 3.3.2, 3.3.3, 3.3.4 and 3.3.5. It should be noted that experimental data presented in fig 3.3.3 are taken from [68] for the same experimental set-up as used by [6].

In this experiment, in order to determine the thermocouple lead wire impact on the measured center temperature, two thermocouples monitored the center temperature, one passing axially and a second passing radially through the particle [6]. Compared to the radial thermocouple, the axial thermocouple is less impacted by heat conduction through the leads since the particle provides some insulation from the radiation and buoyancy-driven bulk-flow convection. Hence the center temperature measured by the radial thermocouple increases much faster than that of measured in the axial thermocouple [6]. This can be observed in fig 3.3.4 and 3.3.5. This can explain the deviation of the

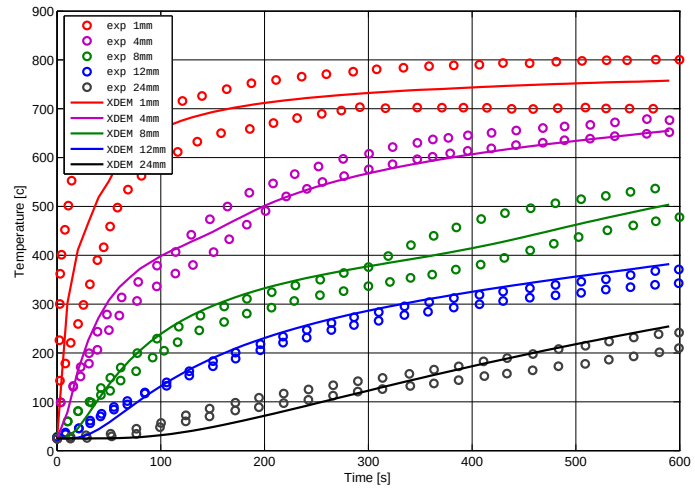

(a)

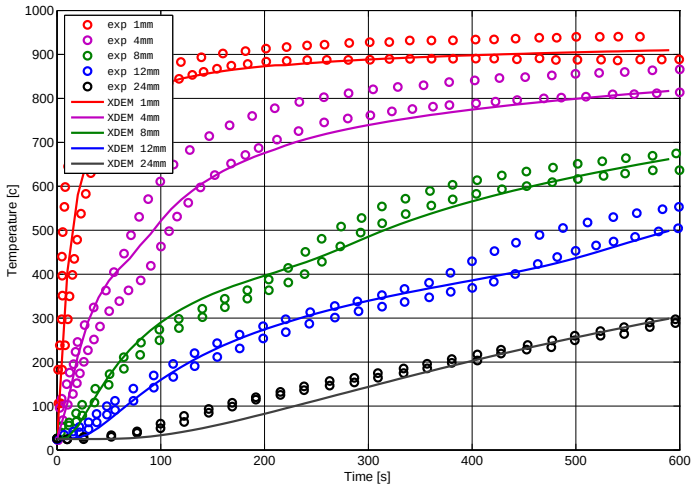

(b)

Figure 3.3.1: Comparison of predicted temperature with measurement [5] for heat flux of a) 80 kW/m^2 (top) and b) 130 kW/m^2 .

predicted center temperature from the measured value for the near-spherical particle (fig 3.3.2 and 3.3.3).

Several experiments have been done by Petek [7] on a single spherical particle to measure conversion characteristics of beech wood and spruce wood at different heating conditions. In the present work, the predicted results are compared with measurements don by Petek for a particle with a diameter of 20 mm and the ambient temperature of 1123 K and 1223 K for beech wood and spruce wood respectively. Figure 3.3.6 and 3.3.7 show good agreements between predicted results and experimental data for both temperature and mass loss.

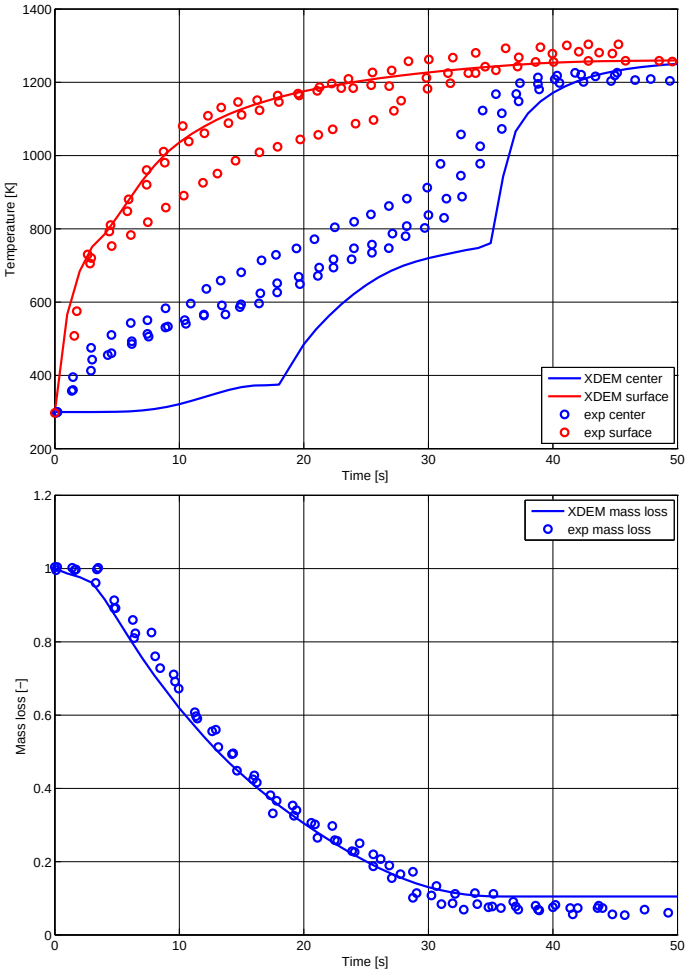

Figure 3.3.2: Comparison of predicted temperature and mass loss with measurement [6], for near-spherical poplar particle with 6.0 wt% moisture content.

3.3.2 Packed-bed validation

In order to validate the numerical model and verify the accuracy of the simulation, the predicted results are compared with experimental data measured by Peters et al. [3]. The experimental reactor shown in Fig. 2.3.1 was considered to investigate heating up, drying and pyrolysis of particles in packed beds. It consists of an outer steel cylinder designed for a maximum temperature of $T = 800\ ^oC$ and a maximum pressure of p = 2 bar. The packed bed is filled into a cylindrical basket, which is positioned in the interior of the reactor. The reactor is 250 mm in diameter and can be filled by solid particles up to 190 mm in height. A rod connects the basket containing the packed bed to a load cell. While the fuel bed is heated, the reaction chamber rests on a metal seat. In order to record mass losses due to evaporation and pyrolysis, the gas flow is turned off and the reaction tube is lifted via an electrical motor, which is connected with the load cell. Afterwards the reaction tube is reinstalled in its previous position and the gas flow is turned on again. By adjusting the intervals of the weight measurements appropriately, a mass loss history for

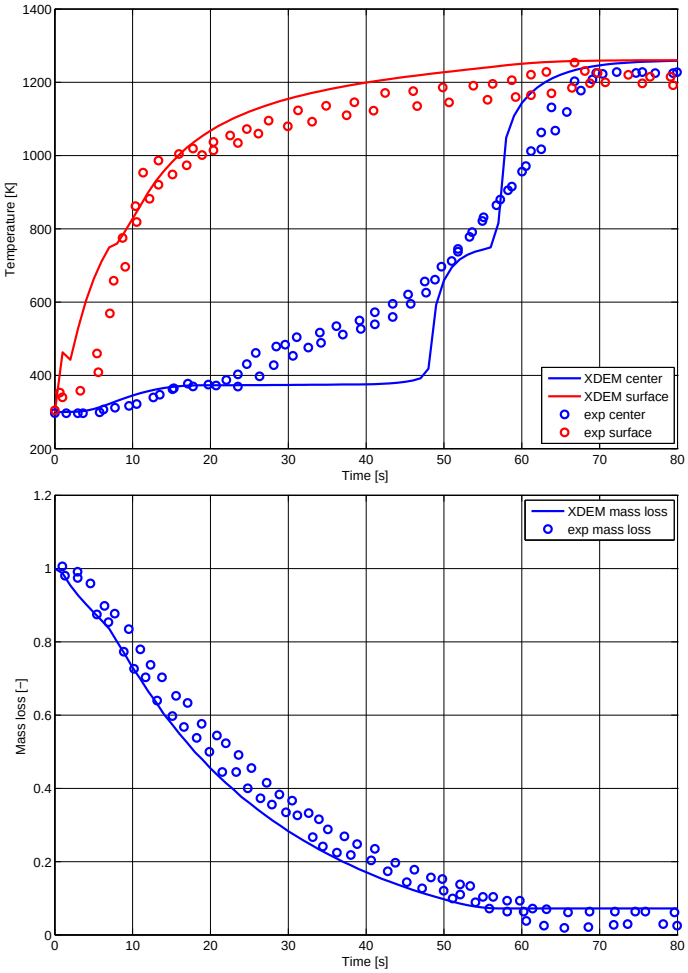

Figure 3.3.3: Comparison of predicted temperature and mass loss with measurement [6], for near-spherical poplar particle with 40.0 wt% moisture content.

the packed bed due to evaporation and devolatilization is produced. The bed is heated by a flow of hot gas entering from top of the container and passed through the reaction tube from top to bottom. More details about the experimental setup is given in [3]. The pyrolysis experiments were carried out with 2 kg of air-dried cube of beech wood $10 \times 10 \times 10\ mm^3$ in size. The moisture content of particles is approximately 8% of dry mass. The relevant properties of the beech wood are listed in Table. 2.3.1 [3]. When the reaction tube has been filled with the particles, the steel containment is closed and the bed is preheated to approximately $T = 90\ ^oC$. A flux of heated nitrogen ($\dot{m}_{N_2} = 16\ kg\ h^{-1}$) as an inert gas streamed through the packed bed. Due to the thermal capacity of the test facility the temperature of incoming gas stream approaches its steady state value after a certain period, whereby the evolution of the temperature follows an exponential relation of following form:

$$T_{in} = T_{dry} - \Delta T e^{\gamma t} \tag{3.3.1}$$

where T_{dry}, ΔT, γ and t stand for the steady state drying temperature, the relevant temperature difference and the time constant and time, respectively. The value for the three different inlet temperatures are given in Table. 3.3.1.

Table 3.3.1: Specification of inlet temperature [3].

Inlet temperature (°C)	ΔT (°C)	γ (1 s^{-1})
530	510	-0.001
500	480	-0.001
385	365	-0.001

According to the experimental setup, the simulation model is prepared as shown in Fig. 3.3.8. In the simulation instead of using cubic particles, spherical particles with equal volume (weight) are used as a simplification. Thus the container is filled with 2667 particles randomly and the height of bed reaches to about 100 mm, same as in the experiment. It should be noted that the computational domain of the reactor is extended

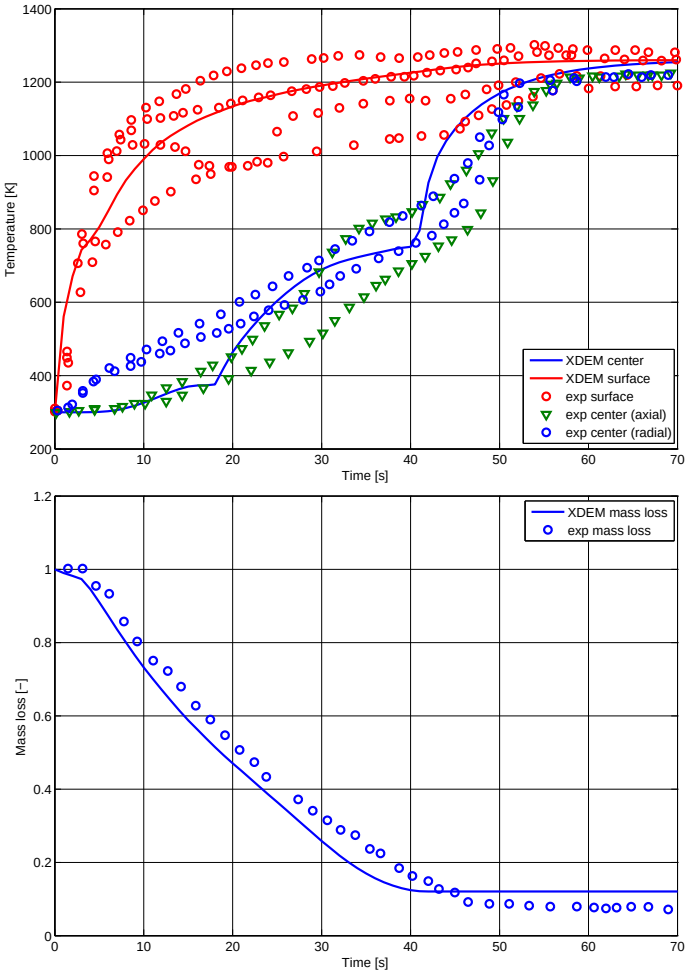

Figure 3.3.4: Comparison of predicted temperature and mass loss with measurement [6], for cylindrical poplar particle with $L/D = 4$ and 6.0 wt% moisture content.

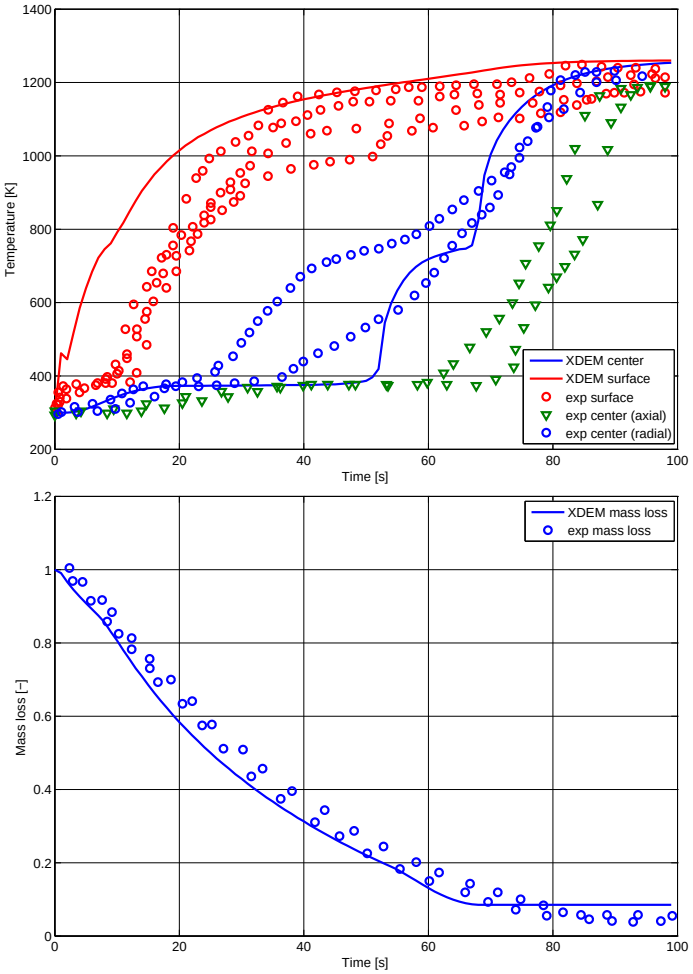

Figure 3.3.5: Comparison of predicted temperature and mass loss with measurement [6], for cylindrical poplar particle with $L/D = 4$ and 40.0 wt% moisture content.

at the top and bottom by 8 and 6 cm respectively, as shown in Fig. 3.3.8.

Fig. 3.3.9 and 3.3.10 present mass loss of bed due to drying and pyrolysis of wood particles at different inlet temperatures for both experiment and simulation with two pyrolysis models. A good agreement for both models between measurement and numerical predictions for a wide range of inlet temperatures has been achieved. This proves that the proposed numerical model can predict accurately drying and pyrolysis of packed bed of wood particles.

3.4 Results and Discussion

Fig. 3.4.1 depicts gas temperature and the mean temperature of particles when inlet temperature is set to 803 K. In order to reveal the state inside the reactor, half of the gas phase has been plotted. It should be noted that a non-unique legend has been used for

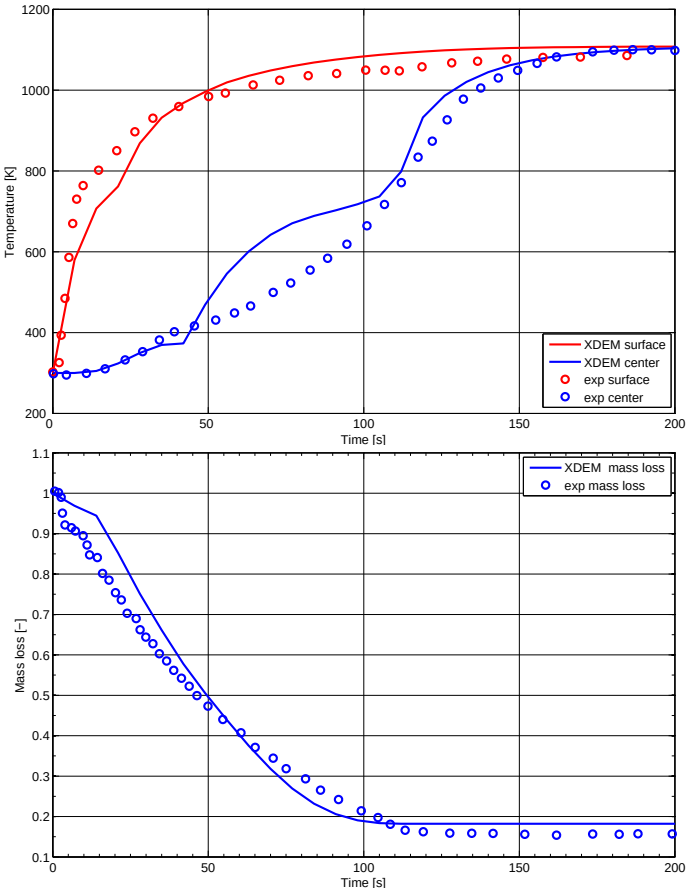

Figure 3.3.6: Comparison of predicted temperature and mass loss with measurement [7], for beech wood particle with $d = 20mm$ and ambient temperature of 1123 K.

different times to illustrate better the temperature distribution in both gas phase and solid particles. Thermal energy of injected gas is transferred to the wood particles by forced convection. The absorbed heat by particles also can be transferred to other particles either by conduction or radiation. As explained above, according to the experiment, at the beginning the inlet temperature is lower than initial temperature of particles in the container, then during the initial stage the inlet gas cools down the bed. It can be seen that the mean temperature of particles decreases from top to bottom at $t = 100\ s$. But at $t = 1000\ s$ all the particles are heated up by injected gas. This transient from cooling to heating of the particle by the inlet gas flow is more clear at $t = 250\ s$. As it will be shown in figure 3.4.2 at $t = 4000\ s$ the pyrolysis already finished but still there is a small temperature gradient in the bed showing the produced char is still heated up to reach the inlet gas temperature.

Conversion of the particles and also the tar yield is depicted in figure 3.4.2. Since it is intended to present species distribution inside the reactor, similar to Fig. 3.4.1, a portion of the gas phase has been shown. Moreover, half of the particles have been shown in this figure to illustrate reaction front within the bed. By increasing the temperature in the bed

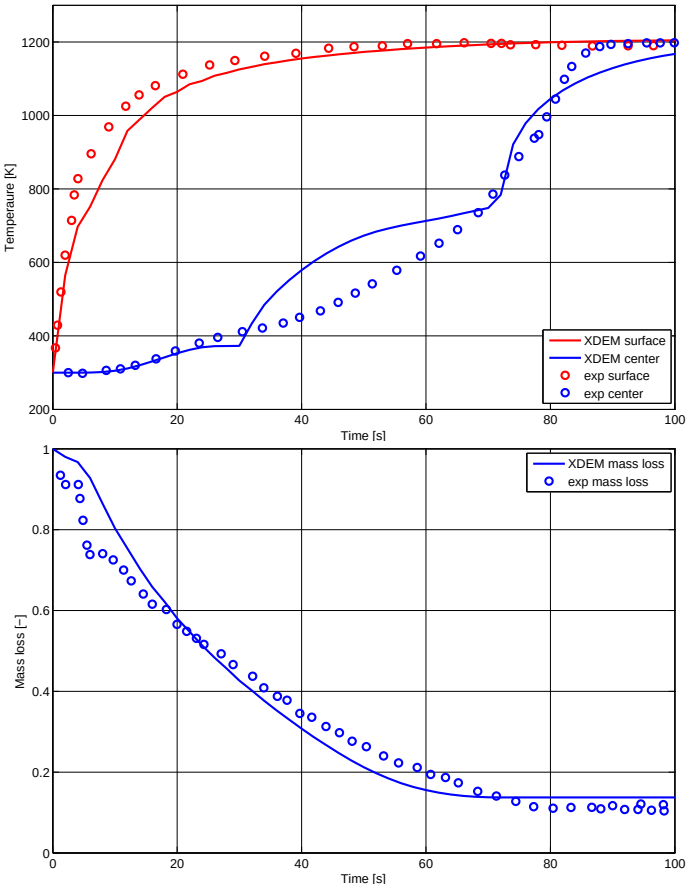

Figure 3.3.7: Comparison of predicted temperature and mass loss with measurement [7], for spruce wood particle with $d = 20mm$ and ambient temperature of 1223 K.

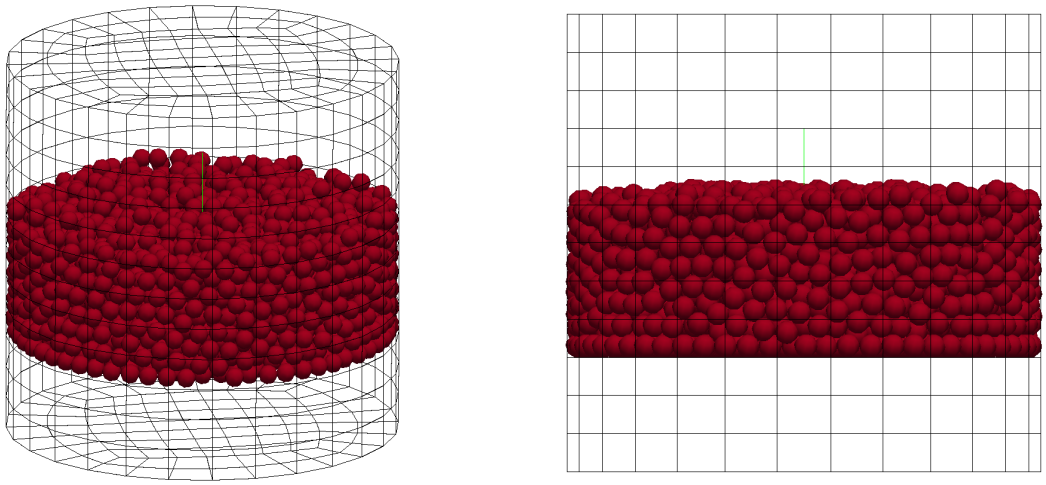

Figure 3.3.8: Problem geometry

from top to bottom as shown in previous figure, the conversion of the wood particles also starts from top. At $t = 1000$ s few particles on the top of the bed start decomposing, and

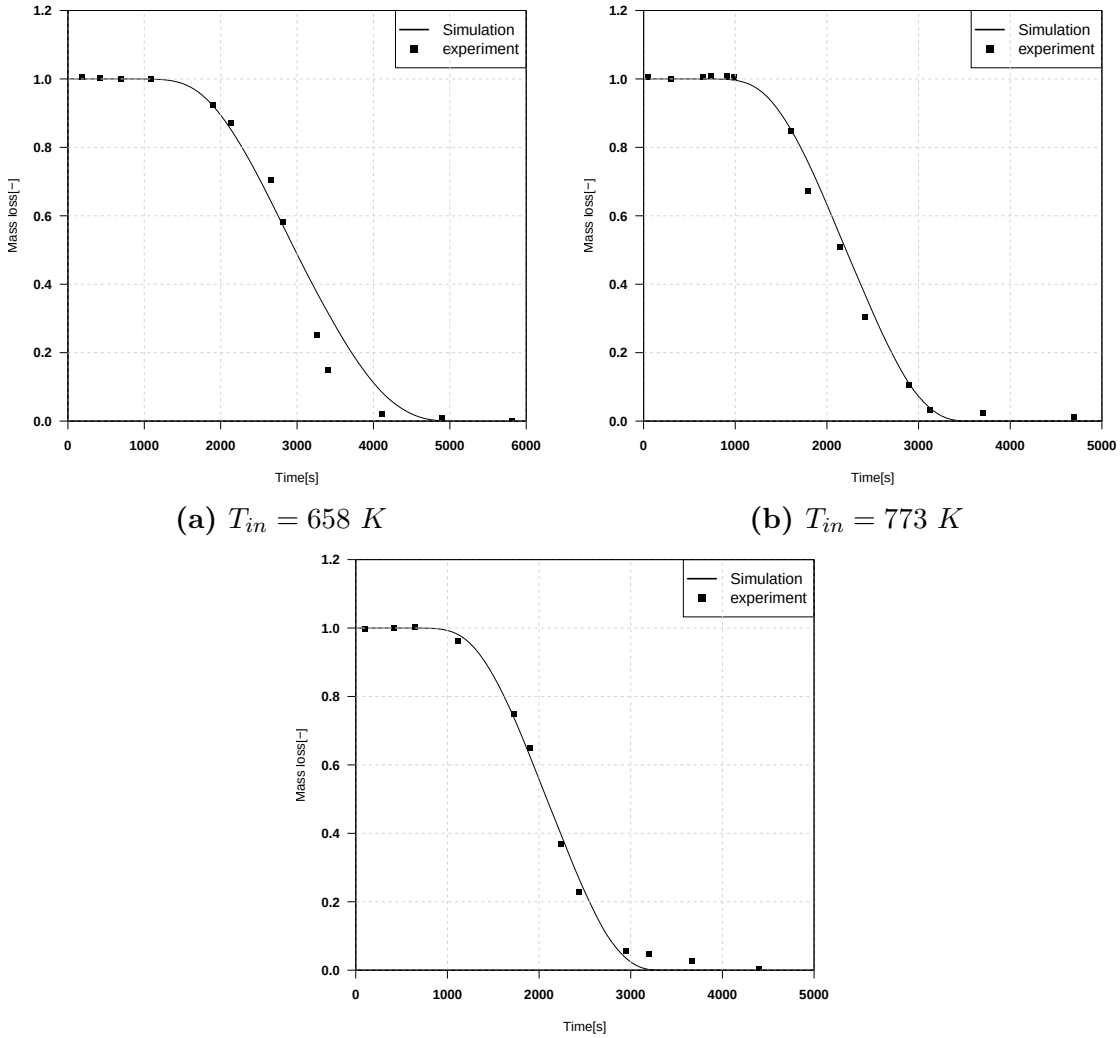

(a) $T_{in} = 658\ K$

(b) $T_{in} = 773\ K$

(c) $T_{in} = 803\ K$

Figure 3.3.9: Comparison of predicted mass loss with measurement [3] at different inlet temperature (using *One step global model*).

therefore a small amount of tar appears in the gas phase. As time proceeds more particles decompose and more tar is produced and transferred to the gas phase. At $t = 2000\ s$ the amount of tar in the gas phase is 7 times higher than that of $t = 1000\ s$. Mass flow rate in the region close to the reactor wall is higher which is due to the higher porosity in this region (see figure 3.4.3). For this reason intensive heat and mass transfer between particles and gas phase near the reactor wall occurs, creating higher tar mass fraction near the wall at the initial stage ($t = 1000\ s$) (see figure 3.4.2). As time proceeds there is more unconverted wood far from the wall, since the particle near the wall converted more compared to other particles, meaning more tar can be produced at the center of the reactor. This can be observed at $t = 2000\ s$. At $t = 3000\ s$ most of the particles have already decomposed completely and just few of them still have some virgin material to decompose; these particles are located mostly at the bottom of the bed and also at locations where the porosity is lower e.g center of reactor. Therefore only at that region

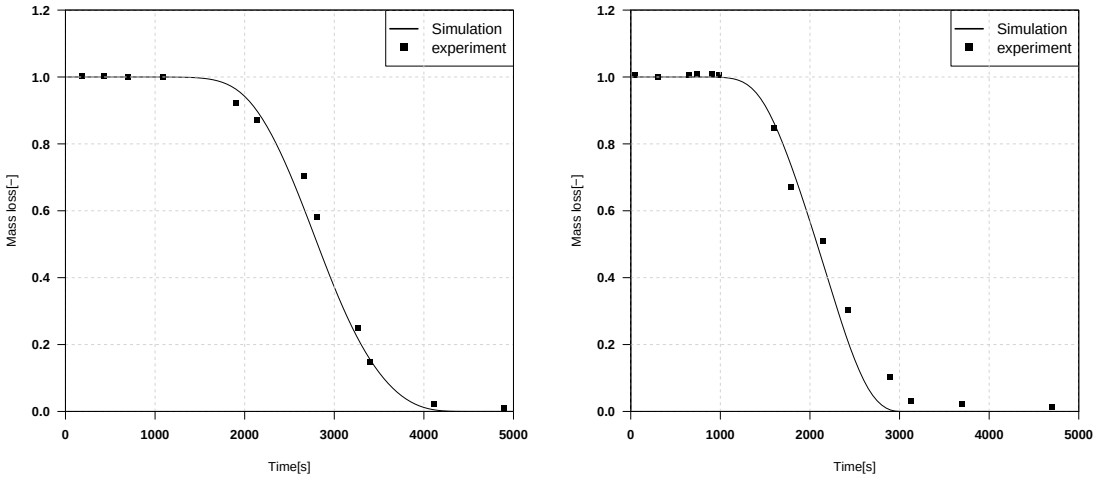

(a) $t_{inlet} = 658\ K$ **(b)** $t_{inlet} = 773\ K$

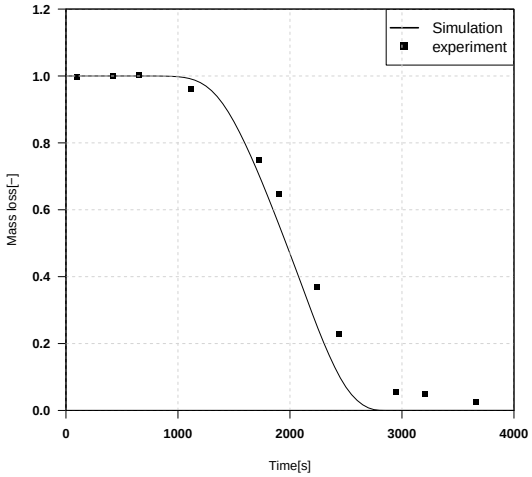

(c) $t_{inlet} = 803\ K$

Figure 3.3.10: Comparison of predicted mass loss with measurement [1], for packed-bed of 2 kg beech wood at different inlet temperature (using *three parallel reactions model*).

some amount of tar can be found in the gas phase.

Fig 3.4.4 and 3.4.5 illustrate the char formation and particle porosity respectively at different times. Due to the pyrolysis, the wood particles are converted into charred material with a higher porosity. Figure 3.4.5 shows that after 1000 seconds the porosity of particles increases from an initial value of 0.55 to 0.67, except for the particles at the bottom of the bed. But according to figure 3.4.2, at $t = 1000\ s$ pyrolysis can be observed just in few particles at the top of the bed. Therefore it is expected that only in those particles porosity changes. Then it can be concluded that the increase of porosity at the initial times is not due to the pyrolysis. These phenomena can be explained by evaporation of the particles' water content which initially has filled the pores of the particles. At the end of pyrolysis, when all particles are converted to char, porosity within the particles reaches to 0.76 which is about 38% higher than initial porosity. As can be seen in figures 3.4.4

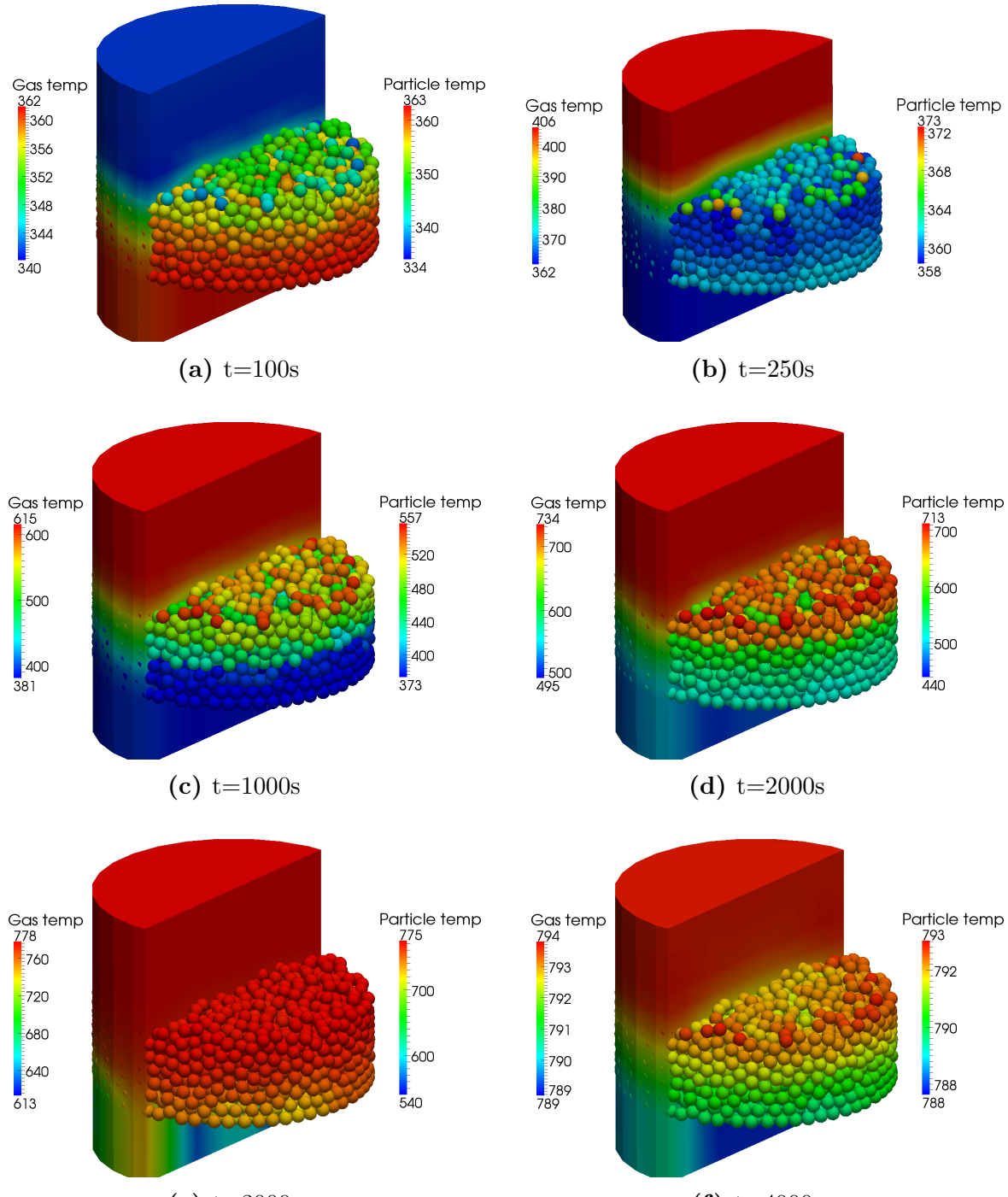

Figure 3.4.1: Gas temperature and mean temperature of particles at different times

and 3.4.5, the char formation and porosity increase follow the same process. This is due to the fact that the reaction front starts from the top of the bed and moves down.

Figure 3.4.6 presents the variation of the gas temperature and CO_2 concentration in the gas phase over time. These gas properties are determined for the central axis of the bed at different heights. As it was explained before, initial decline in the gas temperature

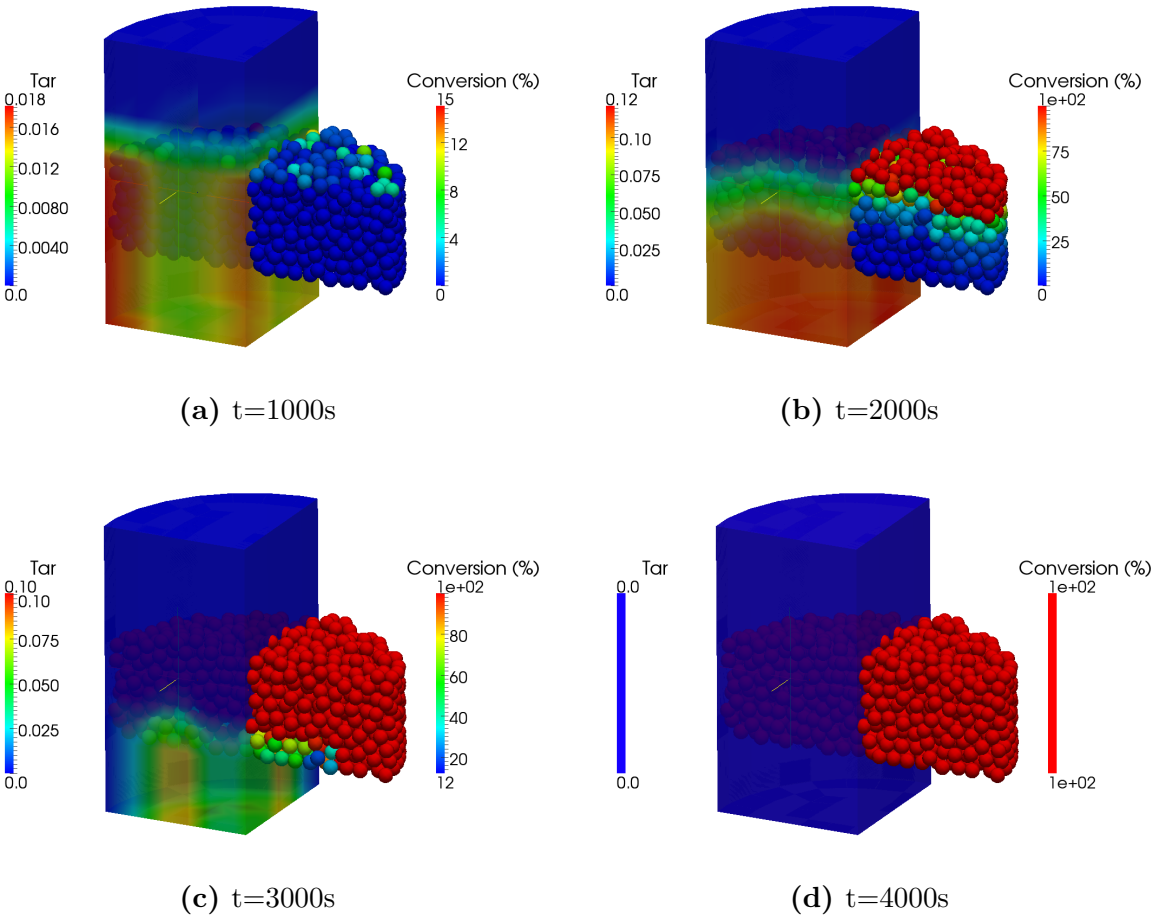

(a) t=1000s **(b)** t=2000s

(c) t=3000s **(d)** t=4000s

Figure 3.4.2: Mass fraction of tar and particle conversion at different times

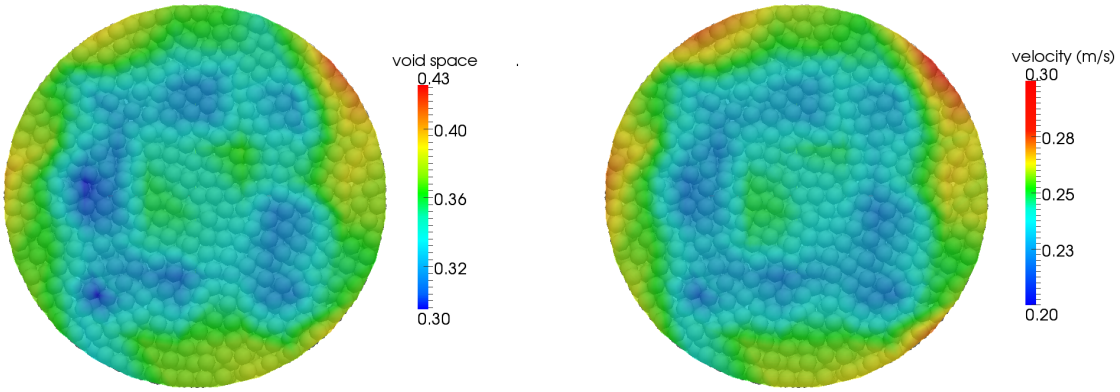

(a) void space **(b)** velocity

Figure 3.4.3: void space of bed and gas velocity at the cross section of reactor

occurs due to the fact that initially the inlet gas temperature is lower than the initial bed temperature. After this stage, gas temperature increases up to 373 K and then it flattens because of the evaporation of the particles' moisture. When particles have finished

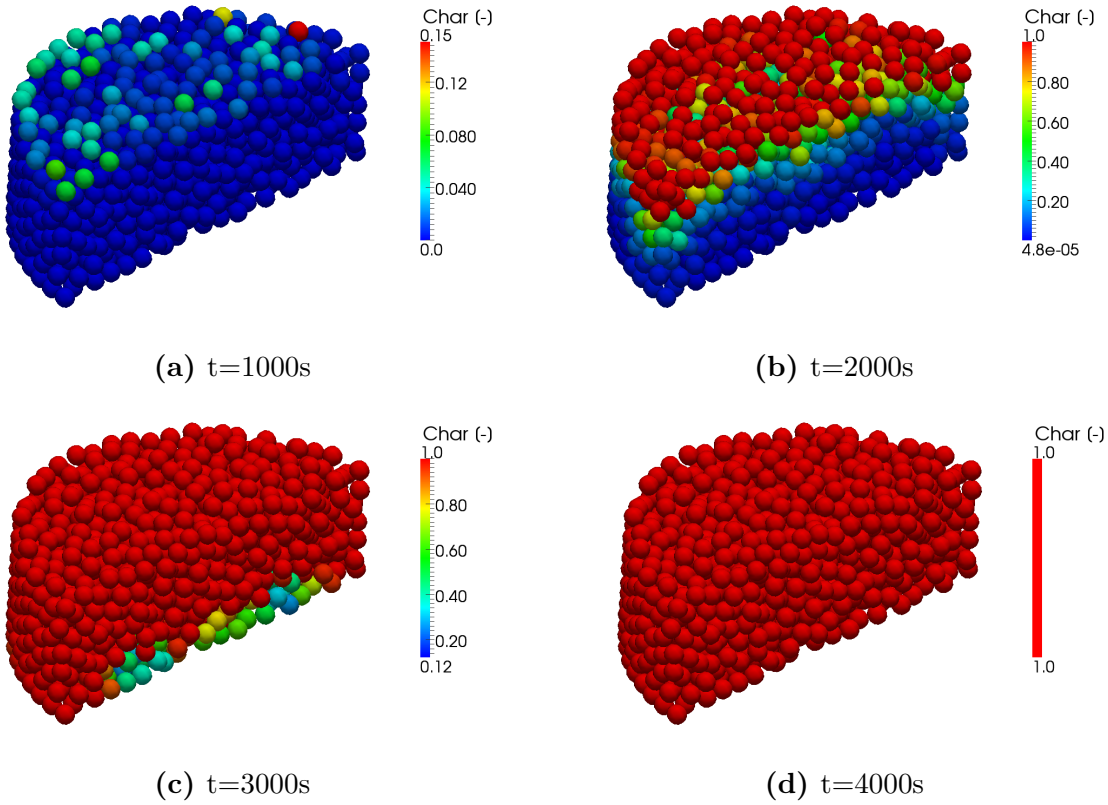

(a) t=1000s **(b)** t=2000s

(c) t=3000s **(d)** t=4000s

Figure 3.4.4: Char formation at different times

drying, the temperature increases more sharply until the pyrolysis in the particles starts. Since the pyrolysis is an endothermic reaction, the particles use the thermal energy of the gas phase for decomposition resulting in a slope change of the temperature curve. When the particles converted completely to the charred material, the gas temperature initially follows an exponential growth with a rapid increase and approaches the inlet gas temperature. At different heights inside the bed the CO_2 content is determined by two factors: locally produce due to pyrolysis of particle and mass transfer from upstream. However CO_2 content of a specific height diminishes by finishing devolatilisation of the particle close to that region. A peak value in curve of CO_2 mass fraction is observed when particles at given height produce more CO_2, or generally volatiles, as a result of higher rate of pyrolysis. This peak corresponds to the second flatten area in the gas temperature curve as it was explained above.

Since in *XDEM* all reactions and governing equations are solved for all particles in the bed, any particle in the bed can be chosen and looked at history to investigate it. Figure 3.4.7 represents the mean temperature and the mass loss of five particles along the center line of the reactor at different heights for two different inlet temperatures. After a small reduction in the particle temperature, for the reasons explained above, the particle temperature increases and then remains constant for a period of time due to drying. This period is corresponding to the first reduction in the mass loss curve (figure 3.4.7b and 3.4.7d).

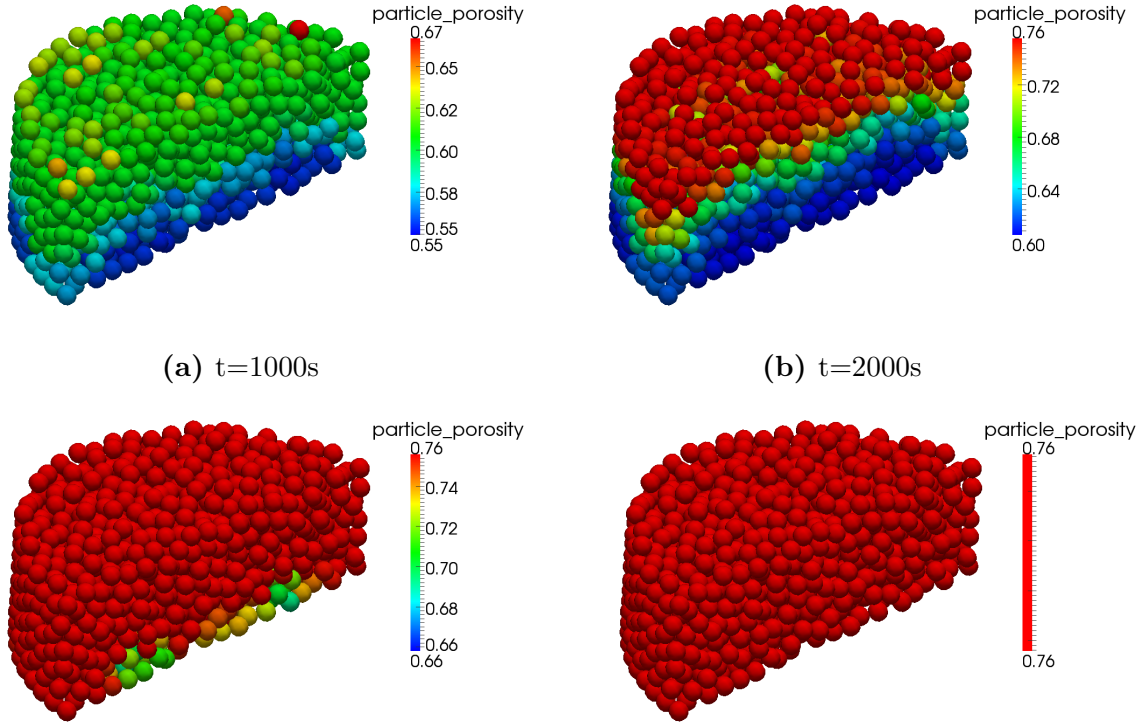

(a) t=1000s **(b)** t=2000s

(c) t=3000s **(d)** t=4000s

Figure 3.4.5: Particle porosity at different times

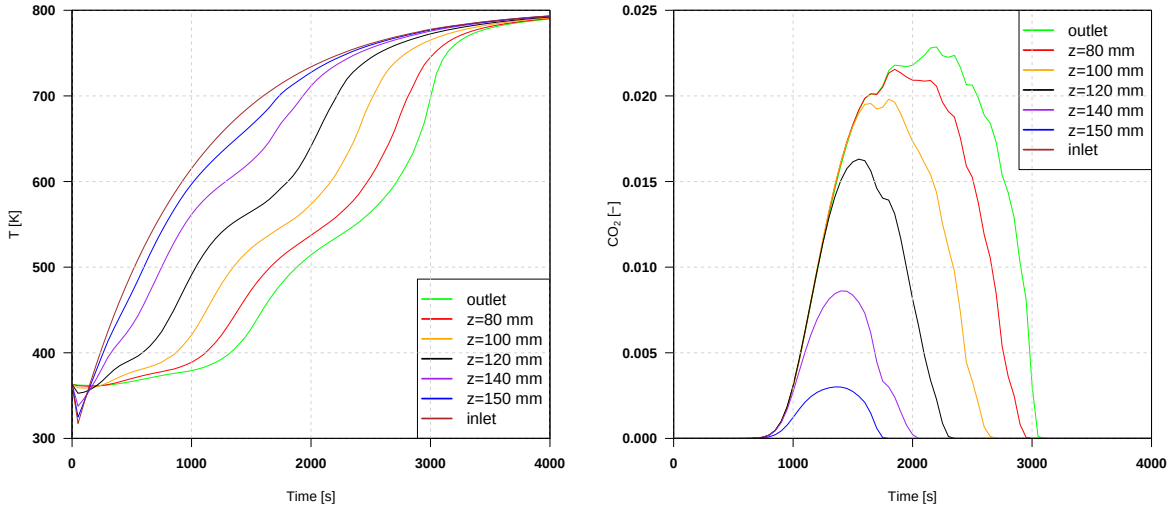

(a) Gas temperature **(b)** CO_2 mass fraction

Figure 3.4.6: Gas temperature and mass fraction of CO_2 in the gas phase versus time on central axis of the reactor

As soon as a particle has finished drying, its temperature increases up to 500 K and devolatilisation starts. Because the external energy transferred to the particle is used to compensate the endothermic heat of the reaction, resulting in a plateau in the predicted

particle temperature. When the particle decomposition is finished the temperature rises to the ambient temperature. Looking at the mean temperature graphs for two different inlet temperatures shows that pyrolysis in case of $T_{in} = 803\ K$ takes place in the temperature range of 500 to 600 K. For an inlet temperature of 573 K it occurs between 500 to 573 K. Although in both cases reaction occurs almost in the same temperature range, there is a considerable difference in the decomposition period. This is explained by the higher heat rate in the first case. Thus for the particle at $z = 140\ mm$, in which $T_{in} = 803\ K$ conversion time is about 840 s but for the case with $T_{in} = 573\ K$ it is about 3700 s.

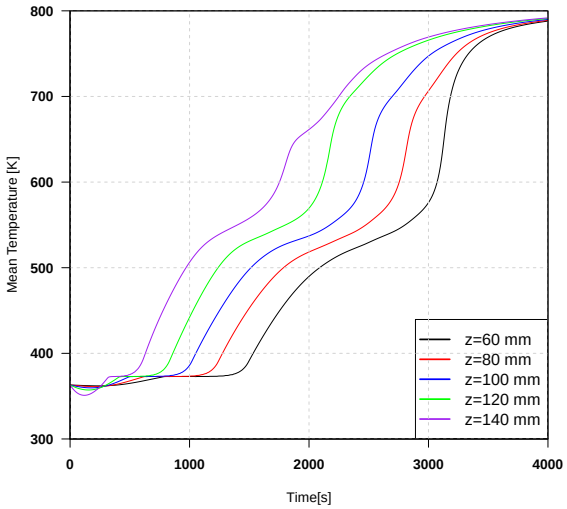

(a) $T_{in} = 803\ K$

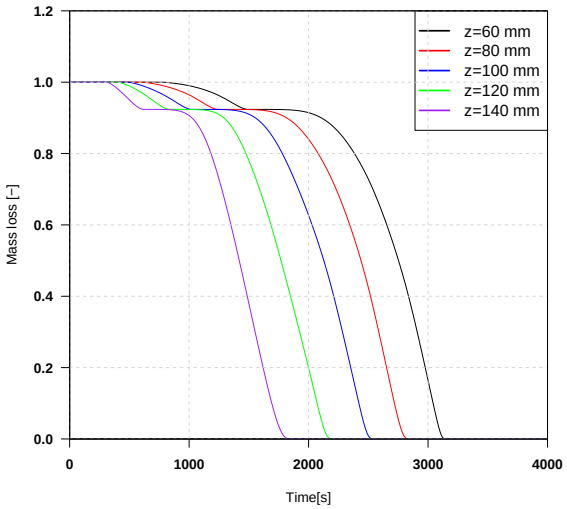

(b) $T_{in} = 803\ K$

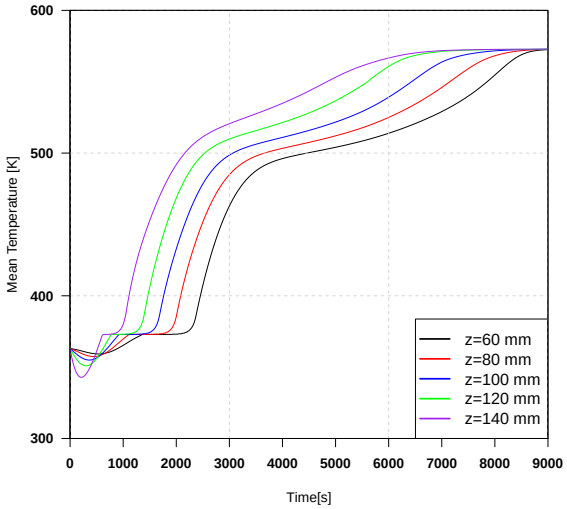

(c) $T_{in} = 573\ K$

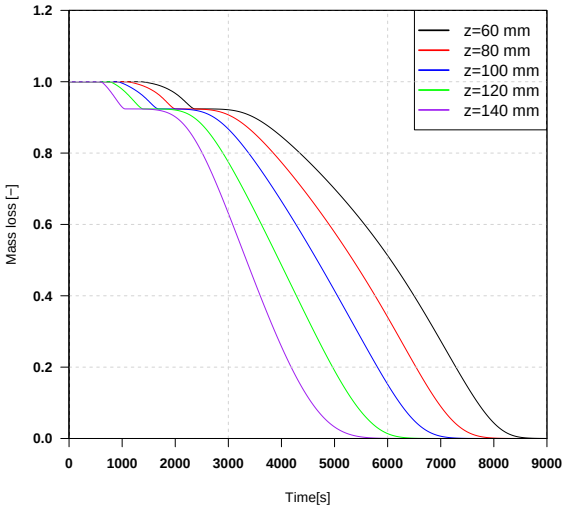

(d) $T_{in} = 573\ K$

Figure 3.4.7: Mean temperature and mass loss of five particles at different positions in the bed for two inlet temperature

Figure 3.4.8 reveals temperature, mass loss and char mass fraction within a particle at the

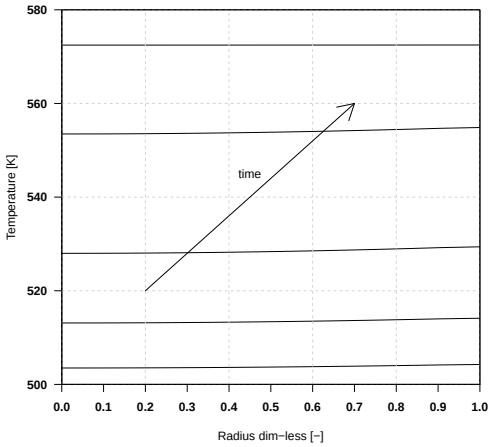

(a) $T_{in} = 573\ K$

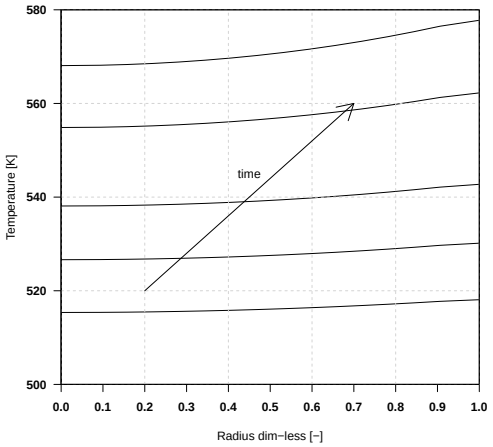

(b) $T_{in} = 803\ K$

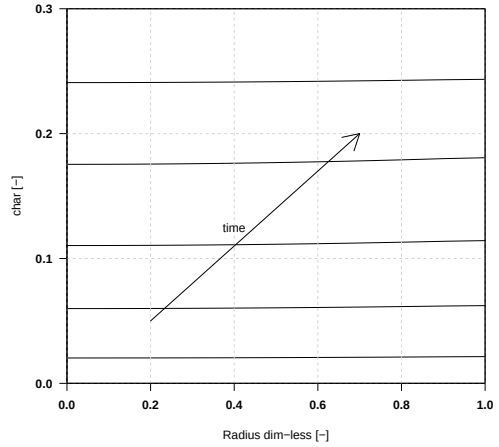

(c) $T_{in} = 573\ K$

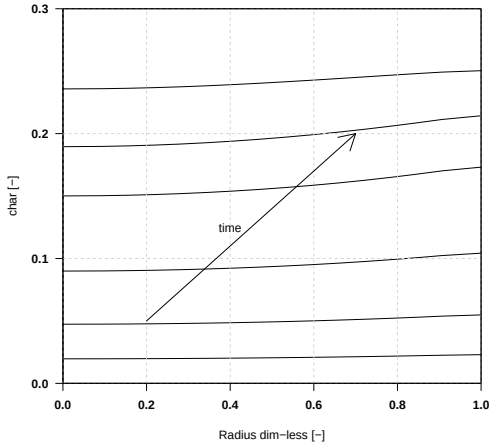

(d) $T_{in} = 803\ K$

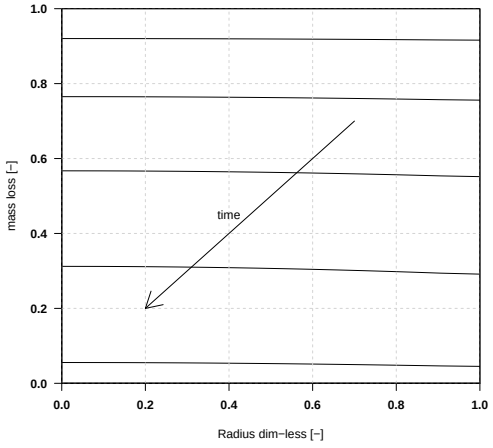

(e) $T_{in} = 573\ K$

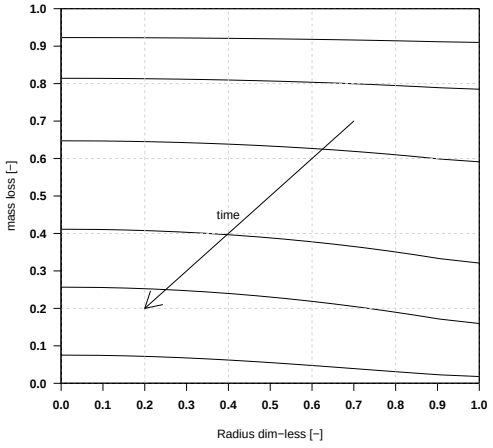

(f) $T_{in} = 803\ K$

Figure 3.4.8: Time and space evolution of char mass fraction and mass loss at $T_{in} = 803$ and $573\ K$

bottom of the bed for two different inlet temperatures. At $T_{in} = 573\ K$ since the heat rate is too low, the temperature gradient inside the particle is not considerable (figure 3.4.8a), leading to an almost uniform conversion and char formation within the particle. These are depicted in figure 3.4.8c and 3.4.8e. But when the inlet temperature increases to 803 K, due to the higher heat rate the conversion shows a noticeable gradient inside the particle, especially close to the end of conversion time. Figure 3.4.8d and 3.4.8f show that the rate of char formation and conversion is higher near the particle surface than the center. This proves that an isothermal particle model is not an accurate assumption for cases with high heating rate, since it does not take into account the considerable species and temperature gradient inside the particles.

3.5 Conclusions

In this chapter the proposed model from the previous chapter was developed to predict pyrolysis of biomass materials in a packed bed. Two models were used to describe the devolatilization of wood particles, *one step global model* and *three parallel reactions*. The simulation results were compared with several experimental data for both the single particle and the packed bed. Good agreement with measurement was achieved that prove the ability and accuracy of XDEM for modeling of pyrolysis in a packed bed. Detailed information about temperature, pyrolysis product distribution and mass loss were presented on both bed and particle scale. Species and temperature gradients inside the particle reveal that isothermal model for particle at high heat rate is not an accurate assumption.

Chapter 4

Modeling of wood combustion in a fixed-bed

During the combustion of biomass in a fixed bed, each particle experiences sequence of processes such as heating, drying, pyrolysis, char combustion and gasification. Furthermore in the gas phase pyrolysis products may react with the oxygen. The aim of this chapter is to develop the proposed numerical model in previous chapters to address detailed information about the phenomena that occur during the combustion of biomass in a fixed-bed. [1]

[1]This chapter is written based on the following published article:
Amir Houshang Mahmoudi, Miladin Markovic, Bernhard Peters, Gerrit Bremb, An experimental and numerical study of wood combustion in a fixed bed using EulerLagrange approach (XDEM), **Fuel** 150 (2015) 573-582

4.1 Introduction

The optimization of the biomass grate furnaces is ongoing to improve the efficiency and emissions control. Therefor it is very important to gain detailed information about the combustion process in the furnace. However combustion and gasification of biomass particles are very complex phenomena because of the involved physical and chemical processes including heating up, drying, pyrolysis, oxidation of pyrolysis product, char oxidation and gasification.

Many authors experimentally investigated the combustion process in the solid layer using batch reactors [69, 70, 17, 71, 72, 73, 74]. In these experiments, the influence of two groups of parameters: operating conditions (airflow, air temperature and oxygen content) and fuel properties (moisture level and fuel composition) were examined, and combustion indicators were observed (combustion rate, ignition rate, temperature profile in the layer, etc.).

Regarding the position of reaction front and the level of primary air preheating, two combustion techniques can be identified: conventional and upward combustion [18]. In conventional combustion ignition is achieved by high heat flux to the top of the fuel layer. The ignition front is formed at the top of the layer and propagates downwards until it reaches to the grate. In upward combustion, or combustion with spontaneous ignition [71] hot primary air is fed below the fuel layer. The ignition front is formed at the bottom of the layer in the proximity of the grate. The biomass layer above the reacting front collapses towards the reaction zone and is consumed in thermochemical conversion process.

Spontaneous ignition is defined as the transition from a negligible or slow fuel reaction rate to a rapid oxidation of either the volatiles or the solid fuel without an external source such as a spark or a flame [71]. Sudden rise in the bed temperature indicates spontaneous ignition, and the temperature that this rise starts is called spontaneous ignition temperature.

Gort [70] investigated the influence of airflow rate at various moisture level and fuel composition on ignition rate in the conventional combustion. The effect of air preheating up to 170 ℃ on the combustion of solid fuels on a grate was described by van Kassel et al. [72]. Spontaneous ignition or ignition with preheated primary air (>220 ℃) in the solid layer was investigated by van Blijderveen et al. [71]. Further study of the processes in the layer after the spontaneous ignition was conducted by Markovic et al. [18].

Experimental investigations of biomass combustion in a packed bed are usually difficult to carry out due to limited access into the bed. Therefor it demands cost-intensive set-ups

to capture all the process and measure detailed information. To be able to gain a better insight into the conversion of a biomass packed bed, numerical modeling is a well accepted affirmation way.

Combustion modeling of a single particle has been reported by many authors [6, 75, 68, 76, 77, 78]. Haseli et al. [75] investigated the effects of pyrolysis kinetic constants on the combustion process. They found that depending on the process condition and reactor temperature, correct selection of the pyrolysis kinetic data is an important parameter in the combustion modeling of the wood particles. Lu et al. [6] studied combustion of cylindrical wood particle with two different diameter-length ratios, considering the surrounding flame combustion of the particle. They compared their results with measurements and obtained a good agreement in prediction of mass loss and particle temperature. Mehrabian et al. [68] divided the particle into four layers corresponding to the main stages of biomass thermal conversion, and solved energy and mass conservation for each layer. By comparing the results with the measurements, they conclude their layer model is accurate and fast enough to be applied in the grate furnace simulation.

Contrary to single particle modeling, only few models of fixed-bed combustion have been reported in literature [65, 11, 79, 13, 51]. Blasi [65] proposed a one-dimensional transient model for prediction of biomass gasification in a stratified downdraft reactor. Beside the pyrolysis and char combustion/gasification they also considered combustion of pyrolysis product and secondary cracking of tar. However they have neglected the intra-particle temperature and species gradients. Later Blasi and Branca [51] used the same model and studied the effect of secondary air entry on the gasification process. Wurzenberger et al. [11] presented a transient 1D - 1D model to simulate conversion of biomass on a moving bed furnace. They assumed that the gradient along the grate is negligible. Hence a fixed bed model can describe entire process of a moving bed. Collazo et al. [13] introduced a three dimensional model (both in solid and gas phase) for simulation of fixed bed combustion. In this model, they neglect movement of bed due to shrinkage of particle during char conversion. Although they obtained an acceptable conformity with measurements, applying particles motion could improve the prediction considerably.

The main objective of this chapter is to develop the proposed model in chapters 2 and 3 to describe combustion and gasification of biomass materials in a packed bed with a high level of detailed information. In this chapter, homogeneous reaction in the gas phase and also secondary tar cracking are considered to address a more accurate gas products composition.

4.2 Experiment

An experimental investigation of the processes in the layer during the upward combustion is conducted in the Energy Technology group of Twente University. For that purpose a batch type combustion reactor is built (see Fig. 4.2.1). The reactor has an inner diameter of 200 mm, an overall height of 4.55 m, and a possibility of fuel layer height up to 1 m. The insulation is made out of two components with a low thermal mass which ensures very low heat losses during experiments. The fuel is stacked on a perforated grate that is made of a low thermal mass and high-temperature-resistant material.

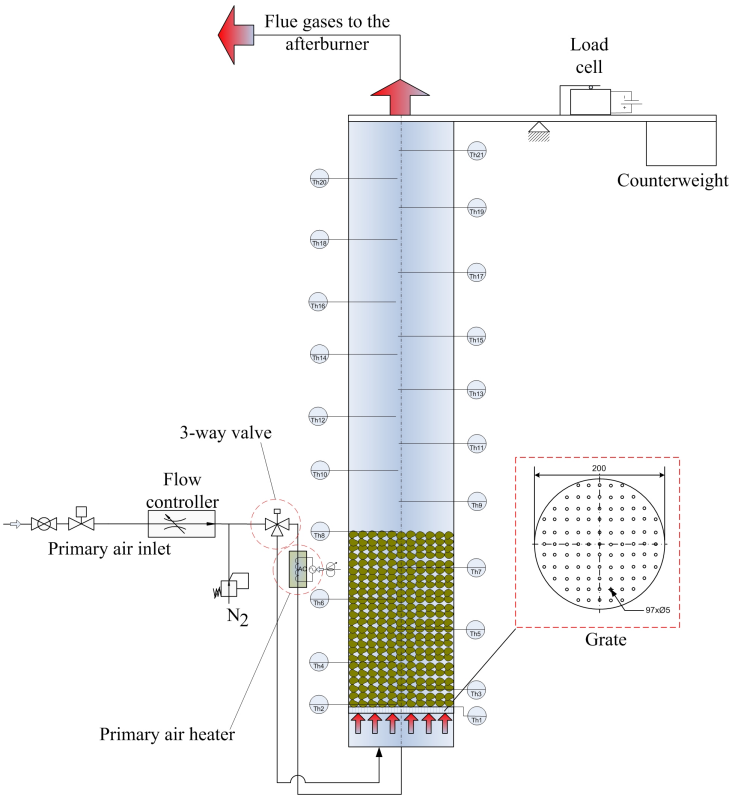

Figure 4.2.1: Experimental setup

The primary air (16.95 m^3/hr in standard conditions) is fed into the reactor from below the grate and it can be preheated by an electric heater. The electric heater can be bypassed via a 3-way valve, so the switch from preheated to not preheated primary air can be made very fast. Nitrogen may be added to the primary air stream in order to vary the oxygen concentration. Temperature profiles are monitored with thermocouples installed along the height of the reactor. For monitoring of the fuel mass reduction during the experiment, a counterweight construction with a load cell is used. Beech wood chips (with size of $6.0 - 10.0$ mm) were used as a fuel in the experiment. The proximate and ultimate analysis of beech wood is listed in Table 4.2.1.

The reactor is filled with prepared wood chips to a height of 0.6 m (for the case with

Table 4.2.1: Proximate and ultimate analysis of the beech wood used in the experiment.

Proximate analysis	
Moisture (wt-%, wb)	30
Volatile Matter (wt-%,db)	77.9
Fixed carbon (wt-%,db)	21.4
Ash (wt-%,db)	0.7
Ultimate analysis (wt%, daf)	
C	48.0
H	6.3
N	0.1
O (by difference)	45.6
HHV (MJ/kg, daf)	19.2

30% water content, the bed height is 0.5 m) and mounted on a load cell. During the experiment the inlet flow rate is constant, with 3% vol. oxygen during the devolatilization phase (when devolatilization is the dominant process in the reactor), and 10% vol. oxygen during the char combustion phase (when char combustion is the dominant process in the reactor). Air is preheated by an electric heater to 250℃ during devolatilization, and when the char combustion stage begins the heater is bypassed via a 3-way valve enabling a sharp decrease of the primary air temperature to the room temperature.

During the experiments three stages of the conversion were noted: drying, rapid devolatilization and char burnout [18]. Drying stages starts immediately when the primary air is introduced. When all of the moisture is evaporated from the reaction zone, the solid temperature increases followed by thermal decomposition of particles. The particle temperature rises until the ignition occurs which is detected by a sharp temperature gradient in the layer. Due to the high rate of heat produced by the reaction, the devolatilization rate increases, as it is observed by large amount of combustible gases production at the outlet of the reactor. This results in very fast mass decrease detected by load cell.

When all of the volatiles are released, only char remains in the container, and in that moment the inlet air feed is set to room temperature by using the bypass valve. Also at that moment the oxygen concentration is increased from 3% vol. to 10%vol.

4.3 Mathematical model

A wet wood particle in a packed bed which is subjected to a hot air experiences heat up, drying, pyrolysis, combustion and gasification. The equilibrium model is used for

calculation of drying rate in this work. This model is based on the hypothesis that water vapor within the pores of the particle is in equilibrium with the liquid and the bound water [11]. In this model drying occurs by the diffusion and convective transport of the water vapor out of the particle. Part of the water in the particle evaporates to compensate the loss of water vapor. An increase in temperature increases the saturation pressure within the particle. Therefore more water must be evaporated to reach to the saturation pressure. Hence drying rate increases with temperature increase.

Devolatilization or pyrolysis occurs during heating up of raw biomass. This leads to decomposition of the biomass into char and volatiles. The latter escapes from the particle by advection and diffusion. The pyrolysis is described with three independent reactions expressing decomposition of wood to its main products (char, tar and gas), as given in Eq (4.3.1, 4.3.2, 4.3.3). Tar may also undergo a secondary cracking reaction and forms light gases as given in Eq (4.3.4).

$$Wood \rightarrow Char \tag{4.3.1}$$

$$Wood \rightarrow Tar \tag{4.3.2}$$

$$Wood \rightarrow \nu_{CO}\, CO + \nu_{CO_2}\, CO_2 + \nu_{H_2O}\, H_2O + \nu_{H_2}\, H_2 + \nu_{CH_4}\, CH_4 \tag{4.3.3}$$

$$Tar \rightarrow \gamma_t\, Tar_{inert} + \gamma_{CO}\, CO + \gamma_{CO_2}\, CO_2 + \gamma_{H_2}\, H_2 + \gamma_{CH_4}\, CH_4 \tag{4.3.4}$$

Where ν_i and γ_i are the mass fractions for the above reactions ($i = CO$, CO_2, CH_4, H_2, H_2O) and are taken from Blasi [65] and Wurzenberger [11] and listed in Table 4.3.1.

Table 4.3.1: Product mass fraction of the pyrolysis reactions.

	CO	CO2	H2O	H2	CH4	Tar_{inert}
ν_i [65]	0.156	0.271	0.521	0.021	0.031	-
γ_i [11]	0.564	0.111	-	0.017	0.088	0.22

Homogeneous reactions in the gas phase play an important role in the whole process and also in composition of gas products. The volatiles released during pyrolysis may react with oxygen and generate heat. The following four gas phase reactions are used in the present work. The rate expression and the kinetic data of these reactions are listed in

table 4.3.2 and 4.3.3 respectively.

$$2\ CO + O_2 \rightarrow 2\ CO_2 \tag{4.3.5}$$

$$CH_4 + 2\ O_2 \rightarrow CO_2 + 2\ H_2O \tag{4.3.6}$$

$$2\ H_2 + O_2 \rightarrow 2\ H_2O \tag{4.3.7}$$

$$Tar + 2.9\ O_2 \rightarrow 6\ CO + 3.1\ H_2 \tag{4.3.8}$$

Table 4.3.2: Rate expressions

reaction number	rate expression	ref
	$K_i = A_i exp(Ei/RT)$	
4.3.4	$\frac{\partial \rho_{Tar}}{\partial t} = K_{4.3.4}\rho_{Tar}$	
4.3.5	$\frac{\partial C_{CO}}{\partial t} = K_{4.3.5}C_{CO}C_{O_2}^{0.25}C_{H_2O}^{0.5}$	[80]
4.3.6	$\frac{\partial C_{CH_4}}{\partial t} = K_{4.3.6}C_{CH_4}^{0.7}C_{O_2}^{0.8}$	[80]
4.3.7	$\frac{\partial C_{H_2}}{\partial t} = K_{4.3.7}C_{H_2}C_{O_2}$	[80]
4.3.8	$\frac{\partial C_{Tar}}{\partial t} = K_{4.3.8}TC_{Tar}^{0.5}C_{O_2}$	[81]
4.3.9	$\frac{\partial \rho_{O_2}}{\partial t} = K_{4.3.9}P_{O_2}S_{a,char}$	[82]
4.3.10	$\frac{\partial \rho_{CO_2}}{\partial t} = K_{4.3.10}P_{CO_2}S_{a,char}$	[82]
4.3.11	$\frac{\partial \rho_{H_2O}}{\partial t} = K_{4.3.11}P_{H_2O}S_{a,char}$	[82]

Table 4.3.3: Kinetic data and heat of reaction

reaction number	A	E (kJ/mol)	ref	$\Delta H(kJ/kg)$
4.3.4	9.55×10^4	93.37	[11]	42
4.3.5	2.24×10^{12}	167.36	[80]	10110
4.3.6	11.58×10^{13}	202.5	[80]	50187
4.3.7	2.19×10^9	109.2	[80]	120900
4.3.8	9.2×10^6	80.2	[81]	17473
4.3.9	2.54×10^{-3}	74.8	[82]	changing with Ω
4.3.10	1.81×10^{-2}	130	[82]	-14370
4.3.11	1.81×10^{-2}	130	[82]	10940

The remaining char from pyrolysis of the wood may undergo heterogeneous reactions, which are gasification and combustion. The following reactions describe these heterogeneous reactions.

$$\Omega\ C + O_2 \rightarrow 2(\Omega - 1)\ CO + (2 - \Omega)\ CO_2 \tag{4.3.9}$$

$$C + CO_2 \rightarrow 2\ CO \tag{4.3.10}$$

$$C + H_2O \rightarrow CO + H_2 \tag{4.3.11}$$

where [83]

$$\Omega = \frac{2(1 + 4.3\ exp[-3390/T_{particle}])}{2 + 4.3\ exp[-3390/T_{particle}]} \tag{4.3.12}$$

The combustion/gasification reactions rate of the char are calculated according to Evan and Emmons [82], which are based on partial pressure of the oxidizing/gasifying agent within the particle.

Solid particles lose mass via, drying, pyrolysis, combustion and gasification. But particle shrinkage is considered only during char conversion (combustion and gasification) due to negligible volume change during drying and pyrolysis process [65, 11]. Therefor particle shrinkage is accompanied with shrinkage of the bed and moving particle downward. It should be noted that shrinking occurs in during char conversion if the reaction takes place at the surface of the particle. However, if diffusion of the gas oxidizer (for example O_2 in the case of the char combustion) into the particle is fast enough, more reaction might take place inside the particle. This increases only the porosity inside the particle and does not influence the shrinkage of the particle.

4.4 Results and Discussion

In order to validate the proposed numerical model, temperature at different heights of the reactor are compared with the measurements while solid fuels contain initially 30% moisture. It should be noted that due to shrinkage of the bed, the temperature at the given height may be read from different particles. Figure 4.4.1a shows accurate prediction of temperature during all processes of wood conversion (drying, pyrolysis, ignition and char oxidation). Total mass loss of the bed is also compared with experimental data. Figure 4.4.1b shows a good agreement between prediction and measurements. These comparisons are able to prove that XDEM is an advanced and robust tool to model complex physical and chemical phenomena in wood combustion.

According to the experimental setup, the inlet temperature increases gradually from ambient temperature to 523 K and it is kept constant until 2570 s. During this period O_2 concentration at the inlet is 3%. After this period concentration of O_2 increases to 10%, at the same time temperature decreases to ambient temperature.

Figure 4.4.1a illustrates different stages that particles experience during the conversion in the reactor. Hot inlet gas heats up wood particles and is accompanied with drying of particles. Then dried particles at higher temperature devolatilize and the volatile products may react with oxygen in the ambient. The remaining char also undergoes

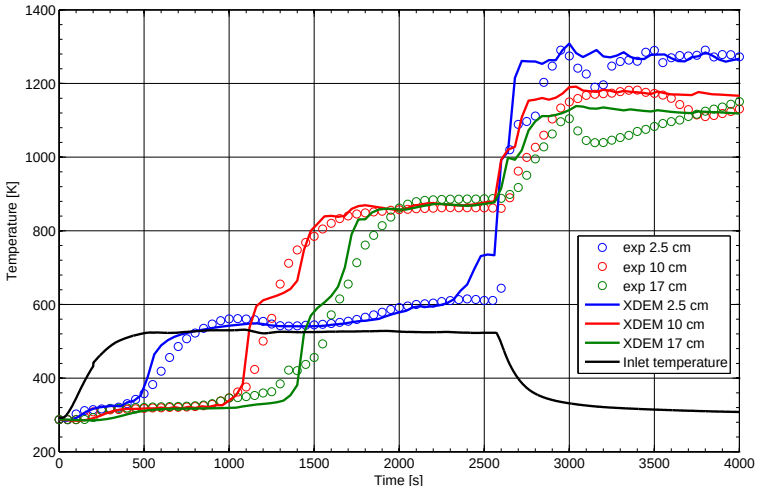

(a)

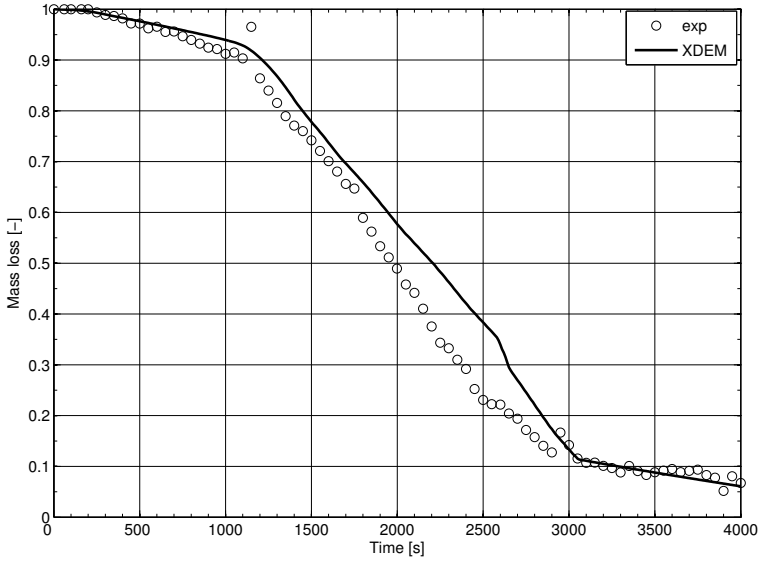

(b)

Figure 4.4.1: Comparison of predictions with measurement (a) temperature at different height of bed, (b) mass loss of the bed

heterogeneous reactions with air. However these phenomena don't happen sequentially. They are strongly coupled and even might occur at the same time in one particle. In the following sections all the details of these series of phenomena will be presented using predicted results.

Drying period is predicted very well at different height of the bed, as it is shown at early stage of fig. 4.4.1a. Due to the equilibrium between water and steam within the particle, drying starts from the beginning of the experiment even at low temperature by mass transfer of steam from the particle to the surrounded gas. However, drying is very slow at low temperature. When the temperature of particles increases and reaches about 50 degree (as a result of heating up by hot inlet gas), drying rate increases considerably. Therefor the most part of thermal energy of the particle is used for the intense water

evaporation, which causes the particle temperature to be almost constant during drying period. Since the hot inlet gas first is in contact with the particles close to the grate, these particles experience a higher heating rate than particles further downstream. This results in earlier drying of particles close to the grate, which is obvious in these figures for particles at position of 2.5 cm above the grate.

Pyrolysis starts first in particles close to the grate at inlet temperature and continues very slowly. This can be seen in fig. 4.4.4a for particle at 2.5 cm above the grate. Although the amount of volatiles released by these particles are very small, they react with oxygen in the gas phase and produce heat. The generated energy is transfered to the particles downstream and increases their temperature to a value which is slightly higher than the inlet gas temperature. Pyrolysis in a particle with a higher temperature is faster, resulting in more production of volatiles, more oxidation of the volatiles and generating more heat. When this process continues for a while, temperature will reach to a value in which ignition may occur. High temperature gradient at 10 cm above the grate after about 1200 s indicates this phenomena (Fig. 4.4.1a). Therefor, it is concluded that spontaneous ignition occurs at area about 10 cm above the grate. The height at which ignition front is formed can be varied by changing the inlet gas velocity and temperature [71].

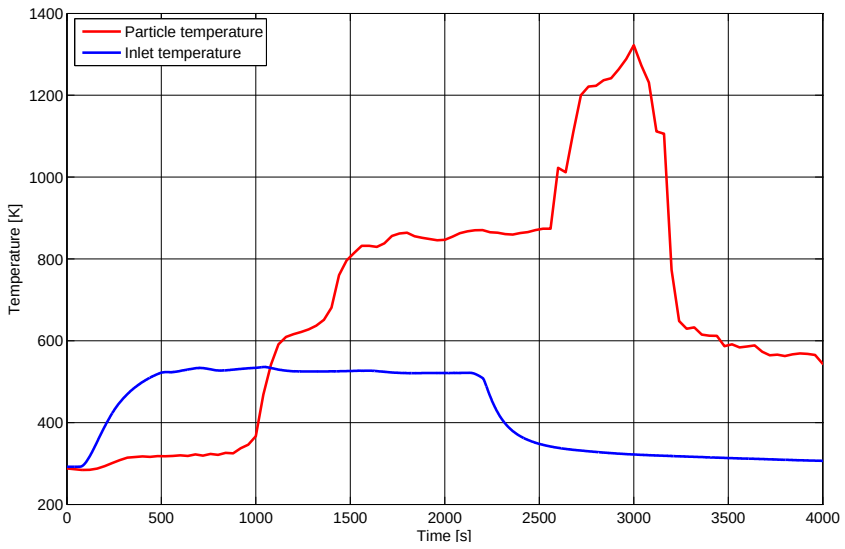

Figure 4.4.2: Inlet gas temperature and particle surface temperature that is located initially at 10 *cm* above the grate versus time

From heat transfer point of view, the inlet gas plays different roles along the reactor during the experiment. At the beginning of the experiment it heats up the particles by convective heat transfer (heating effect) and when temperature of particles increase (due to exothermic reactions) it cools down particles (cooling effect). This is illustrated in fig 4.4.2. The constant temperature after steep temperature gradient (at 10 cm and 17 cm above the grate) is due to an energy balance between convection by inlet gas (cooling effect) and generated heat by exothermic reactions (either homogeneous reactions or char

combustion), fig 4.4.1a.

When the concentration of oxygen at the inlet increases, char combustion becomes more pronounced in particles close to the grate and high temperature gradient is observed. Due to the shrinkage of the bed during the char conversion, there are always char close to the grate. Therefor it can be expected that almost constant amount of energy is generated in this zone and temperature must increase constantly. While in contrary, convective cooling of the inlet gas and endothermicity of gasification cause the temperature stays almost constant during the char conversion period.

Mass loss curve can be split to three zones with different slopes (Fig. 4.4.1b). Until $t = 1100\ s$ (first slope) mass loss is mostly due to the drying, but at the same time mass loss because of pyrolysis is observed at particles close to 10 cm above the grate. From 1100 s until 3000 s (second slope), mass loss mostly results from the devolatilization. Later in fig. 4.4.4b and 4.4.6 will be shown that in this period some portion of mass loss is also due to the char conversion and drying. At the third slope (after 3000 s), the mass loss is only because of char conversion (combustion and gasification).

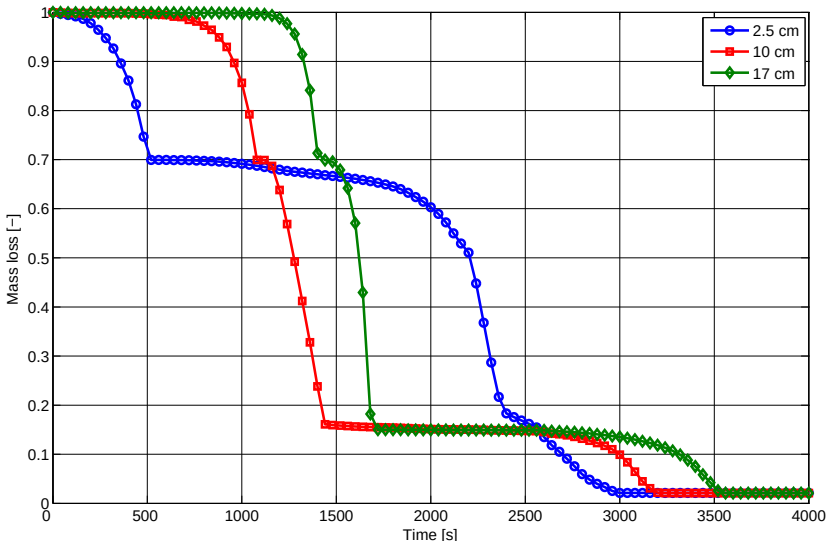

Figure 4.4.3: Mass loss (wb) for three particles at different height of bed

Figure 4.4.3 shows mass loss of three particles that initially are located at 2.5, 10 and 17 cm above the grate. It should be noted that the position of these particles in the reactor will change during the experiment due to the bed shrinkage. Mass loss starts first due to the drying, followed by pyrolysis and then char conversion. The particle at 2.5 cm above the grate is dried first, because it is closer to the grate. When drying is finished, there is a period of about 200 s to heat up the particle with inlet gas and then devolatilization starts very slowly. After a while when temperature of particle increases because of oxidation of volatiles, pyrolysis becomes faster and mass loss gradient increases.

Pyrolysis in the particle at 2.5 cm above the grate is finished at 2400 s (This is more

obvious in fig. 4.4.4a). After this time mass loss is due to the char conversion, which starts with low slope and followed by higher slope. This is caused by the enhanced concentration of oxygen at the inlet at $t = 2570\ s$.

Drying of the particles at 10 cm and 17 cm is faster than particle at 2.5 cm, as they experience higher temperature. When drying is finished in these particles, pyrolysis starts after a very short heating up period and finished very fast. After finishing pyrolysis, mass of these particles remains almost constant for a period of about 1000 s. This is due to the fact that most of the oxygen is used downstream either by homogeneous reactions or char combustion. Therefor char combustion and as a results mass loss is very slow downstream. Figure 4.4.4 presents consumption/formation of wood and char over time

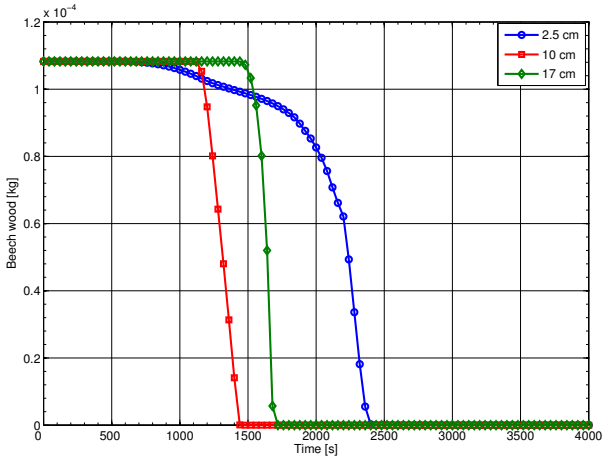

(a)

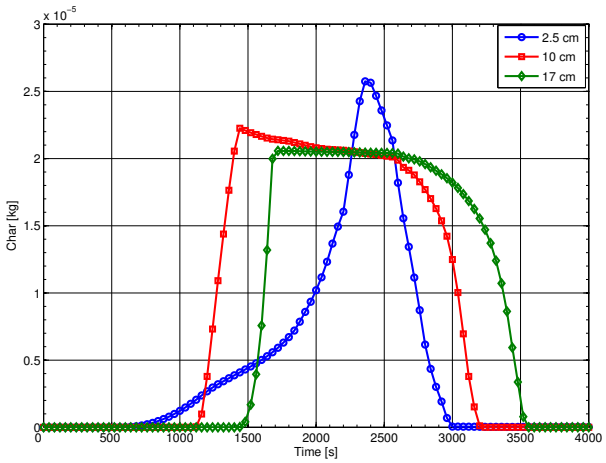

(b)

Figure 4.4.4: (a) Wood conversion , (b) char formation versus time for three particles at different height of bed

for three particles that initially are located at 2.5, 10 and 17 cm above the grate. Their reaction rate are also depicted in fig. 4.4.5. Figure 4.4.5a shows that pyrolysis in the particle at 2.5 cm above the grate starts at $t = 700\ s$ and continues very slowly, while it is very fast for particles at 10 cm and 17 cm. Since slow pyrolysis is associated with more

char formation, more char is formed in particle at 2.5 cm compared to two other particles (Fig. 4.4.4b).

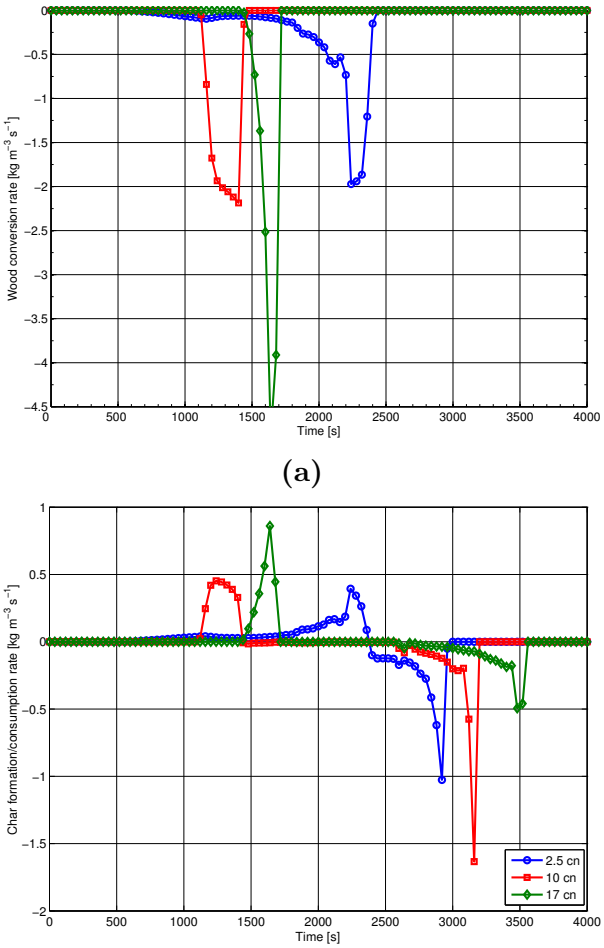

Figure 4.4.5: (a) Rate of wood conversion , (b) rate of char formation versus time for three particles at different height of bed

If the first part of char conversion of the particle at 10 cm (from $t = 1400\ s$ to $t = 2600\ s$) is neglected, it will be observed that char conversion for the particle at 17 cm is longer than particle at 10 cm. This can be explained by the fact that at $t = 2600\ s$, temperature of both particles is high enough (Fig. 4.4.1a) that gasification with CO_2 becomes considerable. Therefor char is consumed in both of them by gasification until the particle initially located at 10 cm above the grate reaches to rich oxygen zone (as a result of the bed shrinkage). Therefor intense char combustion besides the char gasification increases the char consumption rate. The particle which is initially at 17 cm, during this period and even until it reaches to rich oxygen zone is consumed mostly by gasification. Since gasification is a slower reaction compared to the char oxidation, it results in longer char conversion for this particle.

Figure 4.4.6 illustrates gas temperature and tar, steam, O_2, CO and CO_2 mass fraction

along the bed at different times. In order to show shrinkage and height of the bed, the void space along the bed is also included in this figure. Steep steam gradient at $t = 1000\ s$ indicates the drying region propagating along the bed as it is shown at different times. At height of about 7 cm a temperature increase of about 60 degree is observed that can be ascribed to slow oxidation of volatiles. Small amount of CO in that area is also another deviance for oxidation of tar (Eq 4.3.8).

High temperature gradient at $t = 1500\ s$ and $h = 10\ cm$ indicates ignition due to homogeneous reaction of pyrolysis products. After a thin ignition zone, gas temperature decreases because of the convective heat transfer with cold particles downstream and also endothermicity of the pyrolysis.

As can be seen in fig. 4.4.6b, at $t = 1500\ s$ two pyrolysis regions are observed along the reactor. The stronger region moves upward and the weaker one moves downward. Particles close to the grate are heated up by heat flux coming from hot particles at higher position by conduction and radiation and at the same time cooled down by inlet gas. While particles downstream not only receive heat flux due to the conduction and radiation with particles at lower position, but also are heated up by convective heat transfer with hot gas. This causes particles downstream undergo stronger pyrolysis and generate steeper tar gradient.

For the distribution of steam along the bed at $t = 1500\ s$, three different regions can be distinguished: the first and second regions (at $h = 6\ cm$ and $h = 15\ cm$) correspond to those particle layers undergoing devolatilization at weak and strong pyrolysis region. The third region is located downstream where layers of particles are dried by the hot gas. The amount of the produced steam as a result of the devolatilization is much lower than the steam production due to the drying. Therefor higher steam gradient is observed at the second region (drying layer).

At $t = 2000\ s$ the high temperature zone with almost constant value becomes wider. This is due to the thermal equilibrium between hot particles and cold inlet gas. Unlike the drying and pyrolysis layers, the ignition layer does not propagate downstream. It even propagates slightly upstream as depicted in fig. 4.4.6c. Due to the higher heat rate downstream, the second pyrolysis layer moves much faster than the first one. So that after 500 s, it moves from $h = 15\ cm$ to $h = 25\ cm$, but the first pyrolysis layer moves only 2 cm downward.

Some portions of oxygen are used for homogeneous reactions of the volatiles at the first pyrolysis region and the rest is consumed for char combustion. So that oxygen is finished up to $h = 11\ cm$. Hence all the volatiles from the second pyrolysis layer leave the reactor unburned. Although char combustion is not strong at this stage, it causes slight shrinkage

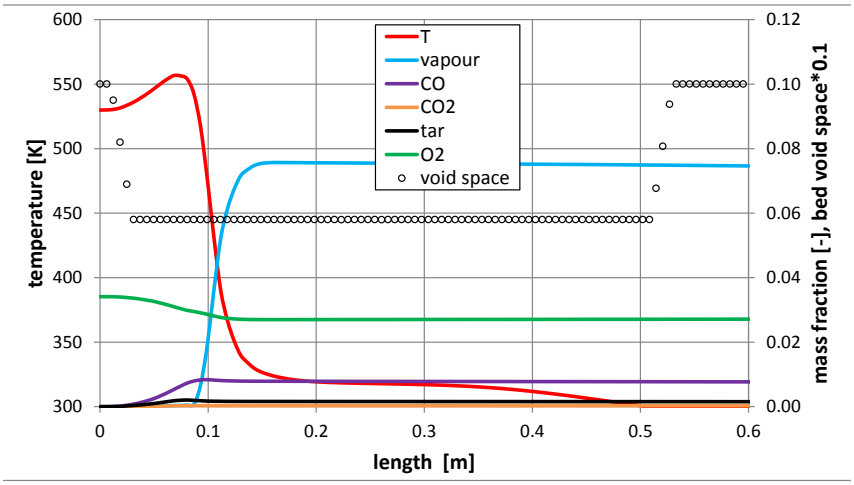

(a) $t = 1000\ s$

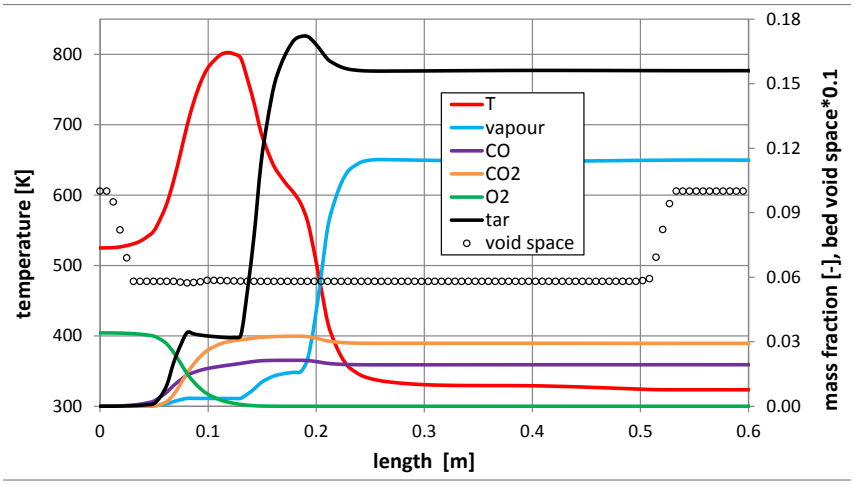

(b) $t = 1500\ s$

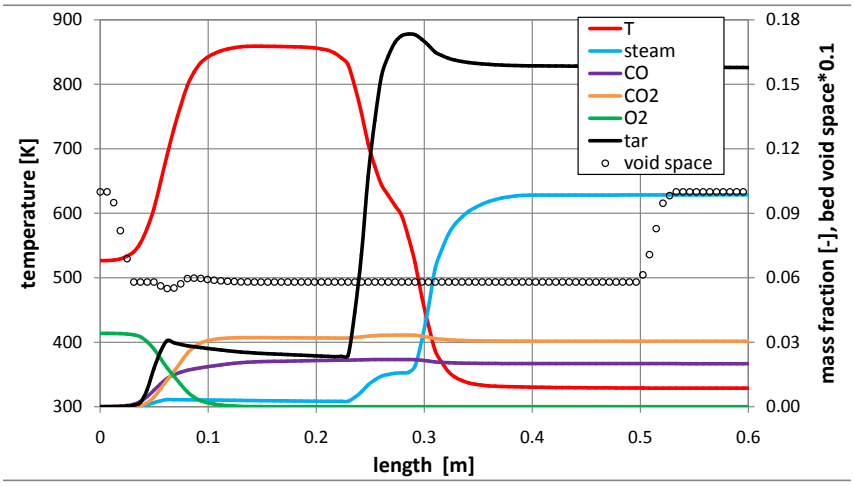

(c) $t = 2000\ s$

Figure 4.4.6: Gas temperature, gas species mass fraction and porosity along the bed at different times (t= 1000, 1500, 2000, 2500, 3000, 3500 and 4000 s)

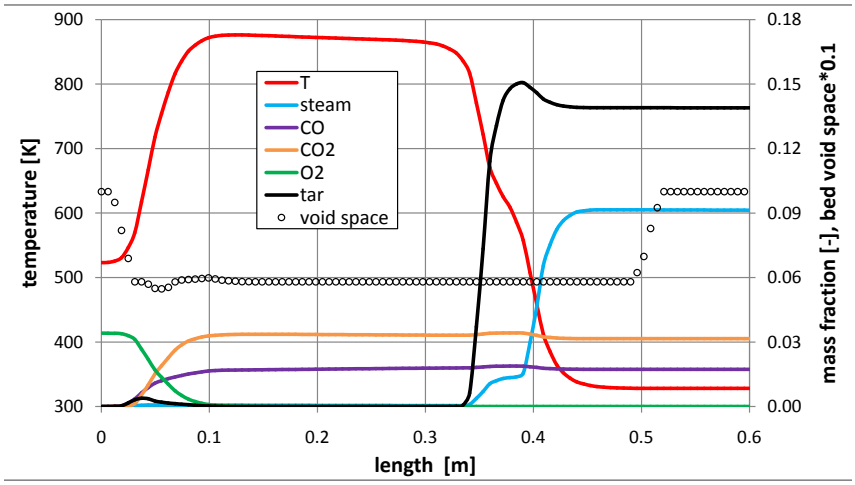

(d) $t = 2500\ s$

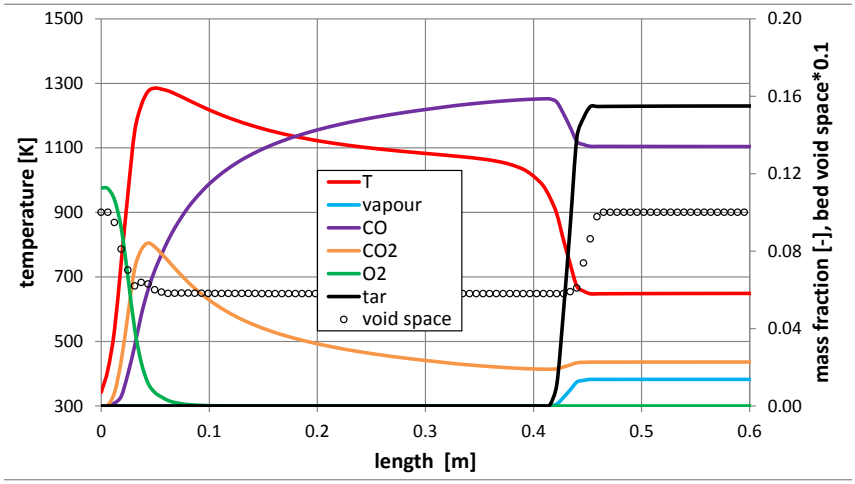

(e) $t = 3000\ s$

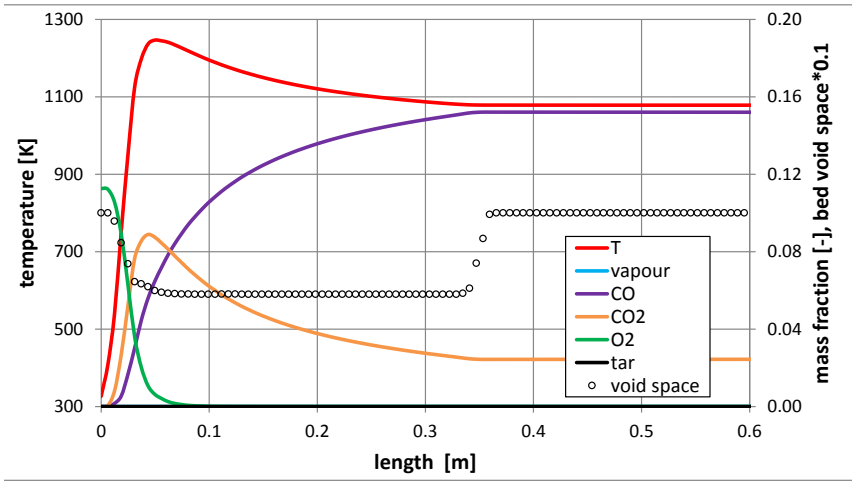

(f) $t = 3500\ s$

Figure 4.4.6: (continued) Gas temperature, gas species mass fraction and porosity along the bed at different times (t= 1000, 1500, 2000, 2500, 3000, 3500 and 4000 s)

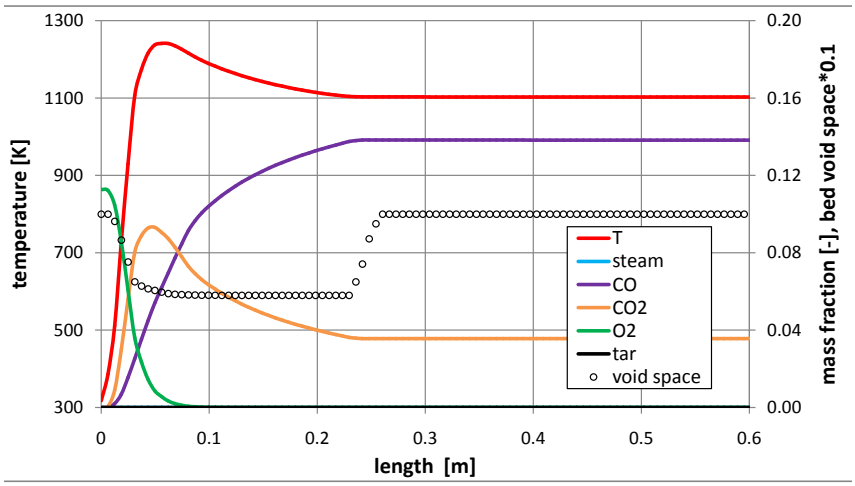

(g) $t = 4000\ s$

Figure 4.4.6: (continued) Gas temperature, gas species mass fraction and porosity along the bed at different times (t= 1000, 1500, 2000, 2500, 3000, 3500 and 4000 s)

of the bed. This can be seen by changing void space at the top of the bed in fig. 4.4.6c.

CO and CO_2 in the reactor can have different origins. Pyrolysis products, homogeneous reactions of volatiles and heterogeneous reactions of char. As can be seen in fig. 4.4.6d, at $t = 2500\ s$ the weak pyrolysis region almost disappears. Therefor it can be concluded that CO and CO_2 from the bottom of reactor up to the pyrolysis layer (at the top of the bed) are only resulting from the char combustion.

As it is shown in fig. 4.4.6e, by increasing O_2 concentration char combustion near the grate becomes more intense and temperature increases up to 1300 K. At high temperature char gasification becomes more important. Hence after a thin layer of char combustion, gas temperature due to convective heat transfer with cold particles downstream and endothermicity of gasification decreases along the bed. Due to stronger char combustion, more CO and CO_2 are produced. But some portions of CO_2 are used for the gasification of the char, producing more CO. This is why after initial increase in mass fraction of CO_2, it decreases and in contrary CO mass fraction increases.

At $t = 3500\ s$ no tar exists in the reactor indicating pyrolysis is already finished. Char combustion zone is placed at a narrow layer close to the grate and does not propagate along the reactor. This can be seen by looking at O_2 consumption at $t = 3000\ s$, $3500\ s$ and $4000\ s$. Intense char conversion (oxidation and gasification) leads to high rate of the bed shrinkage. This is obvious by comparing the void space in fig. 4.4.6f and 4.4.6g.

Figure 4.4.7 shows variation of the mass of different gas species per initial mass of the bed at the outlet. In other word, this expresses total production of each species per initial mass of the bed over time. Steam mass increases constantly from the beginning of

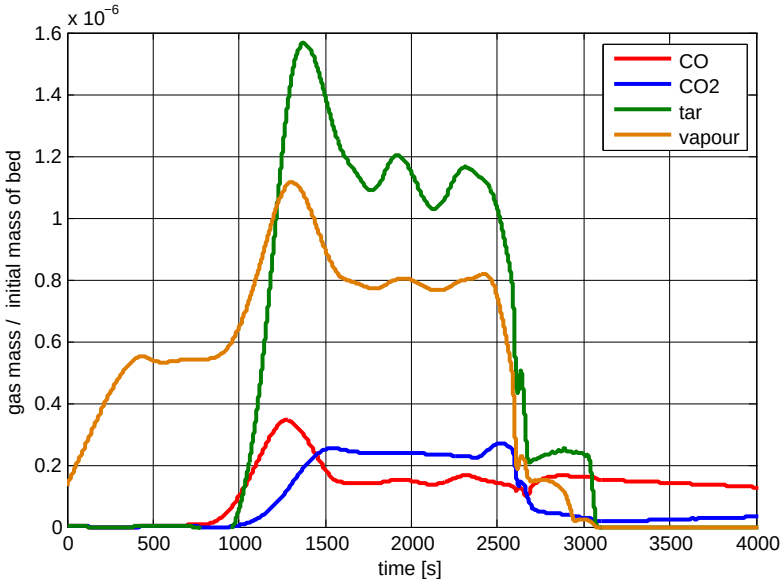

Figure 4.4.7: Variation of the mass of different gas species per initial mass of the bed at the outlet

the experiment until $t = 400\ s$, because the inlet temperature increases gradually from ambient temperature to 523 K. When inlet temperature stays at 523 K for a while, the drying rate and consequently the steam production remains constant. At $t = 1000\ s$, temperature increase due to ignition in the gas phase increases drying rate. However it should be mentioned that at this stage some portions of the steam are pyrolysis product. Steep decrease of the steam at $t = 2600\ s$ shows end of drying, and hence steam after this time is generated by devolatilization.

Similar to the steam, tar production increases by increasing gas temperature after $t = 1000\ s$. It can be observed in fig. 4.4.6b,4.4.6c and 4.4.6d that temperature at the pyrolysis region (the strong one) is almost the same from $t = 1500\ s$ to $t = 2500\ s$. Hence it is expected to have constant global pyrolysis rate. But as it is shown in fig. 4.4.7, the value of the tar mass oscillates about 1.1×10^{-6}. This can be explained by the fact that at $t = 1800\ s$ and $t = 2200\ s$ tar production increases due to the ignition of the volatiles in the pyrolysis region (the weak one).

CO may have different sources: it is produced as a pyrolysis product, product of tar cracking, product of tar oxidation or char gasification. Existence of CO before $t = 1000\ s$ might be due to the pyrolysis (reaction 4.3.3) or/and the tar oxidation (reaction 4.3.8). During that period there is no tar at the outlet, therefor it can be concluded that the entire tar in the gas phase is oxidized before it leaves the reactor, then the CO is mostly produced as a result of this reaction. This can be also the reason for the CO to increase until about $t = 1250\ s$.

After this time, producing the CO is reduced while CO_2 is increased. This can be explained by the fact that at this time char combustion is going to use some considerable fraction of the inlet oxygen. Then, there is less tar oxidation and consequently less products of tar oxidation (e.g. CO). Equation 4.3.12 together with the reaction 4.3.9 show that char combustion produces more CO_2 than CO. This is why the mass of CO_2 increases at the outlet in this period. After $t = 2500\ s$ (as it was already shown in Fig 4.4.6) gasification becomes very important. Hence some portions of CO_2 are used for the gasification of the char, producing more CO. This is the reason that mass of CO_2 decreases while CO increases.

4.5 Conclusions

The proposed model in previous chapter was developed in this chapter by considering heterogeneous and homogeneous reactions. This allows to model combustion/gasification of biomass in packed-bed. Numerical model was validated using experimental data. Temperature variation with time at different heights along the bed and mass loss of the bed were measured. Comparisons of numerical results with experimental data showed excellent consistency, which proves XDEM is an accurate and robust tool to predict all processes during the wood combustion. Due to the size of particles, inlet gas velocity and temperature, drying started at low temperature (about 50 ℃), and equilibrium model predicted this process precisely. Spontaneous ignition occurred at the height of about 10 cm above the grate and during the experiment moved slightly downward. A while after ignition stated, two pyrolysis layers were formed. One layer propagated upward and the other one propagated downward. Unlike the pyrolysis layer, the char combustion zone did not propagate along the bed (after increasing oxygen concentration) and stayed near the grate until the end of experiment.

Chapter 5

Modeling of wood combustion on a forward acting grate

The grate firing system is one of the most common ways for the combustion of biomass because it is able to burn a broad range of fuels with only little or even no requirement for fuel preparation. The main objective of this chapter is to study precisely the involved processes in biomass combustion on a froward acting grate and provide a detailed insight into the local and global conversion phenomena. [1]

[1] This chapter is written based on the following article:
Amir Houshang Mahmoudi, Xavier Besseron, Florian Hoffmann, Miladin Markovic, Bernhard Peters, Modeling of the biomass combustion on a forward acting grate using XDEM, accepted in November 2015 to be published in "**Chemical Engineering Science**"

5.1 Introduction

Grate firing systems are widely used in combustion of coal, biomass and waste because they are able to burn a broad range of fuels with only little or even no requirements on fuel preparation [84]. Grate firing systems are mainly classified into stationary sloping grates, traveling grates, reciprocating grates and vibrating grates [10]. All types function with the same main principle, i.e. the fuel particles are introduced at one side of the grate and are burned while transported to the other end of the grate. The transport of the particles is either solely due to gravity in case of stationary grate or is supported by grate movements [85]

Understanding the details of bed motion, fuel conversion and combustion on the grate helps to improve the fuel burnout efficiency. However, the entire process is of very complex nature due to many involved physical and chemical phenomena such as, gas flow through the void space in the bed, heat and mass transfer between two phases, drying of the wet fuel, devolatization, heterogeneous and homogeneous reactions, motion of the solid fuels either by the movement of the grate or due to the shrinkage.

Peters et al. [86] used DEM to study the mixing and segregation process of a packed bed on a forward acting grate. Sudbrock et al. [87, 88] studied the influence of different parameters such as bar velocity, stroke length and moving patterns on mixing using a grate with vertically moving parallel bars. They found that specific movement patterns of bars could be identified to improve mixing behavior. The influence of particle diameter and material properties of the particles on mixing was investigated both numerically and experimentally by Simsek et al. [89]. Samiei and Peters [85] studied the distribution of particle residence time on forward and backward acting grates using DEM. The effect of different operating parameters including the mass flow and the particles material was studied. Sun et al. [84] presented the distributions of velocity and volume fraction of particles as a function of frequency and amplitude of movable bars in a reciprocating grate.

Due to the complexity of the fuel combustion process together with the motion of the bed, many authors used a batch-type fixed bed reactor to describe the entire process in a moving grate furnace [16, 17, 11, 18, 19]. The main assumption in these studies is that the gradients of, e.g., temperature and concentrations of chemical species in the direction of the movement of the bed are negligible compared to those in the direction of gas flow. Therefore, a vertical slice of the bed is modeled and followed along the grate. However, van Kessel et al. [20], by comparing results from real plants and a fixed bed model, concluded that such a fixed bed is not precise enough to observe certain phenomena in a moving grate neither quantitative nor qualitative. The main reason of this conclusion was the

influence of the solid fuel movement, which is induced by the grate movement, on the entire process.

Rickelt et al. [90] used a CFD-DEM simulation to study heat transient of spherical particles in a packed-bed in which they are mixed with movement of vertical bars. Peters and Dziugys [91] investigated numerically the impact of bar motion (amplitude and frequency) of a forward acting grate on the rate of heat-up. Their results showed that higher bar velocity leads to an increased mixing rate of particles, and therefore, to more homogeneous temperature distribution. They have also compared heat transfer on forward and backward acting grates and found that more homogeneous temperature distribution can be achieved in a backward acting grate [92].

Frey et al. [93] have measured different parameters of solid waste combustion on a furnace grate such as gas composition above the fuel bed. This data has served as the input to the numerical model. Kurz et al. [21] proposed a three dimensional numerical model with an Euler-Euler approach to simulate wood chip combustion on a grate. Although reasonably good an agreement between experimental and numerical results was achieved, they expressed that their heterogeneous reaction model should be improved to consider uneven particle size distribution. Simsek et al. [22] and Brosch et al. [23] proposed a CFD-DEM model to simulate the incineration of the municipal solid waste on a forward acting grate. In their model, a DEM code was coupled to a commercial program (ANSYS FLUENT or ANSYS-CFX) considering a two way interaction between two phases more accurately. Nussbaumer et al.[94] used CFD model to improve the combustion process and extend the part load capability of a grate boiler. They have investigated different secondary air injections and have achieved an optimum condition.

Literature survey indicates that more investigations are required to understand better the complexity of biomass conversion on a moving grate. A deeper understanding of the details of the processes will help to improve the design and the efficiency of the furnace. Therefore, the objective of this chapter is to develop the proposed numerical model in the previous chapters (chapter 2, 3 and 4) by considering the motion of solid particles. This allows simulating combustion and gasification of biomass on a moving bed such as forward acting grate.

5.2 Mathematical model

The developed model in previous chapters is further extended in this chapter by considering the motion of solid particles. This will allow us to simulate biomass conversion in a moving grate.

The particle motion is calculated with the Discrete Element Method which was first introduced by Cundall and Strack [95]. The translational motion of a particle is described by the equation of Newtons second law. It is expressed by the forces acting at the center of gravity of particle i and can be written as

$$\vec{F}_i = m_i \vec{a}_i = m_i \frac{d\vec{v}_i}{dt} \quad \text{with} \quad \vec{v}_i = \frac{d\vec{r}_i}{dt} \tag{5.2.1}$$

where m_i , $\vec{v}_i$, $\vec{a}_i$, $\vec{F}_i$ and $\vec{r}_i$ denote the particles mass, velocity, acceleration, force and position, respectively. Forces on a particle may originate from different sources such as contact forces, gravity or drag forces. However, due to the moderate gas velocity in the simulated gas-solid system (Reynolds number is about 90) it can be assumed that the contribution of drag forces on the motion of the particles is negligible.

$$\vec{F}_i = \vec{F}_{i,contact} + \vec{F}_{i,gravity} \tag{5.2.2}$$

The contact force is the sum of the forces acting on the particle from other bodies (other particles or boundaries) in contact with it:

$$\vec{F}_{i,contact} = \sum_{j=1, j\neq i}^{N} \vec{F}_{ij} \tag{5.2.3}$$

where N is the number of bodies including particles and boundaries in the system.

The rotational motion of particle i is described by the following equation:

$$\vec{T}_{i,contact} = I_i \vec{\alpha}_i = I_i \frac{d\vec{\omega}_i}{dt} \quad \text{with} \quad \vec{\omega}_i = \frac{d\vec{\theta}_i}{dt} \tag{5.2.4}$$

where I_i , $\vec{\omega}_i$, $\vec{\alpha}_i$, $\vec{T}_{i,contact}$ and $\vec{\theta}_i$ stand for the inertia tensor, the angular velocity, the angular acceleration, the torque and the orientation vector of the particle, respectively. The torque is derived from the contact force acting on the particle and is expressed as follows:

$$\vec{T}_{i,contact} = \sum_{j=1, j\neq i}^{N} \vec{T}_{ij} = \sum_{j=1, j\neq i}^{N} \vec{d}_{ij} \times \vec{F}_{ij} \tag{5.2.5}$$

where d_{ij} is the position of the contact between particles i and j relative to the center of mass of particle i. A comprehensive review on the details of equations and modeling particle motion in XDEM have been presented by Samiei et al.[85, 96, 97]

5.3 Results and Discussion

In this section the results are presented for the steady state of combustion of biomass on a forward acting grate. As it is shown in fig 5.3.1, wet particles enter the reactor from the left while they are moving to the right due to motion of the grate. The grate consists of four moving bars (blue bars) and five fixed bar (red bars). Grate motion can be divided into two part. In the first part one bar moves (with a constant velocity) wile the other three bars do not move. When the motion period of one bar finished, it stops and the next bar starts moving. This behavior is applied for all the four bars. In the second part, when all four bars passed their motion period, all four bars will rest for a resting period. This cycle will continue one after the other. In this simulation, the motion period for each bar is $2s$ and resting period is $52s$ The length of the grate is 1.27 m and the height of the boiler is 0.53 m. Air at room temperature is injected uniformly from below the grate and leaves the boiler together with the gas products from the top left corner. Flow pattern in the furnace is shown in fig. 5.3.2 for inlet gas flow rate of 2.73 kg/hr (uniform inlet velocity of 0.05 m/s, air-fuel-ratio of 2.39).

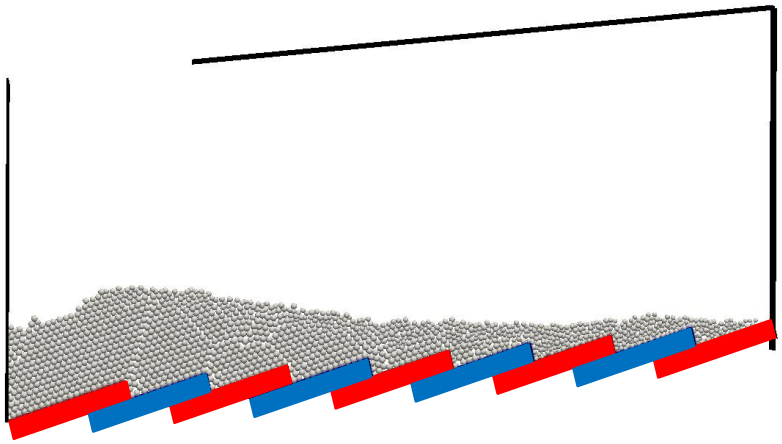

Figure 5.3.1: Simulation setup for forward acting grate

Table 5.3.1: Details of the test case

Inlet gas flow rate	2.73 kg/hr
Inlet solid flow rate	1.4 kg/hr
Inlet gas temperature	298 K
Inlet solid temperature	295 K
Wall temperature	900 K
Solid moisture content	30%db
Particle diameter	1 cm
Length of the grate	127 cm
Height of the reactor	53 cm

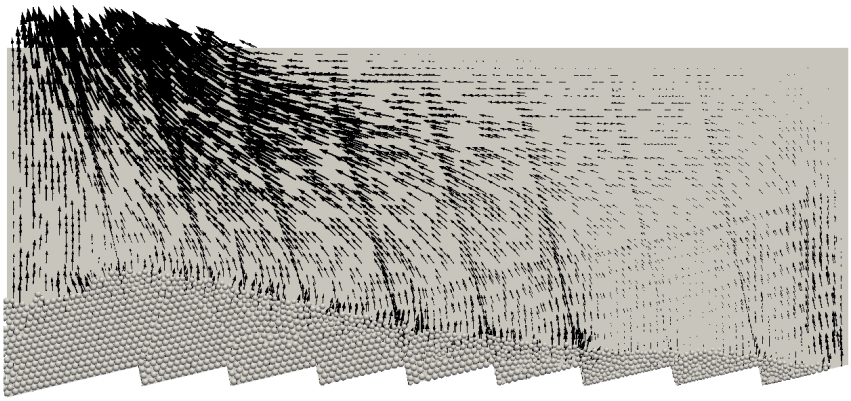

Figure 5.3.2: Distribution of gas velocity vectors for an inlet air velocity of u=0.05 m/s

It is assumed that the top wall of the reactor has constant and uniform temperature ($T_{wall} = 900\ K$) along the grate. While the grate is assumed an adiabatic wall. Particles at the surface of the bed can absorb heat radiated from the walls. The absorbed heat increases particle temperature and also is transferred to particles below the bed surface by conduction and radiation. Mixing of particles due to the motion of the grate, may also speed up heat transfer between hot and cold particles. The reactors steady state was determined by monitoring the total char mass over time. After a transient stage total char mass reached a distinct constant level, thus indicating a steady state of the reactor.

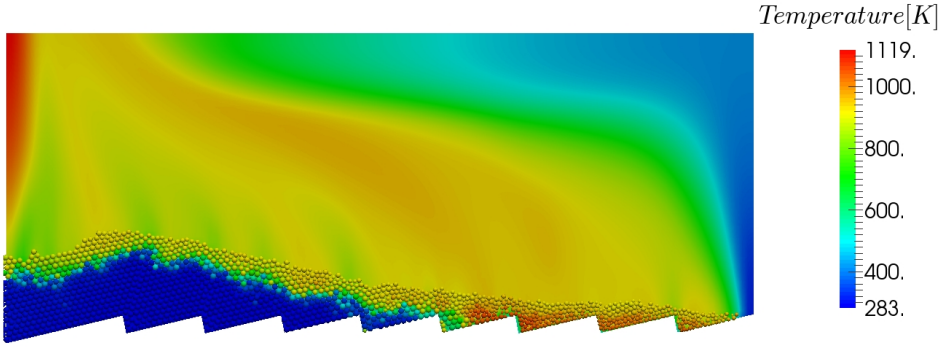

Figure 5.3.3: Temperature distribution in gas and solid phase for the case of an inlet air velocity of u=0.05 m/s

Figure 5.3.3 shows the temperature distribution in the gas and the solid phase inside the furnace. Wood particles containing 30% moisture enter to the furnace at room temperature from the left (with mass flow rate of 1.4 kg/hr). Particles at the surface of the bed absorb radiation from walls and their temperature increases, followed by drying. When temperature of particles increases more, pyrolysis starts and volatiles are released to the surrounded gas phase. Pyrolysis products are oxidized and further increase gas temperature. The remaining char undergoes heterogeneous reactions with oxygen and acts as another heat source in the boiler.

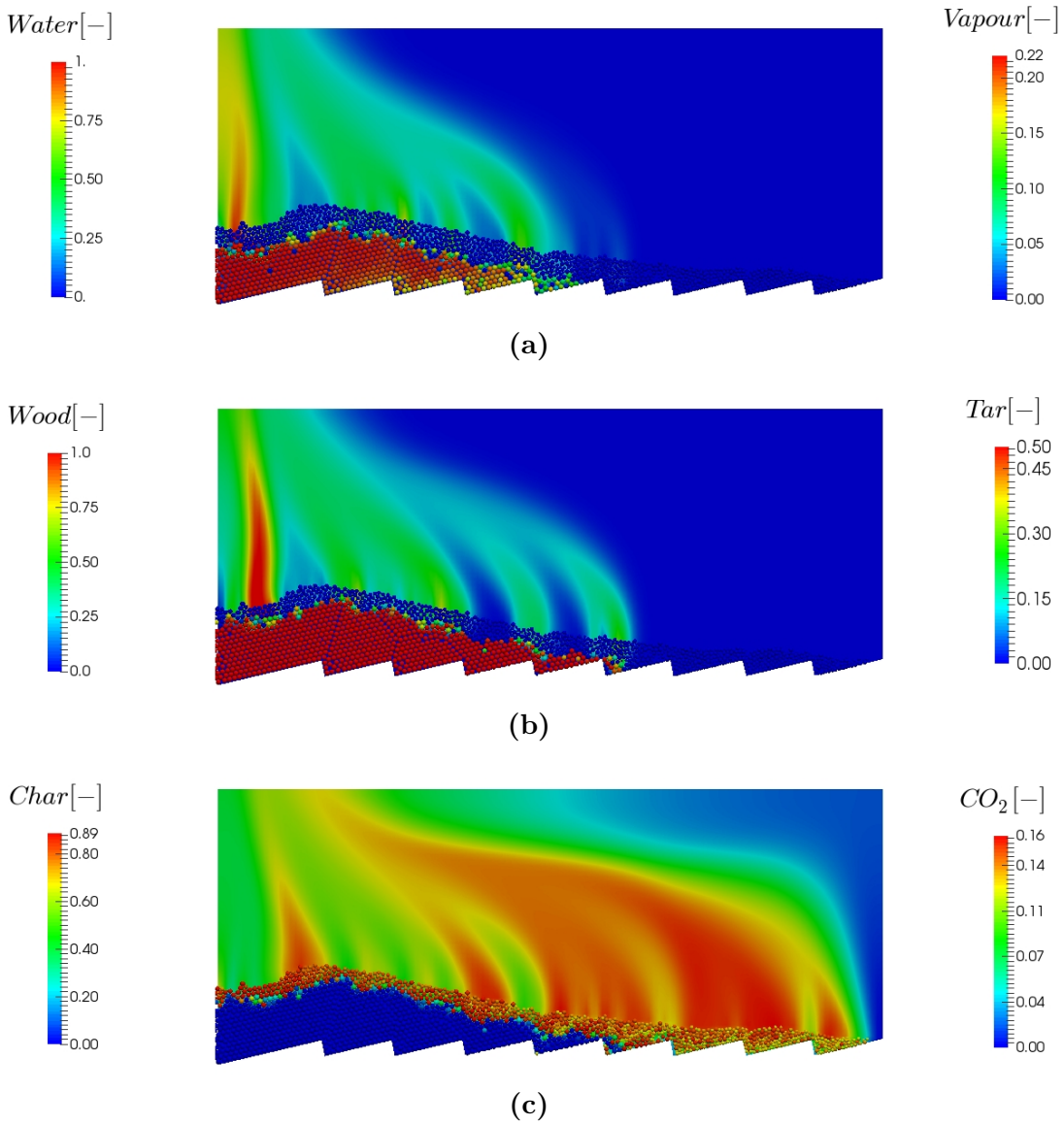

Figure 5.3.4: Distribution of species mass fractions in gas and solid phase for the case of inlet air velocity of u=0.05 m/s

Drying starts in particles at low temperature due to convective transport. However, drying rate increases with rise in temperature. Therefore wet particles at the top surface of the bed, after entering the boiler, are dried quickly due to receiving an intense heat radiation from the walls. This results in high amount of vapor in the gas phase close to the fuel entrance, as it is show in fig 5.3.4a.

As a result of heat penetration by conduction and radiation to the particles below the bed surface, drying front propagates downward. Mixing hot particles with cold wet particles will speed up drying process. Less water content at particles close to the third and fourth bar than particles above them can be explained by mixing.

When particle temperature increases more, devolatilization starts. Pyrolysis observed

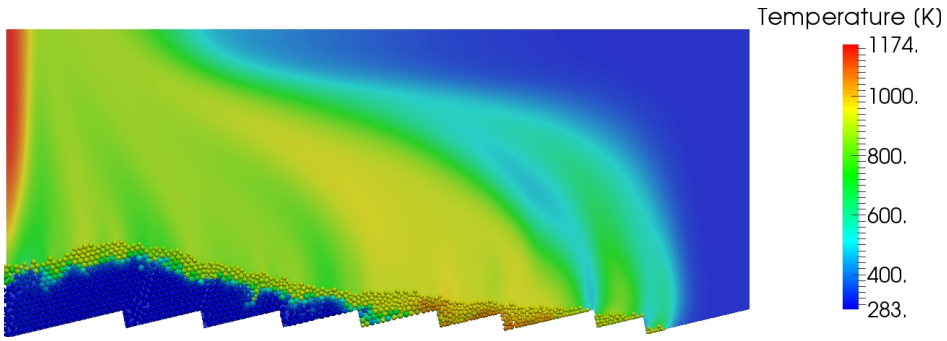

Figure 5.3.5: Temperature distribution in gas and solid phase for the case of an inlet air velocity of u=0.1 m/s

first in particles at the top of the bed. Hence, at the left side of the grate where there are more raw wood at the bed surface, intense pyrolysis is observed. High mass fraction of tar at this region proves this behavior (fig 5.3.4b).

When pyrolysis of those particles at the top of the bed are finished, the surface of the bed is covered by remaining char particles. Hence, wood particles below them are shielded from wall radiation. This reduces pyrolysis rate and consequently tar mass fraction in the gas phase, as it is shown in fig 5.3.4b. Shrinkage of char particles due to combustion/gasification may increase the distance between particles at the bed surface. This will increase the chance of particles at lower location to receive the wall radiation.

At the right half of the grate, there is only char undergoing combustion and gasification (fig 5.3.4c). According to the introduced reactions in this work, CO_2 may be produced by pyrolysis, volatiles oxidation or char combustion. At the left half of the grate, where there are wood, volatiles and char together, it is difficult to find the main source of CO_2. While in the right half, where there is only char, it can be said that high amount of CO_2 is caused only by char combustion and CO oxidation.

In this part, the model is used to calculate the influence of the inlet flow rate on the characteristics of different processes in the furnace. When inlet flow rate is doubled, the general processes in the boiler do not change, while duration of each process and quantity of products change (fig 5.3.6). Higher gas velocity increases heat and mass transfer between solid and gas phase in the furnace. Therefore, drying rate increases, leading to faster drying process on the grate (fig 5.3.6a).

By comparing fig 5.3.6b and fig 5.3.4b, it can be seen that pyrolysis period is shorter in the case of higher inlet flow rate. This behavior is related (directly and indirectly) to more intense char combustion at higher flow rate, because of more available oxygen in the furnace and higher mass transfer between solid and gas phase. This is why the bed is finished before reaching to the end of grate (fig 5.3.4c).

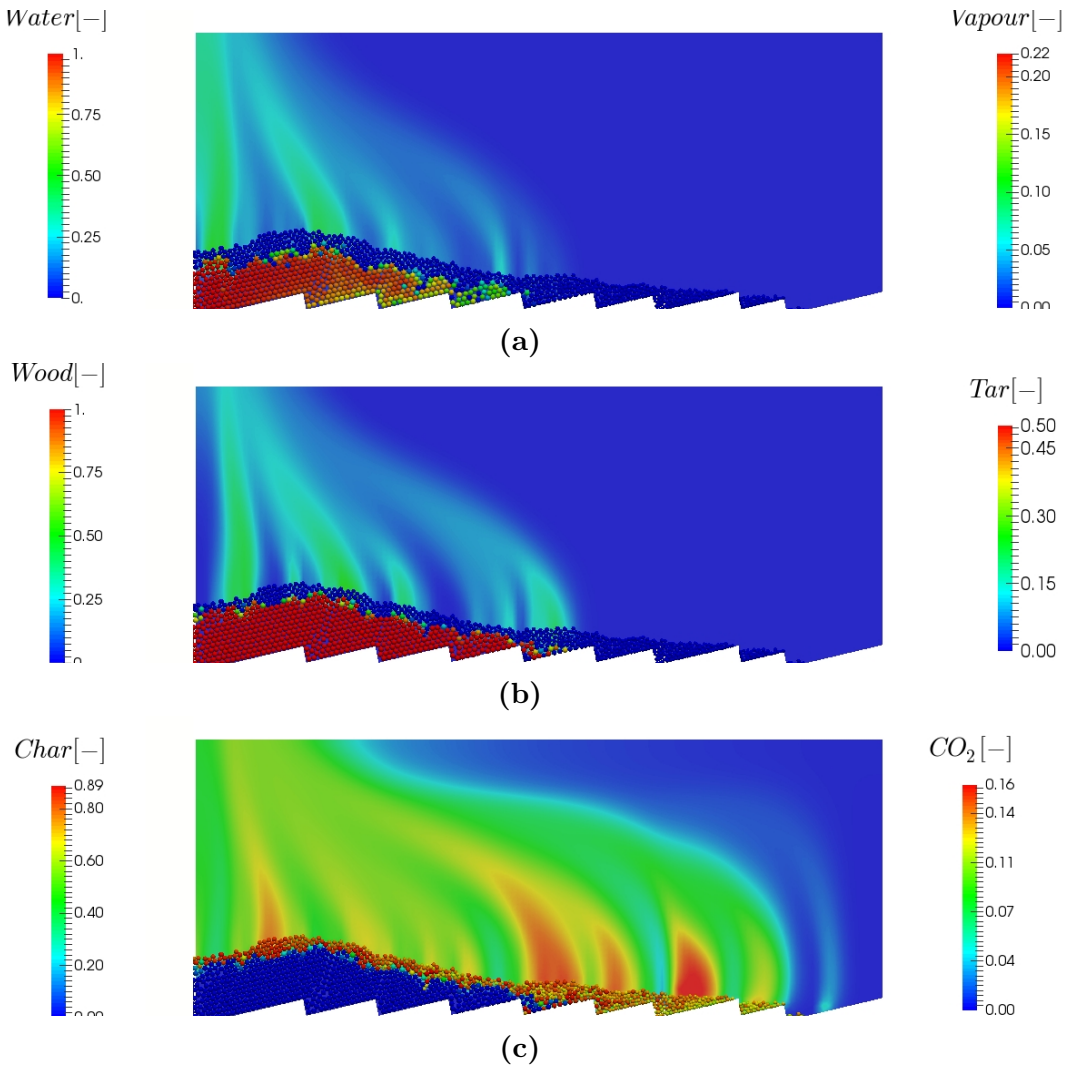

Figure 5.3.6: Distribution of species mass fractions in gas and solid phase for the case of inlet air velocity of u=0.1 m/s

The direct influence is due to the higher heat generation by more intense char combustion, that provides more heat for wood particles below the bed surface. The indirect influence is due to the particle shrinkage. Higher amount of char combustion causes more shrinking and hence, results in more void space between particles at the top of the bed. Consequently, particles below the surface of the bed are able to absorb more wall radiation and more heat transfer to those wood particles increases devolatilization rate and reduces the pyrolysis period.

Figure 5.3.7 presents mass fraction of different gas species and gas temperature above the bed along the grate. High amount of vapor is observed at the left side of the grate where raw wet particles enter to the furnace. Tar mass fraction increases and peaks while vapor mass fraction decreases sharply. This can be explained by the fact that at the beginning while wet particles at the surface of the bed are drying, large amount of vapor is released to the surrounding gas. When they become dry, vapor production is limited to wet particles

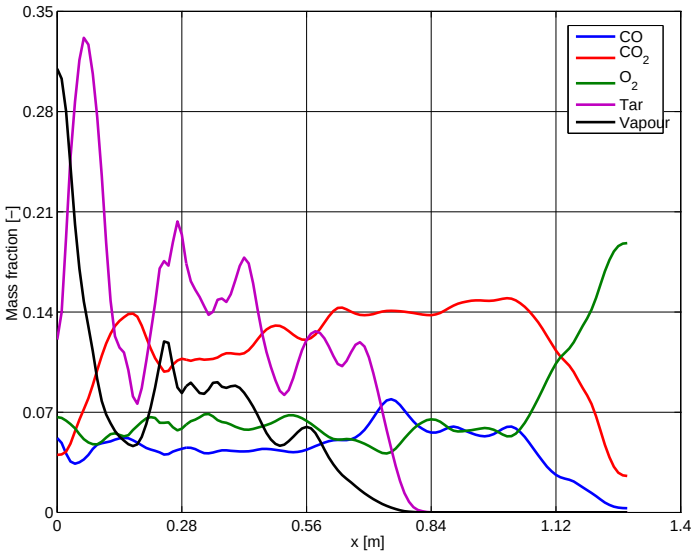

(a)

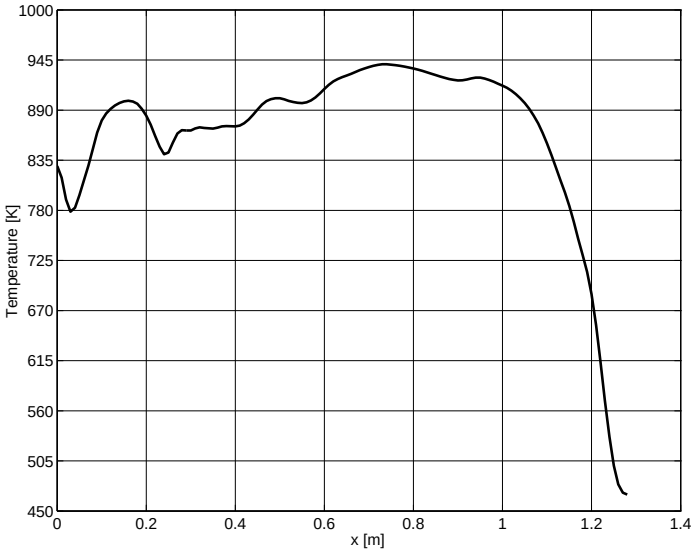

(b)

Figure 5.3.7: Species and temperature distribution in gas phase above the bed along the grate (u=0.05 m/s)

below them, which have low drying rate. Hence vapor mass fraction decreases in the gas phase. At the same time temperature of these dry particles at the top of the bed increases and devolatilization begins. This leads to increased tar mass fraction in the gas phase.

Similar relation is observed between CO_2 and *tar*. At $X = 0.2\ m$ and $X = 0.5\ m$, when *tar* mass fraction reaches to minimum, CO_2 peaks. This is because of finishing pyrolysis of wood particles at the top of the bed and intense char combustion at those particles.

Increase of inlet mass flow rate does not change distribution of gas species along the grates significantly (fig 5.3.8). However, they are shifted to the left indicating faster

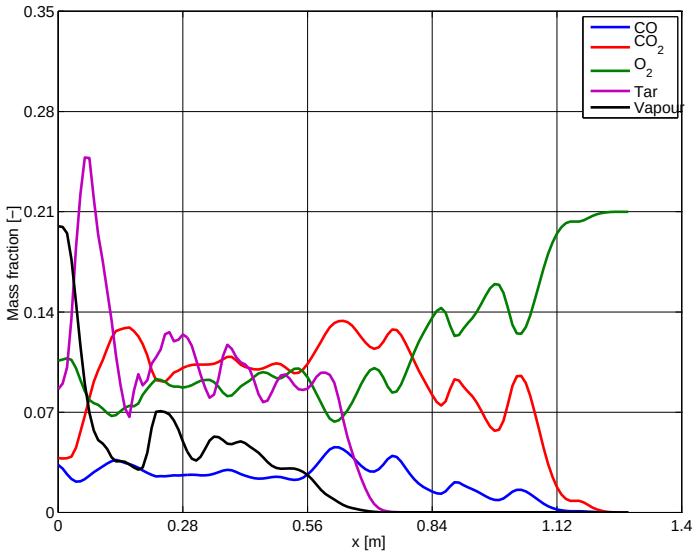

(a)

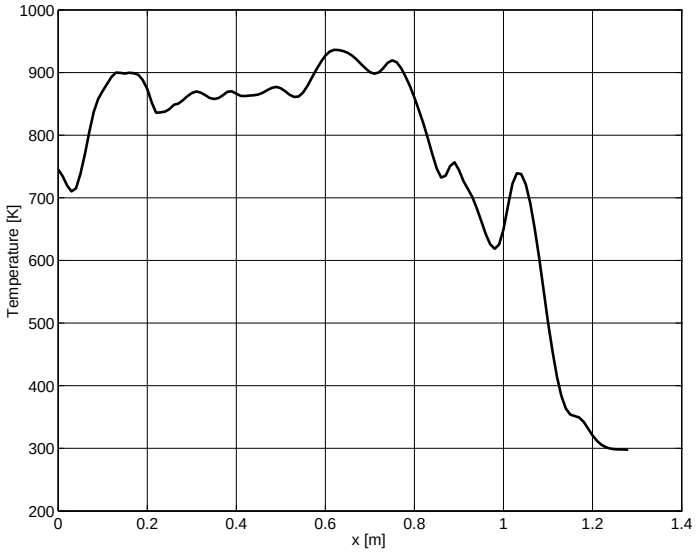

(b)

Figure 5.3.8: Species and temperature distribution in gas phase above the bed along the grate (u=0.1 m/s)

process (drying, pyrolysis, char conversion) by increasing inlet gas flow rate.

Figure 5.3.9 presents mean temperature, water loss, wood conversion and char formation/consumption of a particle while it travels along the grate. Until 600 s, the particle's temperature is about 300 K, meaning that in this period the particle was not at the bed's surface. Although temperature is low, the particle is drying at a low rate. After 600 s, the particle temperature increases, indicating that the particle is approaching the top of the bed and thus receives heat by conduction and radiation from upper particles. Drying rate increases as temperature increases and hence, the water within the particle evaporates

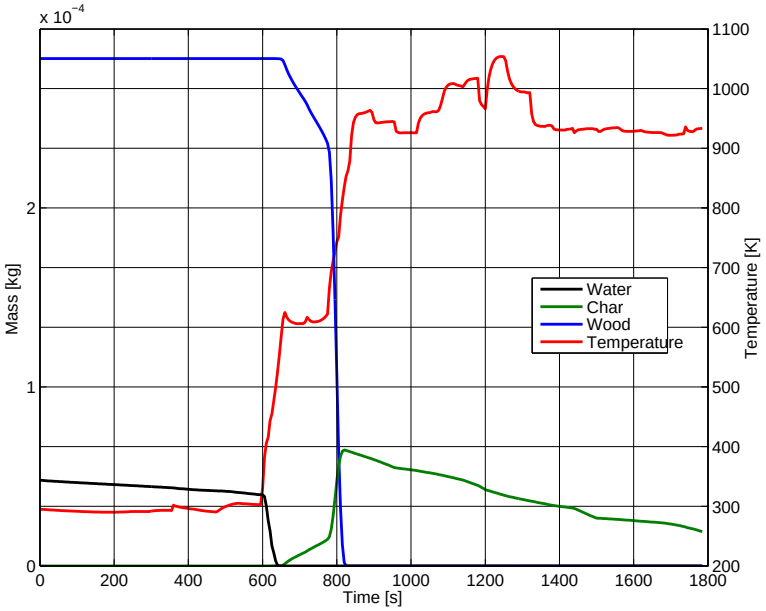

Figure 5.3.9: Temperature, moisture loss, wood conversion and char formation/consumption of a particle on the grate versus time.

quickly.

Devolatilization starts at about $t = 650\ s$ and continues at almost constant rate until $t = 780\ s$. During this period particle temperature is almost constant due to the heat balance between endothermic pyrolysis reaction and energy received by conduction and radiation from neighbor particles. After 780 s, particle temperature increases significantly. This may be explained by the fact that the particle stays on the top of the bed and consequently receives energy from the furnace walls by radiation. As a result, pyrolysis rate increases and wood conversion is finished at $t = 820\ s$.

As time proceeds the remaining char inside the particle undergoes oxidation and particle temperature increases to 1050 K. Despite char conversion at an almost constant rate from about $t = 1300\ s$, the temperature of the particle decreases and continues at a constant level until the particle reaches the end of the grate. As particles approach the end of the grate (as can be seen in fig 5.3.5) they are shrinking in size due to the consumption of char. Thus, they receive less radiation from the furnace walls and convective heat transfer can more effectively cool the particles. Furthermore, the constant temperature level indicates that the energy produced by exothermic combustion balances with energy consumed by endothermic gasification (with CO_2) and convective heat transfer with the cold inlet air.

5.4 Conclusions

The developed model in the previous chapter was further extended by considering the motion of solid particles. This allows simulating combustion and gasification of biomass in a forward acting grate. The presented results show that due to the intensive heating by wall radiation and mixing of particles the moving particle bed is of heterogeneous nature. Mixing of particles takes place but is not able to entirely homogenise conditions an individual particle is experiencing. Shrinking of particles due to char consumption is another important influence. It influences the motion of the bed as well as on the amount of energy a particle receives from the furnace walls by radiation. Furthermore, due to shrinking of particles forming the surface of the moving bed those particles below the surface receive heat input from the furnace walls as well. The results present a high degree of inhomogeneous mechanisms in the bed. In the left half of the grate, higher temperature is observed at the top while it is opposite in the right half. This is due to the fact that at the right half, oxygen is consumed by the char particles at the bottom of the bed (close to the grate surface), and hence less oxygen is available for upper particles. This results in more intense char combustion at lower particles and consequently higher temperature.

Chapter 6

The influence of particle size and packing on pyrolysis products

The main aim of this chapter is investigation of the impact of particle size in combination with particle packing on the char production. For this purpose, three setups of packed beds differing in particle size and packing mode are studied under the same process conditions. The predicted results show that arranging the packed bed in layers of small and large particles may increase the final average char yield for the entire bed by 46%. [1]

[1]This chapter is written based on the following article:
Amir Houshang Mahmoudi, Florian Hoffmann, Bernhard Peters, Xavier Besseron, A study of size distribution of particles in a backed bed on pyrolysis products using XDEM, accepted in September 2015 to be published in "**International communications in heat and mass transfer**"

6.1 Introduction

Pyrolysis/devolatilization is one of the most common way of using biomass, in which biomass is decomposed to char and volatiles. Each of the pyrolysis products can be industrially interesting, but generally chemical plants aim to obtain mainly one of them. For example char can be used as a reducing agent in the metallurgical industry or a domestic cooking fuel. Pyrolysis gas can be used for power generation, heating, or synthesized to produce methanol or ammonia, whereas the tarry liquid (pyrolysis oil or bio-oil) can be used for combustion engines. It can be also used directly for power or heat generation [5]. Therefore it is very important to predict precisely the composition and the amount of pyrolysis products in different thermal conditions of the reactor. A comprehensive review on pyrolysis products has been done by Neves et al. [98]. This illustrates the level of complexity of this process because of many involving chemical and physical phenomena.

Based on heating rate, pyrolysis may be classified as slow and fast. Slow pyrolysis is associated to conversion of biomass with slow heating rates and long resistance time. Slow pyrolysis mostly is applied to produce high char yields. In contrast, in fast pyrolysis, biomass is heated rapidly to temperatures between 700 and 850 K. In this case, there could be two different objectives, that is, the production of a maximum gas or liquid yield (tar), which is mainly depending on temperature and residence time of volatiles [60].

Particle size has a major influence on the heating rate of solid fuel, hence it is a key parameter to control the pyrolysis rate and composition of pyrolysis products. Larger tar yields are obtained from smaller particles because the temperature is successively higher at the reaction front. This is favorable for tar production. Another reason is tar residence time which becomes shorter for smaller particles. This avoids tar cracking inside the particle and results in more tar yields. In contrast larger particles are able to produce more char due to lower temperature gradient within the particle.

Nik-Azar et al. [99] studied experimentally the influence of heating rate and particle size on the product's yields from rapid pyrolysis of beech-wood. They found as particle size increases from 53-63 μm to 270-500 μm, the maximum tar yield decreases from 53% to about 38%. They also found that due to tar cracking at high heating rates in large particles, the maximum tar yield decreases with increasing the heating rate from 70% at 100 ℃/s to 48% at 10,000 ℃/s heating rates. Blasi [60] studied the effect of particle size and heating condition on the amount of the pyrolysis production using single particle modeling. She presented a map in terms of particle size as a function of the reactor temperature, to identify the transition from a kinetically controlled conversion to a heat transfer controlled conversion and from fast to slow pyrolysis.

Lu et al. [62] investigated the effects of shape and size of biomass particles on devolatiliza-

tion. They studied three different shapes (disk/flake-like, cylindrical/cylinder-like and near-spherical) using a one-dimensional, time dependent model and found the near-spherical particles yields slightly lower volatiles relative to other shapes. Their simulation results showed that for all the shapes, volatiles decrease with increasing particle size. Haseli et al. [59] also studied numerically the impact of particle shape and size on conversion time and final char density of biomass at high heating rate. Contrary to Lu [62], they found that less char (more volatiles) is produced in spherical particles compared to cylindrical and slab particles. Similar to Lu [62], their predicted results indicate that as the size of particle increases the final char yield increases.

Although particle size has a major influence on the pyrolysis process, literature review indicates the lack of a comprehensive study about it. The objective of this chapter is to use the proposed model in previous chapters to investigate the influence of size distribution of solid particles in the bed on pyrolysis products. For this purpose three different packed beds are tested under similar operating conditions and the results are discussed in details.

6.2 Results and Discussion

In this section XDEM is used to investigate the impact of the size distribution of the solid particles in a packed-bed, on the amount of final char yield. For this purpose three different packed-beds are modeled which are formed with two particle sizes; $d = 2.5\ mm$ and $d = 10\ mm$ in a rectangular cube reactor.

Three cases are presented in Fig 6.2.1: case I, which includes only big particles; case II, in which only small particles exist; case III, where there is a mixture of small and big particles. The packed bed in case III is formed in a way that at the bottom of the bed, a layer of big particles with about 30 mm height exists. At the top of it, there is a layer of about 20 mm of small particles. This sequence repeats once more to produce a packed-bed with about 100 mm height.

In all three cases the same mass of beech wood is used. The height of the beds are about 100 mm for the case II and III, while it is about 110 mm for the case I. The hot nitrogen with the flow rate of $2.5 \times 10^{-3}\ m^3 s^{-1}$ and the temperature of 1200 K is injected from the bottom of the reactor. The walls are assumed to be adiabatic in each case. The solid particles are initially at 300 K containing moisture 30% wb. Figure 6.2.2,6.2.3 and 6.2.4 show the temperature evaluation in the solid and gas phases at different times for three cases. In order to have better insight into the bed, only half of the bed and half of the gas phase are shown in these figures.

Higher void space near the wall causes higher flow rate passing around the particles located

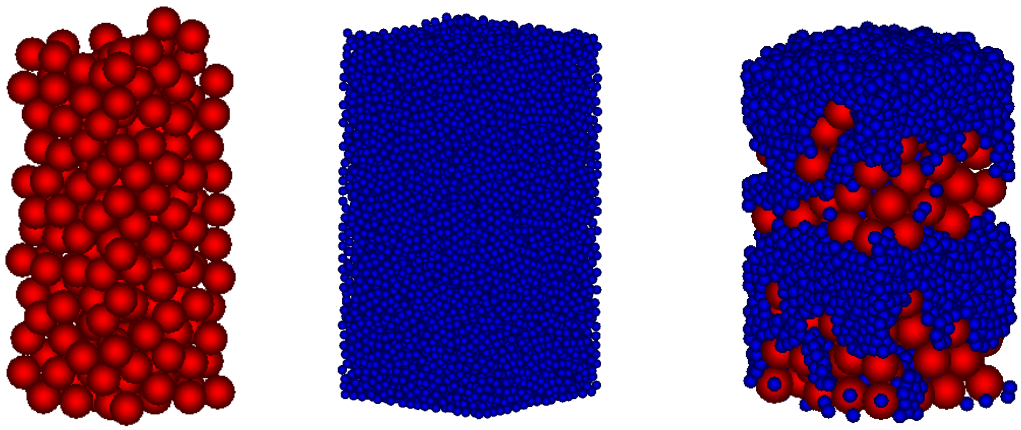

(a) Case I **(b)** Case II **(c)** Case III

Figure 6.2.1: Problem configuration

near the wall, hence heat exchange between the gas and the solid is stronger there. This is the reason why particles close to the wall have higher temperatures compared to particles at the center of the packed-bed.

As it can be seen in fig 6.2.3 for the case II, the observed temperature gradient in the bed is in a narrow layer of about 2 or 3 cm, while the temperature difference between the solid particles and the surrounded gas phase is very small. This is due to the high rate of convective heat transport between two phases, so that the inlet hot gas losses almost its entire thermal energy as soon as it touches the cold particles. As a result, gas reaches with low temperature to the particles above this narrow layer and can not heat up them.

Larger particles have less surface area for heat exchange and lower convective heat transfer coefficient. Hence in case I, when the hot gas touches the first layer of the cold particles, it does not lose its entire thermal energy, therefore it still has considerably high temperature for particles downstream. This can explain the wider range of temperature variations observed in fig 6.2.2. So that in the case I at $t = 300\ s$, about 9 cm of the bed is at temperature between the inlet gas temperature (1200 K) and 700 K, while it is about 2 cm for the case II.

In the case III, similar to the case I and II, it is seen that due to the wall effect the temperature of the particles near the wall is a bit higher than the particles located at the center of the bed. Here, the interesting point is that small particles at higher positions have higher temperature compared to the big particles at lower position (see fig 6.2.4). As it was explained before, this is due to the fact that the inlet gas after passing through the big particles still has considerably high temperature. Furthermore, the small parti-

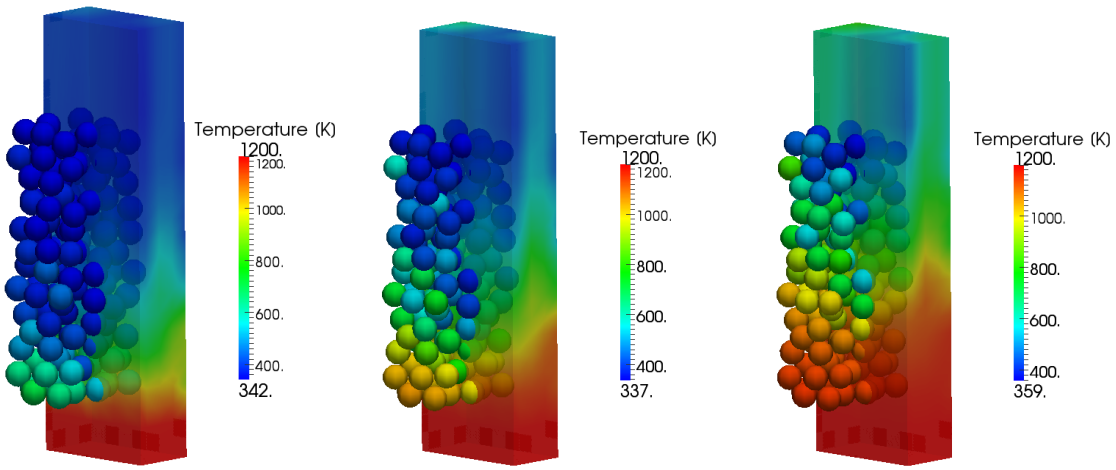

(a) $t = 100\ s$ **(b)** $t = 200\ s$ **(c)** $t = 300\ s$

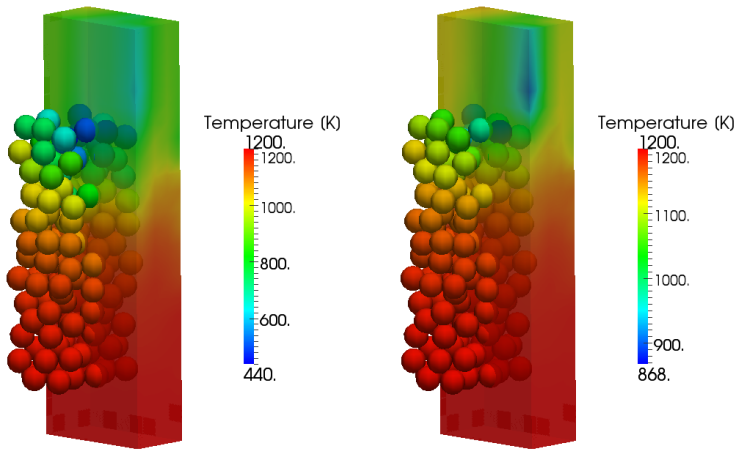

(d) $t = 400\ s$ **(e)** $t = 500\ s$

Figure 6.2.2: Particle temperature and gas temperature for case I at different time

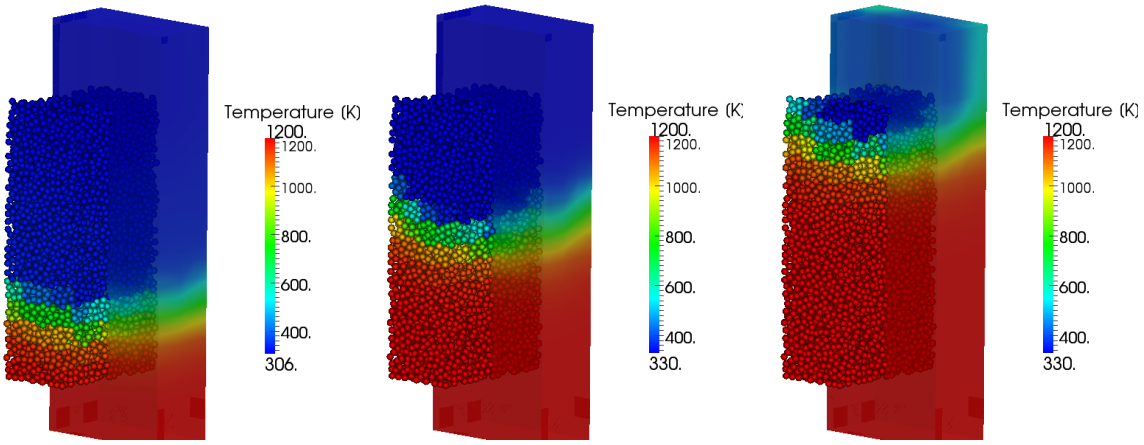

(a) $t = 100\ s$ **(b)** $t = 200\ s$ **(c)** $t = 300\ s$

Figure 6.2.3: Particle temperature and gas temperature for case II at different time

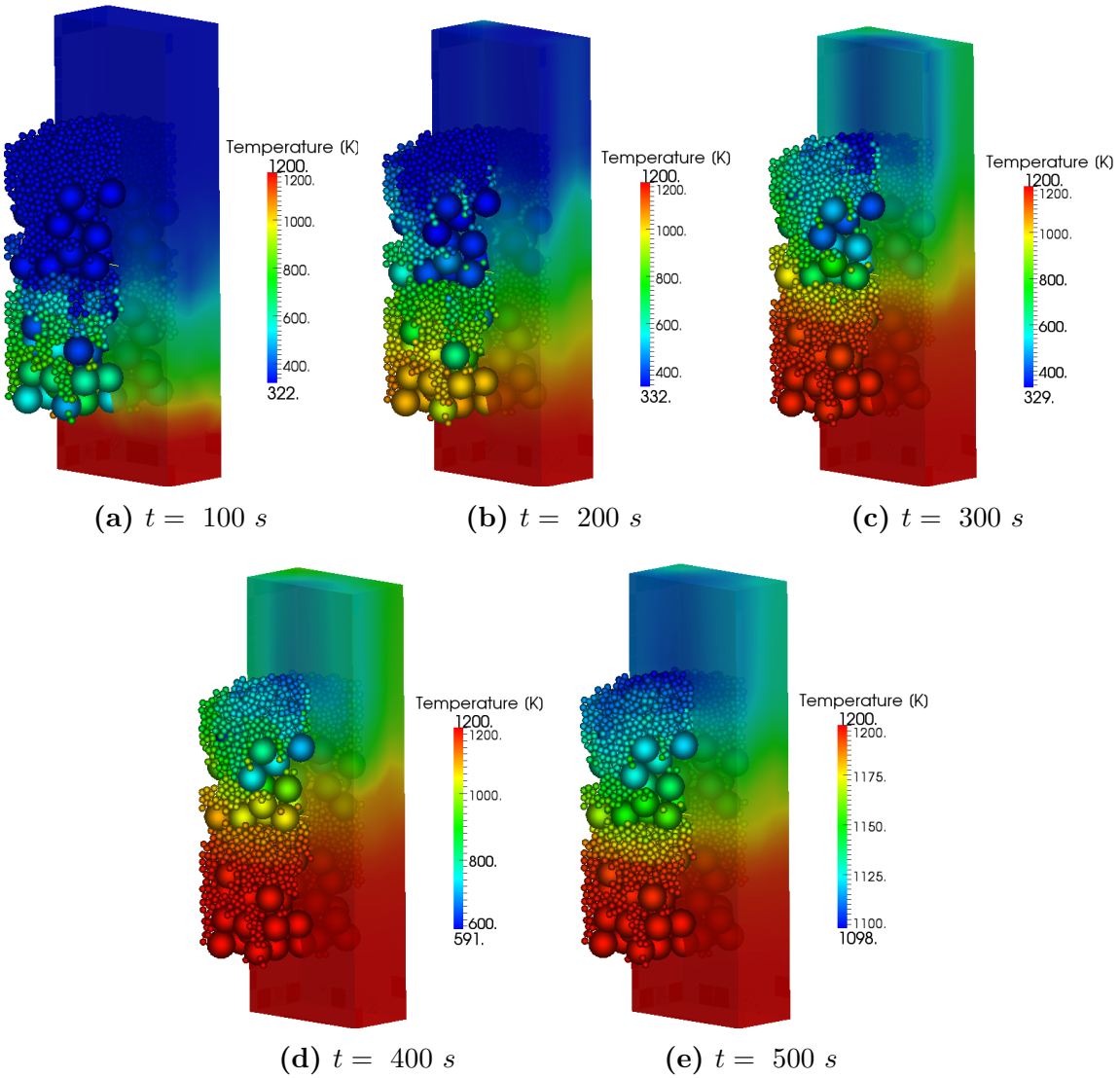

(a) $t = 100\ s$ **(b)** $t = 200\ s$ **(c)** $t = 300\ s$

(d) $t = 400\ s$ **(e)** $t = 500\ s$

Figure 6.2.4: Particle temperature and gas temperature for case III at different time

cles located above them have bigger heat exchange surface and higher convective heat transfer coefficient. Then gas loses its remaining thermal energy within this layer. The temperature of small particles may rise above the big particles located below them, as they have small volume. This can be observed in fig 6.2.4. Larger temperature difference between big particles and gas phase and smaller difference between small particles and gas phase, confirms this explanation. This is the main difference between case III and two other cases, which influences the conversion of biomass significantly.

Figure 6.2.5 illustrates the moisture loss of particles for case III at different times. In order to depict clearly inside the bed, just half of the bed is presented in this figure. Due to the convective transport, drying may start at temperature lower than boiling point. However drying rate increases with an increase in temperature. Impact of convective transport on drying is more pronounced for the small particles as a result of larger S_p/V_p compared to

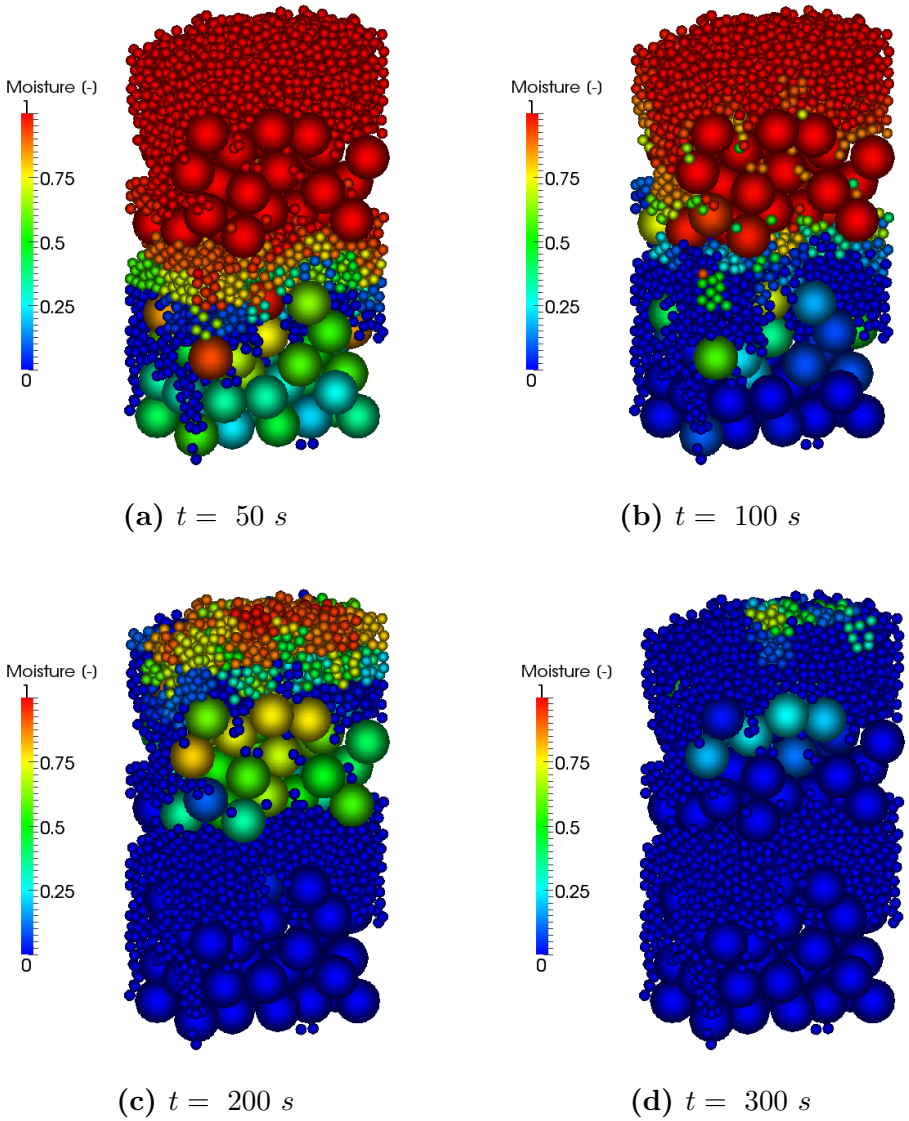

(a) $t = 50\ s$ **(b)** $t = 100\ s$

(c) $t = 200\ s$ **(d)** $t = 300\ s$

Figure 6.2.5: Moisture loss in particles for case III at different time

the bigger particles; hence small particles may be dried at the lower temperature. For this reason and also because of the higher convective heat transfer coefficient (as explained before), the small particles are dried faster than the big particles even though they are located at higher position.

Since the small particles are dried faster, pyrolysis may start earlier than the big particles below them. Therefore, it is expected the wood conversion in the bed has similar pattern as water loss as presented in fig 6.2.6.

Figures 6.2.4, 6.2.5 and 6.2.6 can be summarized in fig 6.2.7. In this figure moisture loss, wood consumption and mean-temperature evaluation of a small and a big particle (located close to the center line of the reeactor, at $z = 87\ mm$ and $z = 55\ mm$ respectively) are presented over the time. Drying of the small particle is shorter and starts earlier. The

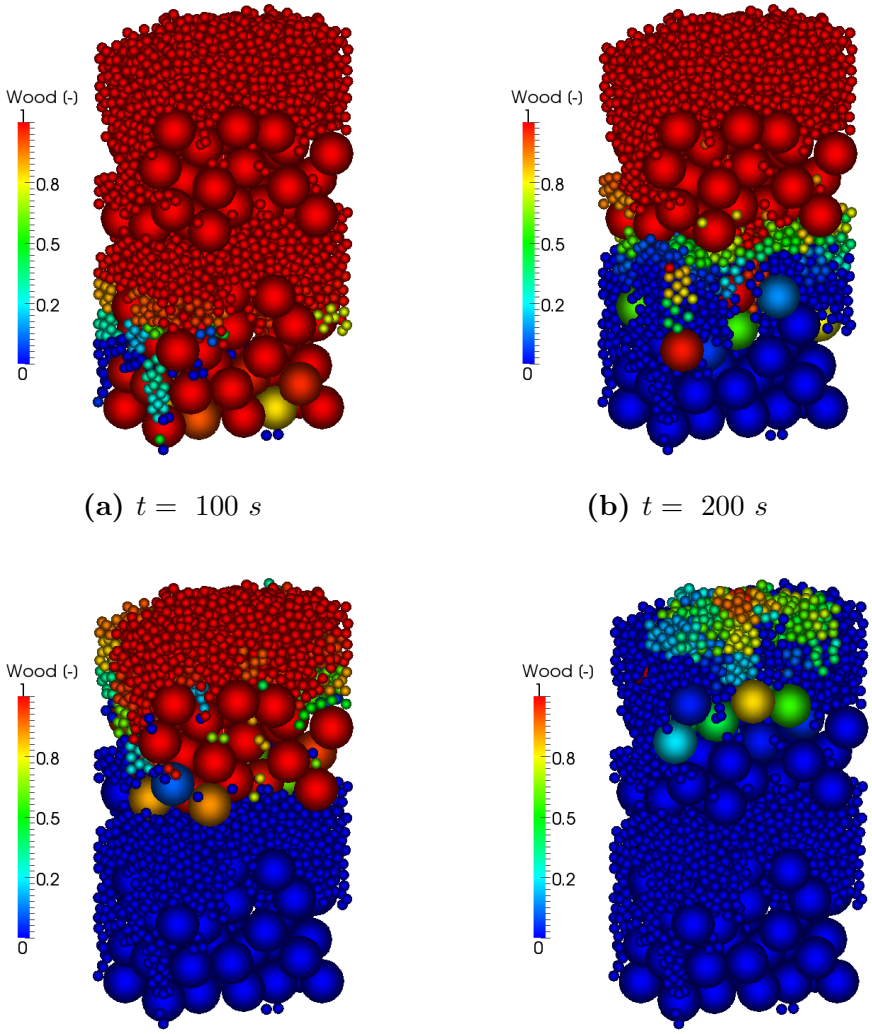

(a) $t = 100\ s$ **(b)** $t = 200\ s$

(c) $t = 300\ s$ **(d)** $t = 400\ s$

Figure 6.2.6: Wood conversion at different time for case III

results indicate that 90% of water content of small particle is evaporated at a temperature about 330 K, while in the big particle only 30% of water is evaporated in this temperature. For the big particle, some parts of drying occur even at mean-temperature about 440 K.

Since drying in the small particle is finished earlier, then temperature in this particle reaches earlier to the value in which devolatilisation can start. So that at about $t = 270\ s$ when pyrolysis begins in small particle, the mean-temperature is about 560 K while the mean-temperature of the big particle is about 400 K and it is still in the drying period.

Similar to drying, it is expected that pyrolysis period of the small particle becomes much shorter than of the big particle, however the results show opposite. So that pyrolysis of the small particle takes about 100 s, while it is about 60 s for the big one. This can be explained by the fact that the inlet gas has lower temperature after heat exchange

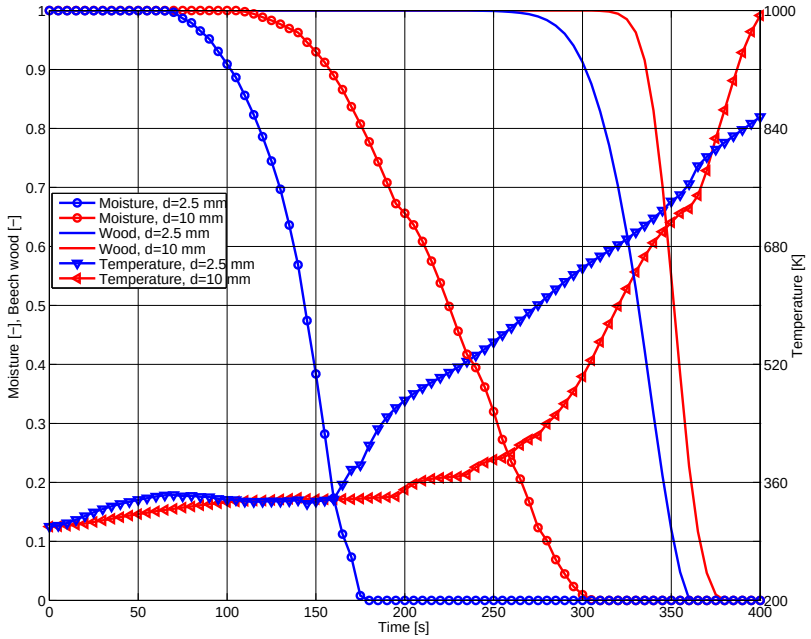

Figure 6.2.7: Variation moisture content, wood consumption and mean temperature for one small and one big particle in case III

with big particles. Therefore the small particles experience the lower gas temperature compared to the big particles. This results in a slower pyrolysis for the small particles, which is favorable for the char production.

Figure 6.2.8 shows tar mass fraction in the gas phase and the dimensionless char yield ($Char[-] = \frac{char\ mass}{initial\ wood\ mass}$) at different times for the case III. At $t = 100\ s$, $200\ s$ and $300\ s$ mass fraction of tar is higher near the walls of the reactor which is because of the wall effect. This results in stronger heat exchange between the solid and the gas phase, more intense reaction within the particle and hence more reaction products in the gas phase in that region. But at $t = 400\ s$, more tar is observed at the center of the bed. That is due to the fact that most of the raw wood near the wall have already been consumed, therefore there are less tar there.

Normally small particles are used to produce more volatiles (particularly tar) and big particles for more char yield. Hence, it is reasonable to expect in the case III more char to be gained from the bigger particles. However, fig 6.2.8 shows if the particles are mixed in a particular way, it is possible to produce more char in the small particles than the big particles. As it was explained before, since the gas around the small particles has lower temperature, they experience slower pyrolysis compared to the case that they are subjected directly to the hot inlet gas (like case II). Slow pyrolysis is associated with more char production, therefore higher percentage of wood is converted to char in these small particles.

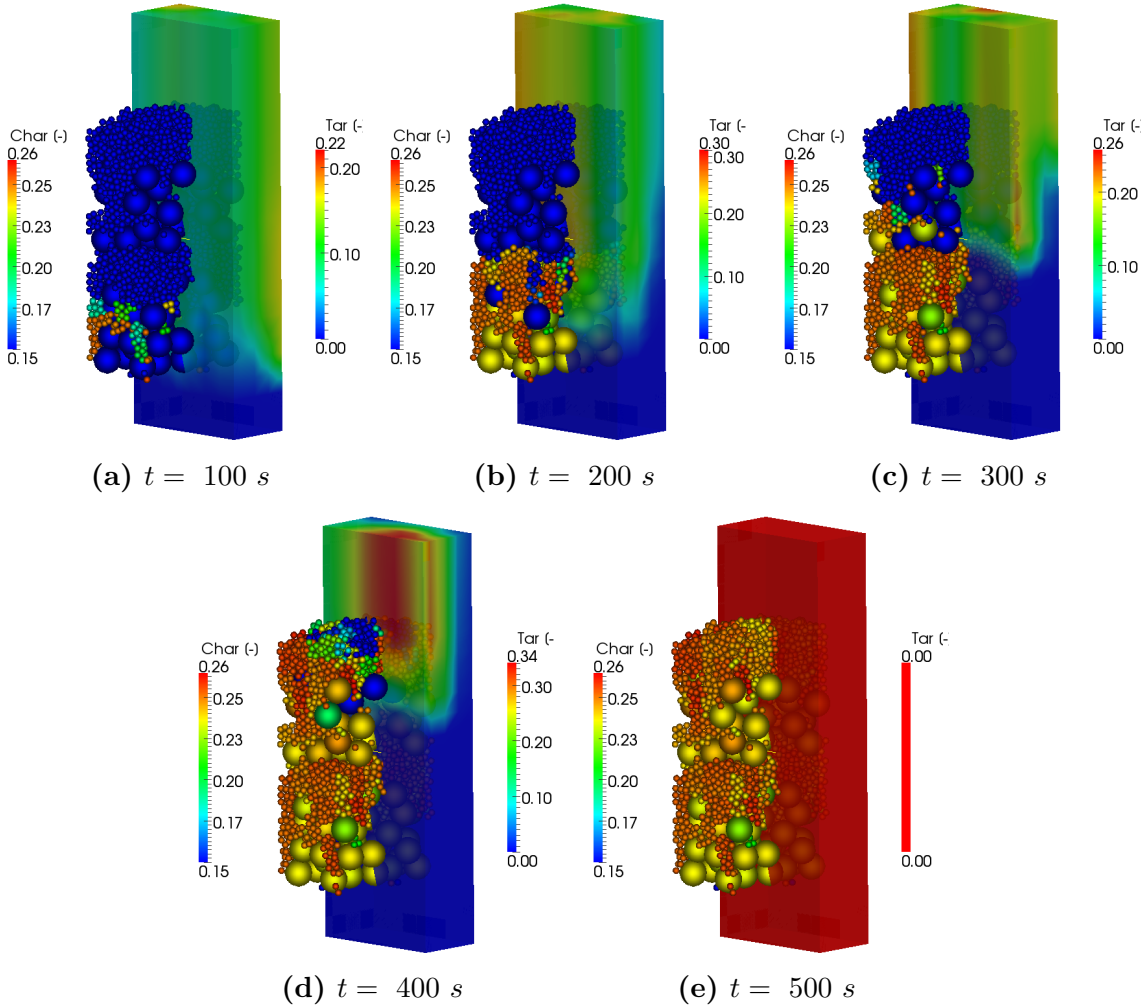

(a) $t = 100\ s$ **(b)** $t = 200\ s$ **(c)** $t = 300\ s$

(d) $t = 400\ s$ **(e)** $t = 500\ s$

Figure 6.2.8: Char yield in particles and tar mass fraction in the gas phase for case III at different time

For the bed with the big particles (case I), it is expected to gain high amount of char. Figure 6.2.9 shows more char is produced even at the higher position in the bed. Similar reason as of the case III (lower heat rate and hence slower pyrolysis), can explain this behavior in the case I.

Following fig 6.2.8 and 6.2.9, it can be expected to have more char yield as it goes toward top of the bed. According to the fig 6.2.3, there are very severe temperature gradients in the bed in the case II. Therefore less particles along the bed experience the low heat rate during their pyrolysis period. This means, there is no region in the bed with the high amount of the char yield, except for some scattered particles which is due to the non-uniformity of the void space in the bed that results in non-uniformity in the gas flow and the heat transfer.

Figure 6.2.10 shows the char yield of the whole bed versus time for two different flow rates. The results indicate that at the flow rate of $2.5 \times 10^{-3}\ m^3/s$ the same amount of

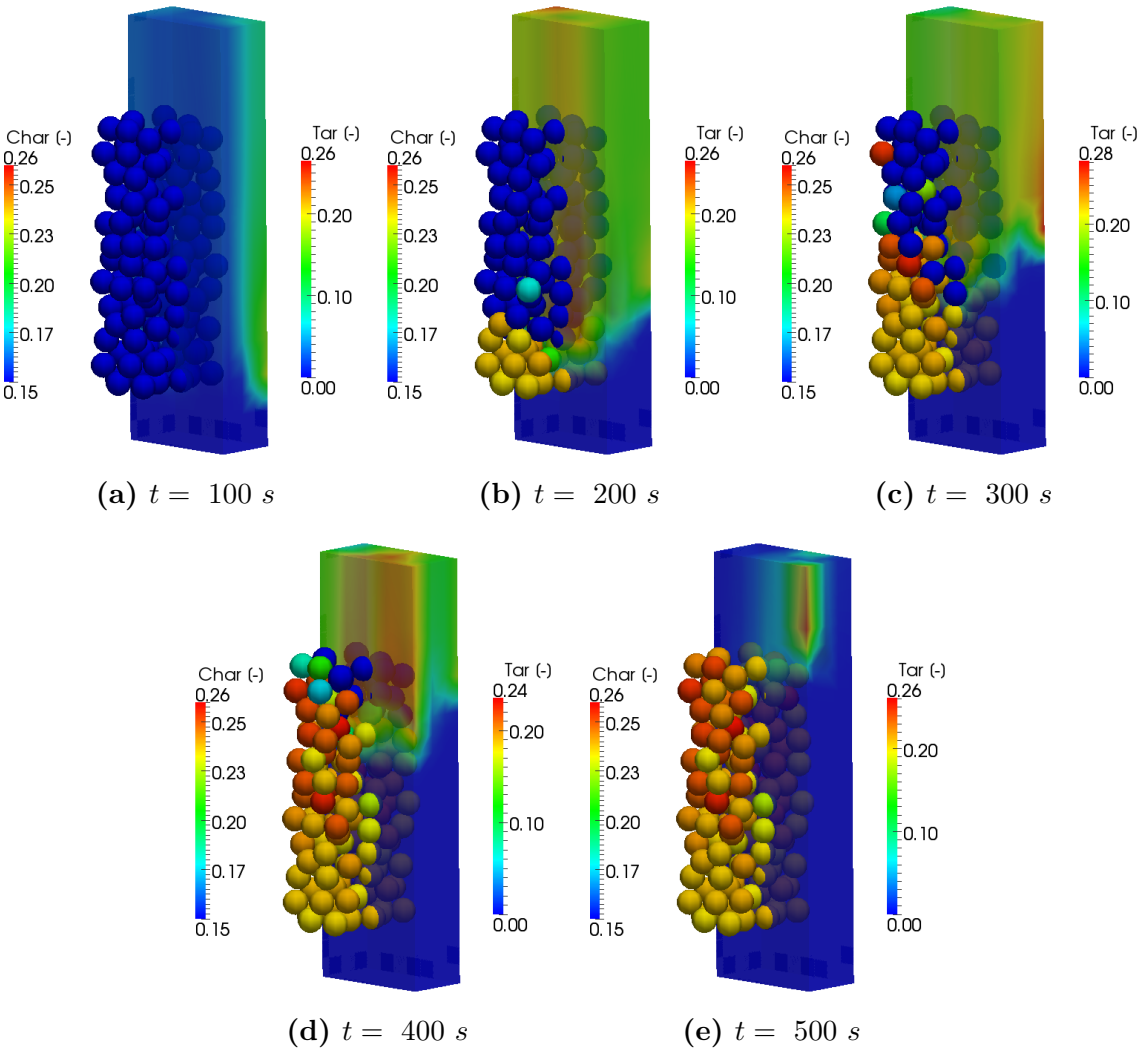

(a) $t = 100\ s$ **(b)** $t = 200\ s$ **(c)** $t = 300\ s$

(d) $t = 400\ s$ **(e)** $t = 500\ s$

Figure 6.2.9: Char yield in particles and tar mass fraction in the gas phase for case I at different time

char is produced in the case I and III, while 28% less char is produced in the case II. This difference even increases to 46% when the flow rate rises to $5 \times 10^{-3}\ m^3/s$. Increasing the flow rate has higher impact on the char production in the case II. So that by increasing the flow rate from $2.5 \times 10^{-3}\ m^3/s$ to $5 \times 10^{-3}\ m^3/s$, the final char yield in the case I and III decreases about 9%, while in the case II it decreases about 24%.

To show how much char yield in the small particles increases (using particular mixture), it is interesting to compare the char production of only small particles in the case III with case II. The results indicate that the final char yield of only small particles in the case III is about 31% and 51% more than the case II for the lower and higher flow rate, respectively.

6.3 Conclusions

The proposed numerical model in previous chapters was used to investigate the influence of specific particle size in combination with particle packing on the char production. For this purpose, three packed beds were generated consisting of the same mass but differing in particle sizes and packing of particles.

Predicted results show, when a layer of small particles is located between a layer of larger particles (case III), the average char yield from small particles increases by 31% when compared to a packed bed consisting of only small particles (case II). This is due to the fact that, small particles in case III experience lower heat rate compared to case II which is favorable for char production. When doubling the inlet flow rate the difference between the two cases even rises to 51% for the average char yield of small particles. These insights highlight an important effect arising from changes in particle size and particle packing on the pyrolysis product. Furthermore, the results show how layering of small and large particles may highly improve the char yield for small particles. Therefore, as a future work, it would be very useful to find the optimum size distribution, packing and operating conditions to maximize the yield of favorable pyrolysis products.

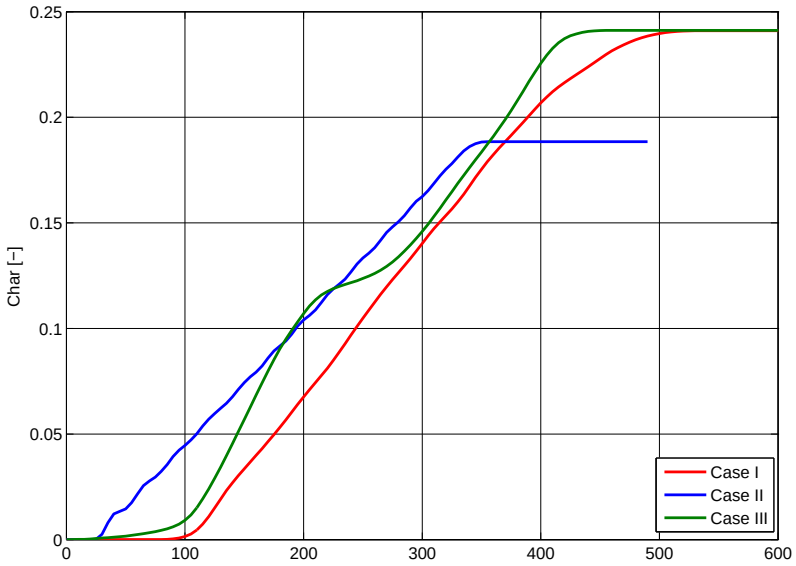

(a) $Q = 2.5 \times 10^{-3}\ m^3/s$

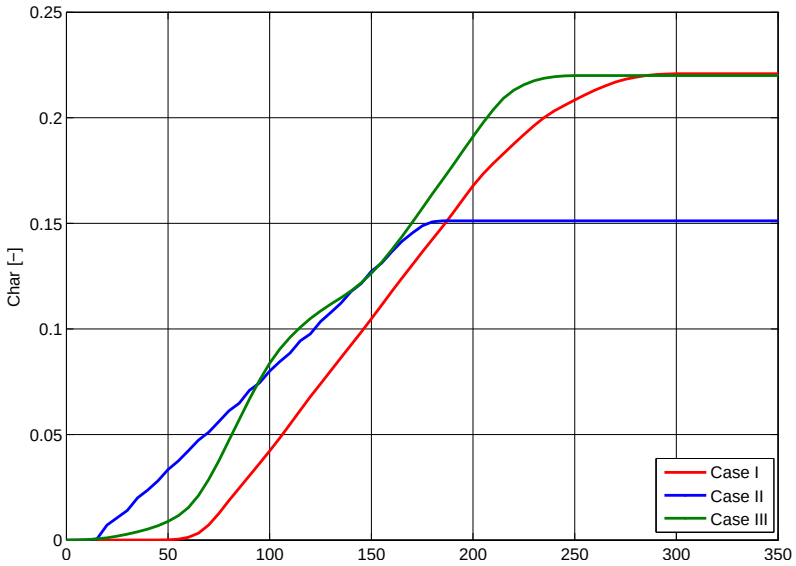

(b) $Q = 5 \times 10^{-3}\ m^3/s$

Figure 6.2.10: Total char yield of the bed for all three cases at two different flow rate

Chapter 7

Self ignition

In a packed bed of biomass, spontaneous ignition might occur due to oxidation of volatiles and causes a serious and unforeseen risk. On the other hand self-ignition may be useful in gasifiers and combustors if it occurs at the expected location and time. Therefore self-ignition can be categorized as a favorable or an unfavorable process, which can be controlled by managing some parameters such as gas velocity and temperature. The main aim of this work is to investigate the characteristics of self-heating and self-ignition in a packed bed. The influence of different parameters such as gas velocity, gas temperature, particle size and moisture content will be studied and discussed in details. [1]

[1]This chapter is written based on the following article:
Amir Houshang Mahmoudi, Florian Hoffmann, Miladin Markovic, Bernhard Peters, Gerrit Brem, Numerical modelling of self-heating and self-ignition in a packed-bed of biomass using XDEM, accepted on October 2015 to be published in "**combustion and flame**"

7.1 Introduction

Packed bed dryer is one of the most common types of industrial dryers, in which hot air flows through the bed and evaporates the moisture content of the particles. However, spontaneous ignition might occur due to the oxidation of volatiles and causes a serious and unforeseen risk. On the other hand, the self-ignition can be useful in gasifiers if it occurs at the expected location and time. Therefore, self-ignition can be categorized as a favorable or an unfavorable processes. This can be controlled by managing some parameters such as gas velocity and temperature [71].

Different experimental investigations have been conducted on self-ignition of various materials such as coal, RDF (Refuse Derived Fuel) and sewage sludge [100, 101, 102]. Moreover, ignition time and temperature for different types of wood samples were measured by Shi et al.[103]. Anez et al. [104] analyzed the emitted gases of various fuel samples and found that it is possible to detect incipient spontaneous combustion processes using measurements of CO and CO_2 emissions during heating process. Torrent et al. [105] studied the influence of some factors (such as chemical composition, physical treatments and flammability characteristics) on self-ignition of biomass fuel. They reported that the chemical composition of the biomass has an overriding role in characterizing the self-ignition tendency. Yafei et al. [106] investigated the altitude effects on spontaneous ignition characteristics of wood. The results showed that mass loss rate of wood at high altitudes (3650 m) was higher than the one at low altitudes (50 m), while ignition delay time of the sample at high altitude was shorter.

Ejlali et al. [107] studied numerically the self-ignition of a wet coal stockpile. They developed a correlation to estimate the time that a typical coal stockpile can be kept safe as well as the maximum temperature inside the pile. Gao et al. [108] proposed an analytical model based on the principle that the spontaneous ignition is determined by the combination of convective heat transfer between the gas flow and the particles and the heat generated by the oxidation reactions. Blijderveen et al. [109] used a similar model to predict the ignition temperature and ignition delay for different types of fuel. Although the analytical model can predict the ignition temperature well, it is not able to calculate ignition delay. This is due to the fact that the effect of the heat released by particles upstream on particles downstream in the bed is neglected. As a results, the position where ignition starts cannot be calculated.

A literature survey indicates that there are few works investigating the parameters involved in spontaneous ignition of biomass fixed-bed. More knowledge about self-ignition allows designers to control this process either as a favorable or unfavorable phenomena. Therefore, the objective of this chapter is to use a comprehensive and precise numerical

model (chapter4) to predict self-ignition in a packed-bed of biomass at different operating conditions. The effect of different parameters such as gas velocity, gas temperature, particle size and moisture content on self-ignition will be investigated; in each case the ignition delay and ignition position will be calculated. Prediction of the position that ignition starts is one of the most challenging part of the work and to the best knowledge of the authors, no related study has been yet reported in the literature in this regard.

In this chapter, a map is presented which related gas temperature, gas velocity, ignition delay and ignition position together. This results provide a guidance for design and operation of packed bed dryers or gasifiers. Moreover, to examine the accuracy of the model, the predicted results are compared with experimental data.

7.2 Validation

In order to validate the numerical model, the predicted results are compared with experimental data, conducted in the Energy Technology group of University of Twente [18]. The reactor has an inner diameter of 200 mm, an overall height of 4.55 m, and a possibility of fuel layer height up to 1 m. The insulation is made out of two components with a low thermal mass which ensures very low heat losses and accumulation during experiments. Air is fed into the reactor from below the grate and it can be preheated by an electric heater (see Fig. 7.2.1).

Comparisons are done with three experiments; Exp-1: initial moisture content of 30% and flow rate of 16.95 m^3/hr, Exp-2: initial moisture content of 20% and flow rate of 16.95 m^3/hr and Exp-3: initial moisture content of 20% and flow rate of 11.30 m^3/hr

In fig 7.2.2, temperature at different heights of the reactor are compared with the measurements for the Exp-1. According to the experimental setup, the inlet temperature increases gradually from ambient temperature to 523 K and it is kept constant until 2570 s (when devolatilization is almost finished). During this period O_2 concentration at the inlet is 3%. After this period, when there are mostly char combustion/gasification in the bed, concentration of O_2 increases to 10%. At the same time temperature decreases to ambient temperature [18].

Pyrolysis starts first in particles close to the inlet and then continues very slowly. Although the amount of volatiles released by these particles is very small, these volatiles react with oxygen in the gas phase and produce heat. The generated energy is transferred to the particles downstream, increasing their temperature to a value which is slightly higher than the inlet gas temperature. Pyrolysis in a particle with a higher temperature is faster, resulting in more production of volatiles, more oxidation of the volatiles and generating

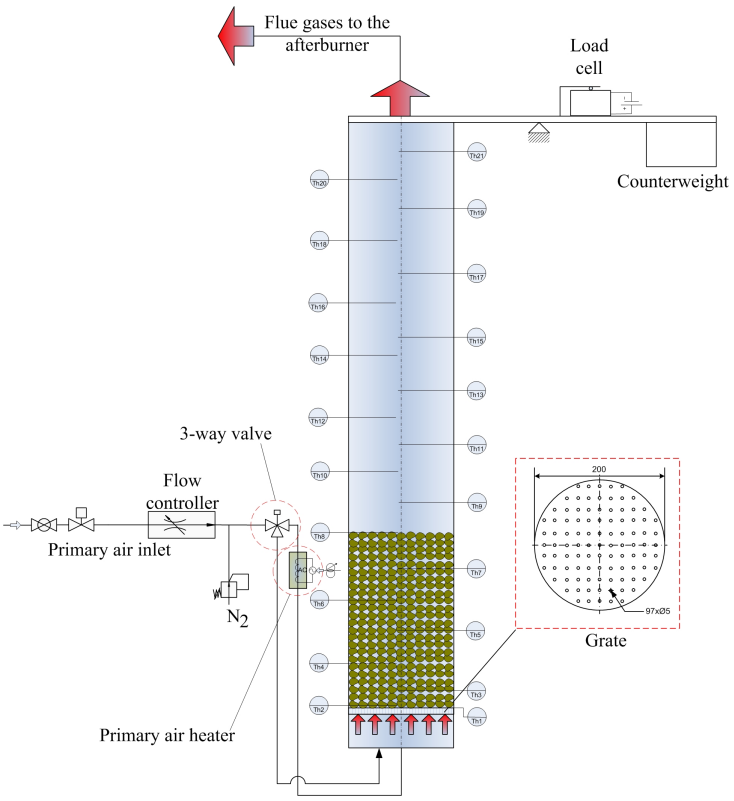

Figure 7.2.1: Experimental setup

more heat. When this process continues for a while, temperature will reach to a value in which ignition may occur. High temperature gradient at 10 cm above the grate after about 1200 s indicates this phenomena (Fig. 7.2.2). Therefore, it is concluded that the spontaneous ignition occurs in the region about 10 cm above the grate.

Similar behavior is observed for Exp-2. Due to the lower moisture content in the bed, compare to Exp-1, ignition occurs earlier. Comparison with measurements shows that numerical model could predict accurately different stages in this case (fig. 7.2.3).

In Exp-3, where lower flow rate is used, still similar stages for conversion of wood particles can be observed. However, ignition occurs at the different height in the bed (fig. 7.2.4). This is due to the energy balance between the convective heat transfer of the inlet gas and generated heat by oxidation of pyrolysis products. This will be explained in more details later in the results section.

By comparing the predicted results with these three experiments, it can be concluded that the numerical model is able to predict precisely spontaneous ignition characteristics (e.g., ignition delay and position of ignition).

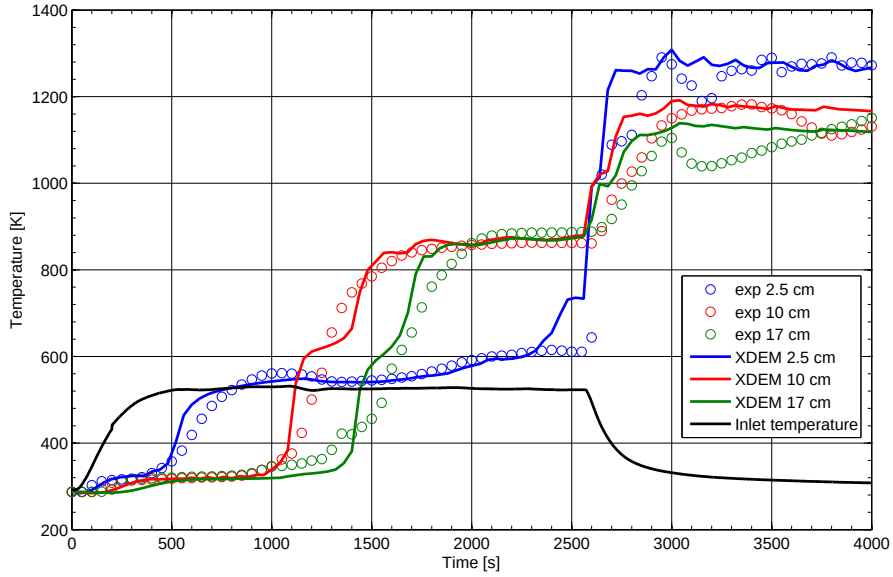

Figure 7.2.2: Comparison of predictions with measurement, temperature at different heights of the bed, Exp-1: initial moisture content of 30% and flow rate of 16.95 m^3/hr

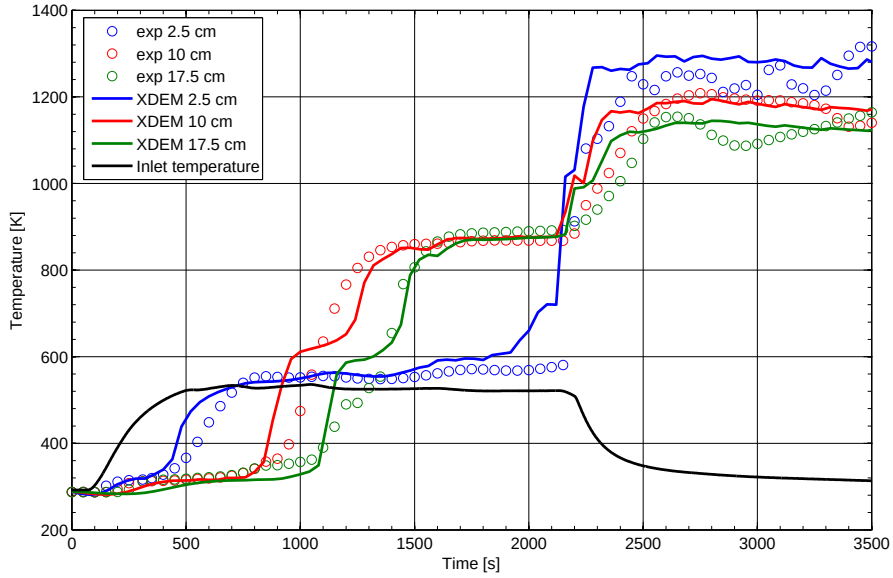

Figure 7.2.3: Comparison of predictions with measurement, temperature at different heights of the bed, Exp-2: initial moisture content of 20% and flow rate of 16.95 m^3/hr

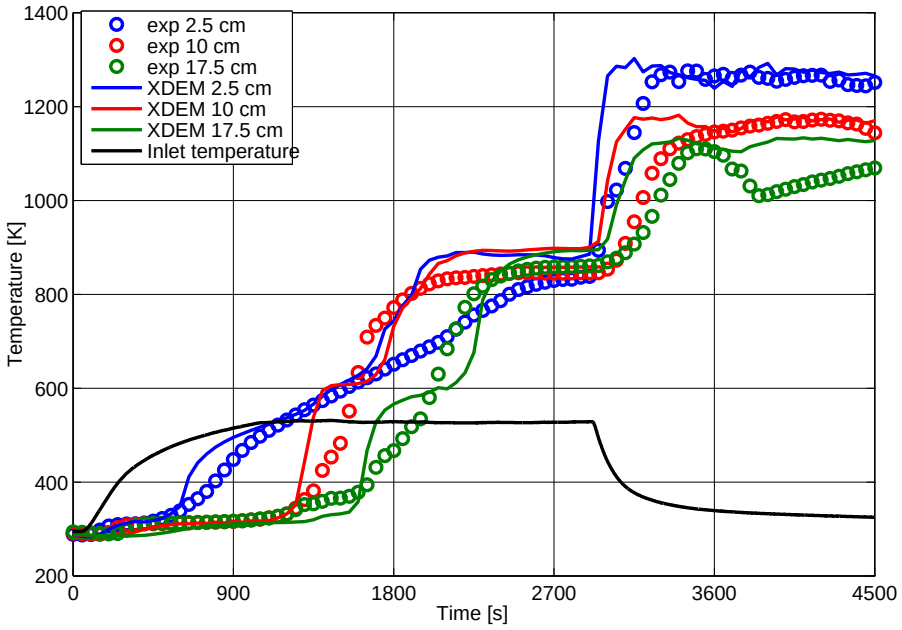

Figure 7.2.4: Comparison of predictions with measurement, temperature at different heights of the bed, Exp-3: initial moisture content of 20% and flow rate of 11.30 m^3/hr

7.3 Results and Discussion

In this section XDEM is used to investigate the impact of different parameters such as gas velocity, gas temperature, particle size and moisture content on the self-ignition characteristics. However, it would be very useful to illustrate first the details of the self-heating and self-ignition formation in a bed. For this purpose, a packed bed 16 cm in height is formed by beech wood particles with a diameter of 1 cm is studied (fig 7.3.1). Solid particles are initially at room temperature and they contain 20% moisture. Hot air at a temperature of 533 K and velocity of 0.4 m/s is injected at the bottom of the bed and leaves the reactor at the top.

Figure 7.3.2 illustrates moisture content in the solid particles and vapor mass fraction in the gas phase at different times. In order to show clearly vapor distribution in the gas phase and also the drying in the bed, an axial cut through the gas domain is shown in this figure. Moisture distribution in the particle phase shows the drying front in the bed, which starts from the bottom and moves upward. Due to the wall effect, larger void space near wall, heat exchange between the solid and the gas phase is higher near the wall. Therefore, drying of particles close to the wall is more intense than particles on the centreline of the bed.

Vapor in the gas phase can have two origins: one due to the evaporation of the moisture

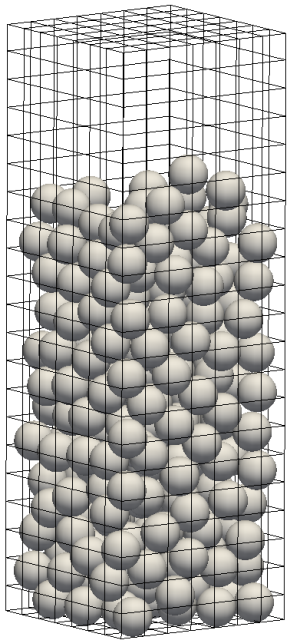

Figure 7.3.1: Simulation configuration

content in the bed and the other one is due to the pyrolysis of wood particles. As it will be presented later in fig 7.3.4, devolatilization will be observed after about 500 s. Hence it can be said that, until 500 s, the vapor in the gas phase is mostly due to the drying.

Temperature distribution, wood conversion and tar mass fraction in the bed are shown in fig 7.3.3 and 7.3.4 at different times. Hot air is injected into the bed at the bottom of the reactor. After exchanging heat with cold particles, it leaves the reactor with lower temperature from the top. At $t = 500$ s, some particles reach the gas' inlet temperature. Although 533 K is still a low temperature for pyrolysis, it can be started with a low rate, fig 7.3.4a. As a result, some combustible species as pyrolysis products are released into the gas phase. They might oxidize and generate some heat that will increase the gas temperature and consequently particle temperature. Hence at $t = 650$ s, temperature in the gas phase and in the particles raises above the gas' inlet temperature. This phenomenon is called self-heating which is the first step in the process that might finally result in spontaneous combustion.

An increase in temperature of solid particles will rise the pyrolysis rate and consequently the amount of pyrolysis products in the gas phase. More exothermic reactions release more heat, causing higher temperature which finally leads to self-ignition. Figure 7.3.3d shows that ignition occurs after 750 s at a height of about 7 cm.

Increase of tar mass fraction in the gas phase can be observed over time in fig 7.3.4. However, extinction of tar downstream is either due to mass transport into the particles located downstream or due to oxidation in the gas phase.

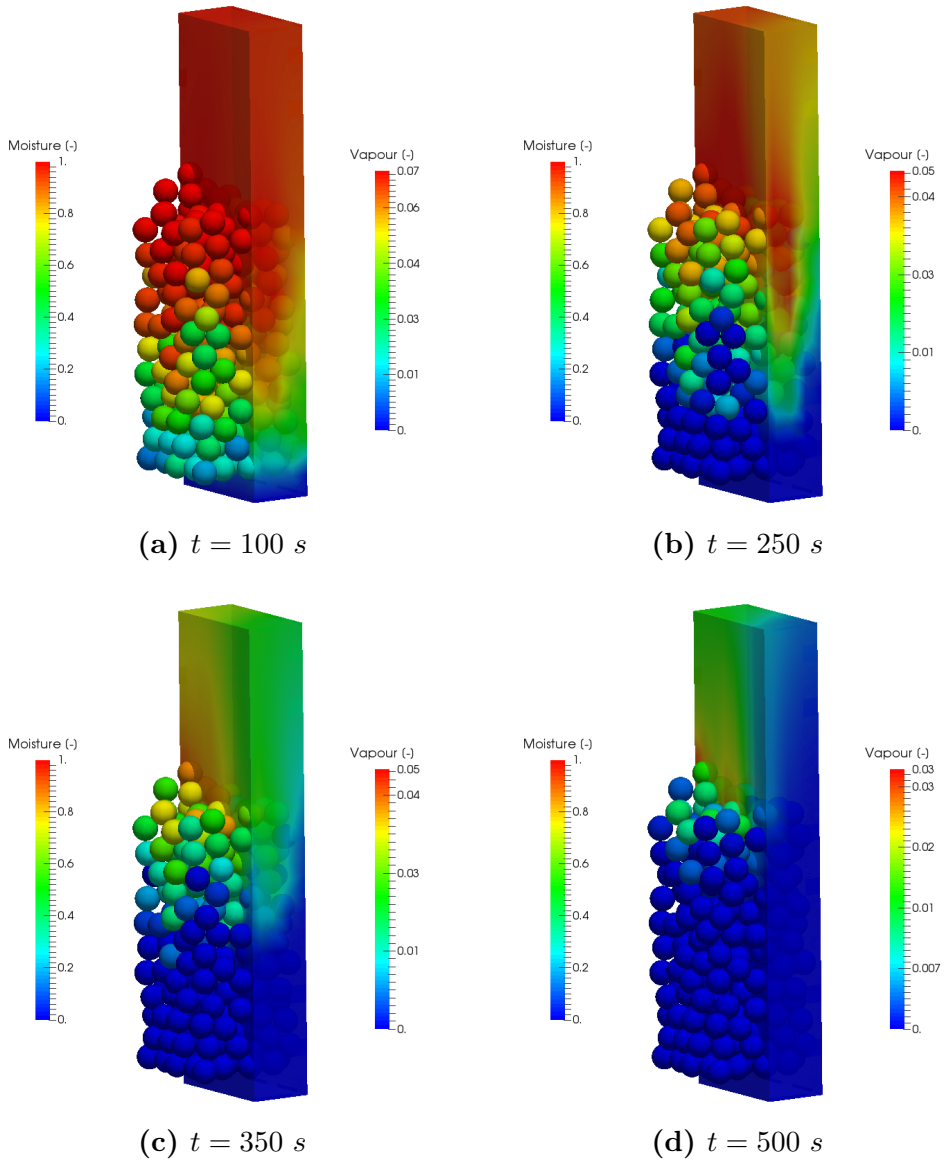

(a) $t = 100\ s$ **(b)** $t = 250\ s$

(c) $t = 350\ s$ **(d)** $t = 500\ s$

Figure 7.3.2: Moisture content in the solid particles and vapour mass fraction in the gas phase at different times

By comparing the temperature of the inlet gas and solid particles over time, it can be seen that for a period of time the inlet gas has a heating effect on the bed ($t = 250\ s$ and $t = 500\ s$). However, when the temperature of the bed rises due to self-heating, it has a cooling effect ($t = 650, 750, 850\ s$). This is the key point in the spontaneous ignition study. It means if the heat generation caused by the oxidation is greater than the heat loss due to the convection between the gas and the particle, temperature continuously rises and spontaneous ignition occurs.

Several parameters can influence this heating balance. Being aware of these parameters could help to understand and control the process precisely. In the following section the impact of process conditions such as gas velocity, gas temperature and fuel properties

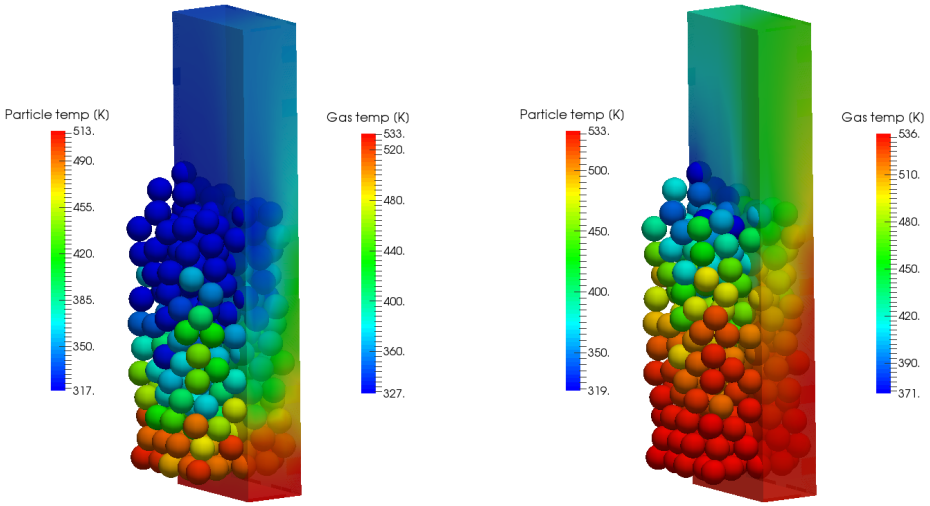

(a) $t = 250\ s$

(b) $t = 500\ s$

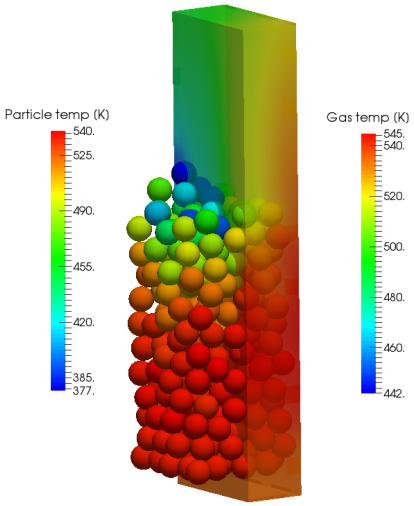

(c) $t = 650\ s$

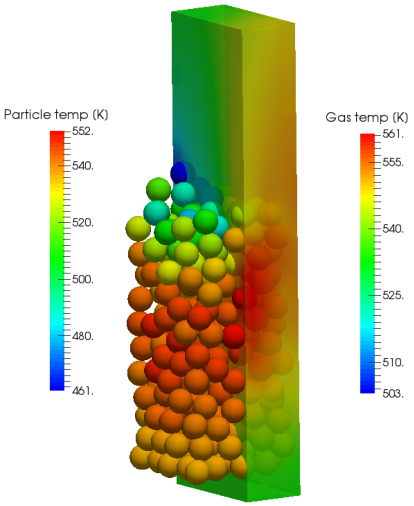

(d) $t = 750\ s$

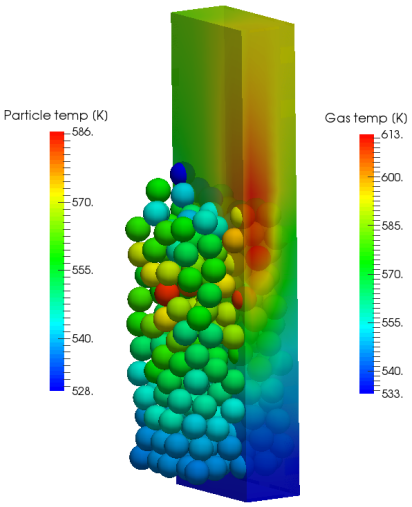

(e) $t = 850\ s$

Figure 7.3.3: Particle and gas phase temperature at different times

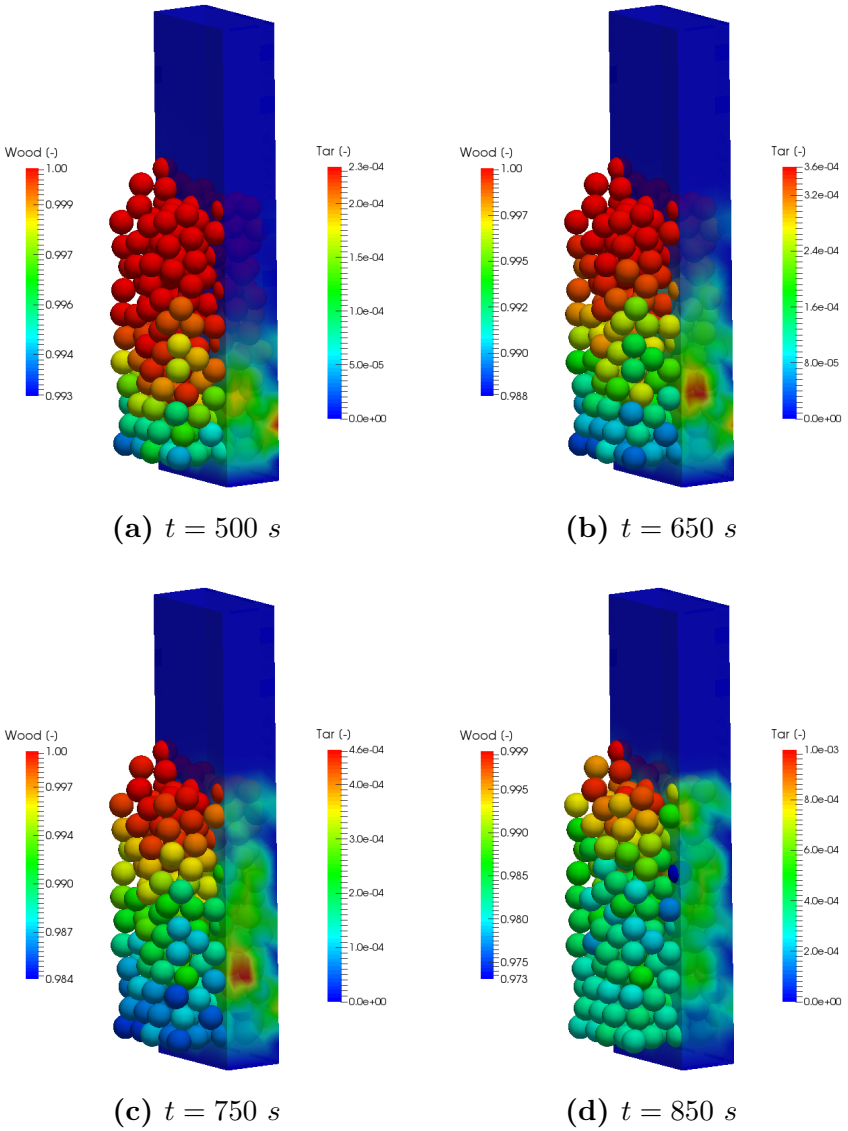

(a) $t = 500\ s$ **(b)** $t = 650\ s$

(c) $t = 750\ s$ **(d)** $t = 850\ s$

Figure 7.3.4: Particles' wood mass fraction and tar mass fraction in the gas phase at different times

such as particle size and moisture content on the self-ignition is investigated and results are discussed in details.

Figure 7.3.5 shows variation of ignition delay (for dry wood particles of 10 mm) and position of ignition with the inlet gas temperature for different inlet velocities. As it is expected, ignition delay decreases with increasing the inlet temperature. Higher gas temperatures shorten the heat-up period of particles. Moreover, devolatilization rate is more intense at higher temperature, therefore, more pyrolysis products are released to the gas phase that might cause earlier ignition.

Figure 7.3.5a indicates that regardless of the inlet gas temperature, ignition delay decreases with increasing the inlet gas velocity. Higher inlet gas velocities intensify the

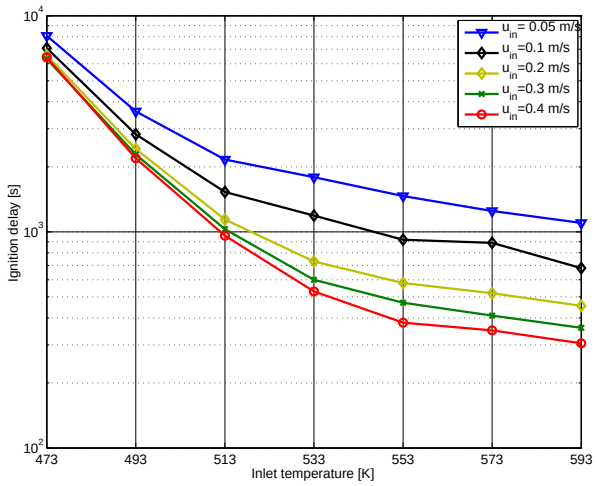

(a)

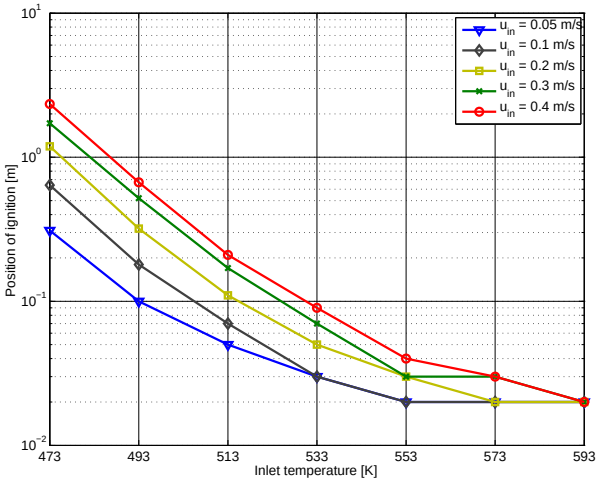

(b)

Figure 7.3.5: Position of ignition and ignition delay versus inlet temperature for different inlet velocities (particle diameter = 10 mm, moisture content = 0 %)

convective heat transfer between the gas and the solid phase. The time required for the particles to reach to the inlet gas temperature is reduced due to the enhanced convective heat transfer between the two phases. Moreover, with a higher flow rate, more energy is inserted into the bed. However, during the self-heating period the inlet temperature is lower than the bed's temperature and consequently retards the ignition formation due to a cooling effect. Nevertheless, the presented results show that the influence of the enhanced convective heat transfer on the heat-up phase is greater than on the cooling effect during the self-heating period. This explains why ignition delay is reduced by increasing gas velocity. This decrease is more pronounced at higher inlet temperatures. So that, at $T_{in} = 473\ K$ ignition delay decreases by 20% if inlet velocity increases from 0.05 to

0.4 m/s. Whereas at $T_{in} = 593\ K$ it is reduced by 72%.

Figure 7.3.5b shows that regardless of the inlet gas velocity, the ignition position approaches the inlet port with increase of the inlet gas temperature. However, at higher inlet velocities, ignition occurs at higher positions. This can be explained by the fact that at higher velocities, the generated heat at a specific height (as a result of oxidation of pyrolysis products) has less time for heat transfer with the solid particles around it. Therefore, the generated heat is transferred downstream by advection where it heats up more particles. Hence, self-heating (and consequently ignition formation) is shifted to a higher position.

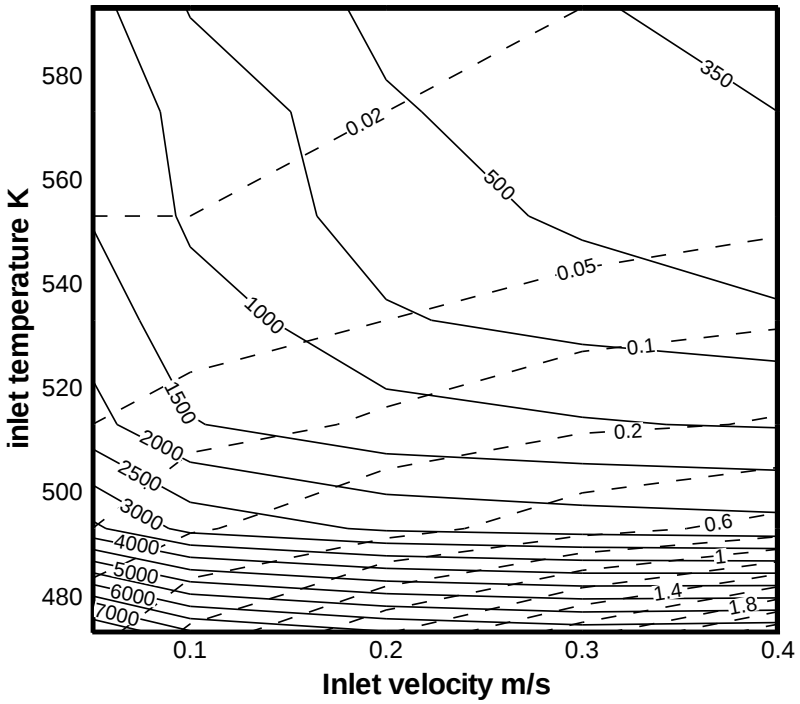

Figure 7.3.6: Contour of ignition delay (solid line) in s and height of ignition (dashed line) in m for a range of inlet velocities and inlet temperatures (particle diameter = 10 mm, moisture content = 0 %).

By combining fig 7.3.5a and 7.3.5b, a map of ignition delay and ignition position for a range of inlet gas velocity and temperature can be assessed, fig 7.3.6. This figure provides very useful information especially for designing a boiler. For example, it shows whether it is possible to have self-ignition in a certain time and position. Moreover, in the case of self-ignition, it will provide the inlet gas condition. It can also determine for a certain inlet condition at a boiler, when and where ignition occurs.

Figure 7.3.7 presents the influence of the moisture content on the ignition delay and ignition position for different inlet gas temperatures and velocities. Ignition delay increases

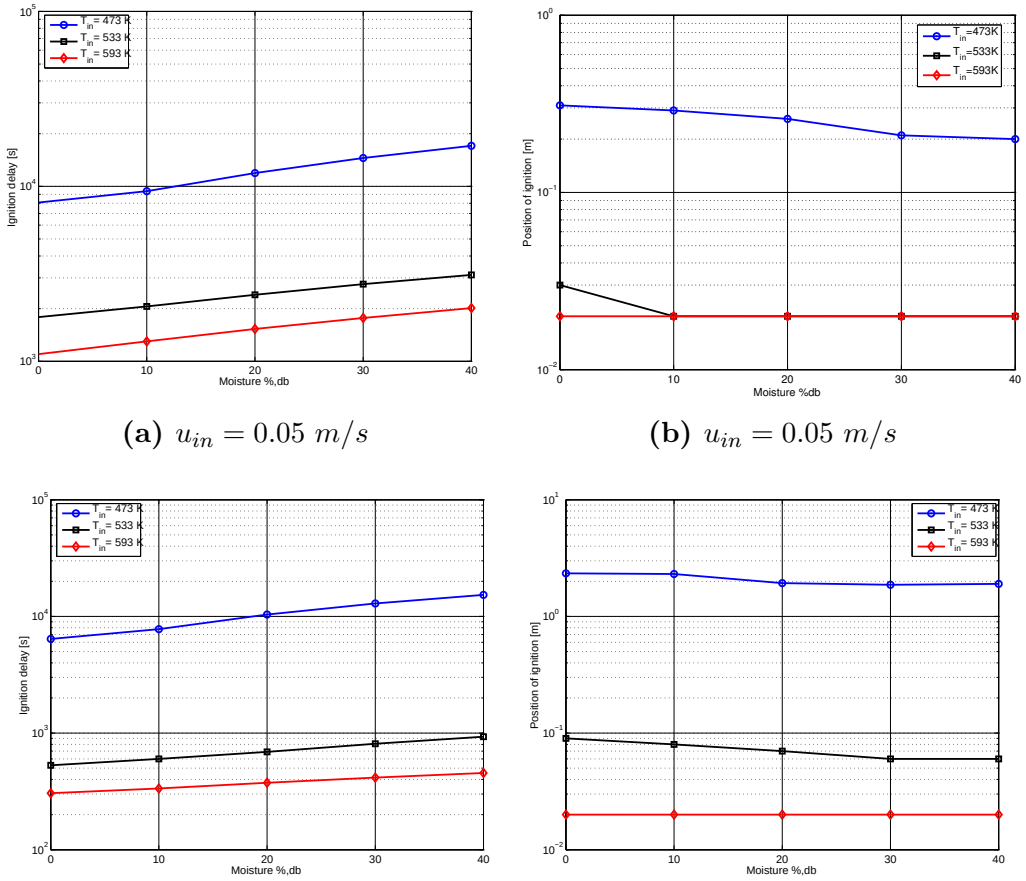

(a) $u_{in} = 0.05\ m/s$ **(b)** $u_{in} = 0.05\ m/s$

(c) $u_{in} = 0.4\ m/s$ **(d)** $u_{in} = 0.4\ m/s$

Figure 7.3.7: Position of ignition and ignition delay versus moisture content for different inlet temperatures and two inlet velocities (particle diameter = 10 mm)

with moisture content as it needs more time for drying. However, this increase does not have the same magnitude for all the cases.

Impact of moisture content on the ignition delay at lower temperatures is more pronounced at higher inlet velocities. By increasing 40% in moisture content of the bed at $T_{in} = 473\ K$, ignition delay increases 110% when $u_{in} = 0.05\ m/s$. While for $u_{in} = 0.4\ m/s$, it increases by 138%. However, at high temperature ($T_{in} = 593\ K$) this behavior is inverse. So that, 40% moisture content increases the ignition delay about 83% for $u_{in} = 0.05\ m/s$ while 49% for $u_{in} = 0.4\ m/s$.

Existence of water vapor in the gas phase increases convective heat transfer coefficient and improves heat transfer between the gas and solid particles. This causes the hot gas, which contains some water vapor from drying of wet particles, to lose its thermal energy more at lower part of the bed. Therefore less amount of energy remains for particles downstream. Hence, particles which are located at lower height in the bed reach earlier

to the pyrolysis stage compare to the case with no/less vapor in the gas phase. This leads to ignition to occur at lower height in the bed as can be seen in fig 7.3.7d.

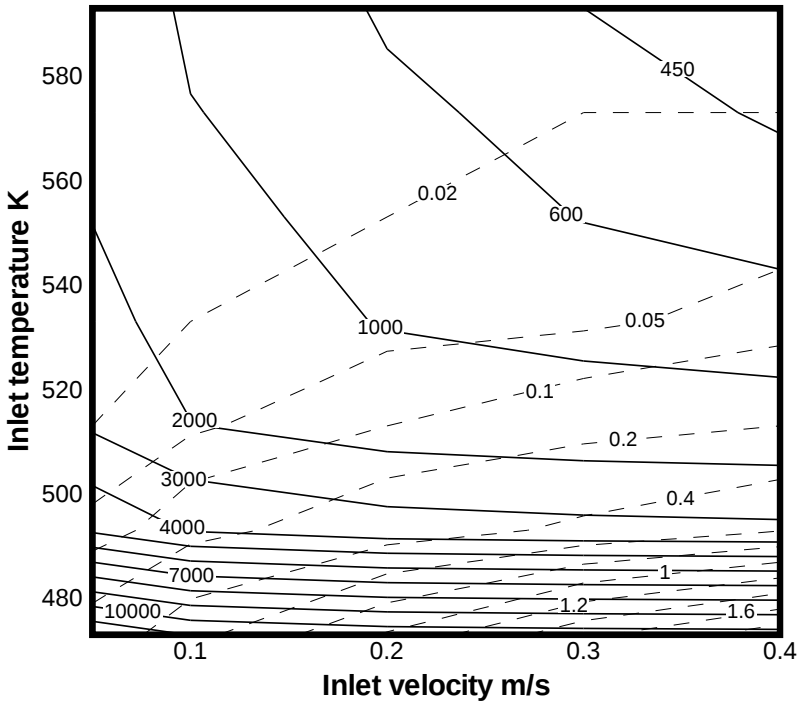

Figure 7.3.8: Contour of ignition delay (solid line) and height of ignition (dashed line) for a range of inlet velocities and inlet temperatures (particle diameter = 10 mm, moisture content = 20 %).

Similar to fig7.3.6, a contour of ignition height and ignition delay for a wide range of inlet velocities and temperatures is shown in fig 7.3.8. In this case 20% moisture was assumed in the bed. Ignition delay (dashed lines) is squeezed to the bottom while ignition position (solid lines) is expanded. This indicates a decrease in the ignition height and an increase in the ignition delay.

Figure 7.3.9 shows variation of the ignition delay and ignition position with the particle size for different inlet gas temperatures and velocities. The ignition delay increases with the particle size. This is due to the fact that larger particles have smaller surface area to volume ratios. Therefore, heat and mass transfer between the two phases decreases with the particle size. This increases the heating up period and slows down the pyrolysis, which causes the ignition to occur later.

Particle size has more influences at higher temperatures. When $T_{in} = 493\ K$, for $u_{in} = 0.4\ m/s$, by increasing particle diameter from 2.5 mm to 20 mm, the ignition delay becomes 1.7 times larger. While at $T_{in} = 593\ K$ it becomes 5.7 times larger. The results also indicate that the particle size has negligible impact on the ignition position.

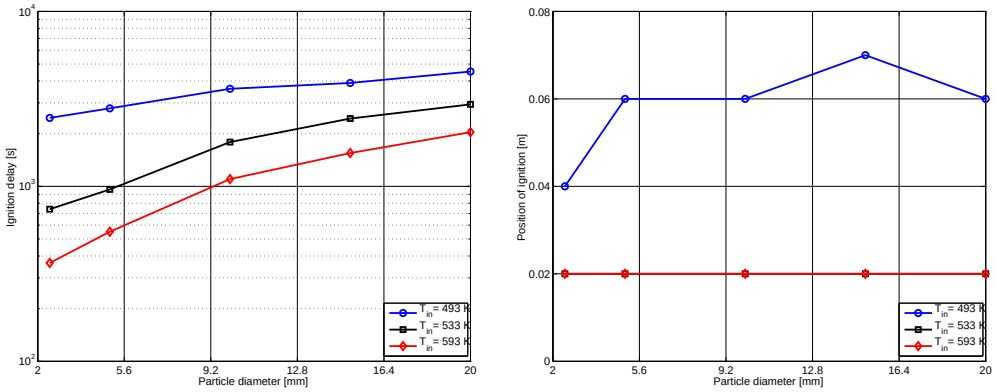

(a) $u_{in} = 0.05\ m/s$ **(b)** $u_{in} = 0.05\ m/s$

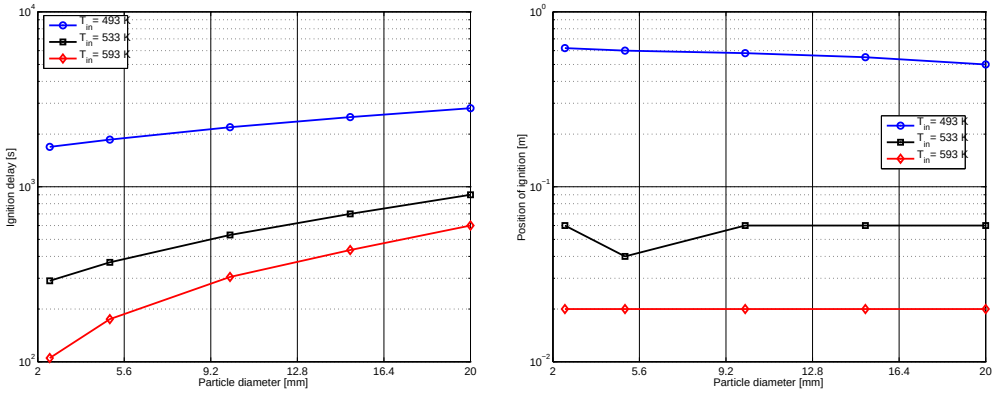

(c) $u_{in} = 0.4\ m/s$ **(d)** $u_{in} = 0.4\ m/s$

Figure 7.3.9: Position of ignition and ignition delay versus particle size for different inlet temperatures and two inlet velocities (moisture content = 0 %)

7.4 Conclusions

The main aim of this chapter was to investigate the characteristics of self-heating and self-ignition in a packed bed. However, study of spontaneous ignition is very complex due to many involved physical and chemical phenomena such as gas flow through the void space of the bed, heat and mass transfer between two phases, drying, devolatilization, gas phase reaction and char combustion and char gasification.

After describing the details of spontaneous ignition, the effect of different key parameters such as gas velocity, gas temperature, particle size and moisture content on self-ignition has been studied. The results have shown that ignition delay increases with increasing moisture content and increasing particle size, while it decreases with increasing gas velocity and increasing temperature. However the impact of moisture content and particle size on ignition delay does not have the same magnitude in all the range of temperature and velocity. For example, at low temperature, adding moisture to the bed is more pronounced at higher gas velocity while at high gas temperature, it has more influence on

lower gas velocity. Ignition height showed an increase with gas velocity and a decrease with gas temperature and moisture content. The results have indicated that particle size does not have a significant effect on ignition position.

Chapter 8

Semi-resolved model

The main aim of this chapter is to present a new approach for modeling multi-phase systems of granular media in which solid phases are fully resolved while the surrounding gas phase is semi-resolved. The presented method is based on a volume averaging model implemented in the XDEM framework in which the fluid phase is a continuous phase and individual particles are tracked with a Lagrangian approach. In the semi-resolved model the gas phase is described on a length scale smaller than the particles size. This method facilitates mesh generation for complex geometries. Moreover, it is computationally less expensive than a fully resolved model since it allows for coarser grids to solve gas flow through the void space between particles. In this chapter, the proposed model is used to predict heat-up of steel particles and pyrolysis of wet wood particles in a packed bed.
[1]

[1]This chapter is written based on the following article:
Amir Houshang Mahmoudi, Florian Hoffmann, Bernhard Peters, Semi-resolved modeling of heat-up, drying and pyrolysis of biomass solid particles as a new feature in XDEM, "**Applied thermal engineering**", 93 (2016) 1091-1104

8.1 Introduction

The proposed model in chapters 2, 3 and 4 used an Euler-Lagrange approach, where the fluid phase is a continuous phase but each particle is tracked with a Lagrangian approach. This approach includes a three-dimensional model for the gas phase and a one-dimensional model for the solid particles. Since the real particles are represented by the model, heat transfer between solid particles (conduction and radiation) are accurately predicted. The gas flow is treated as superficial flow through a porous media and thus is resolved with a low degree. This implies that the gas phase is described on a scale larger than the size of the particles. The predicted results were in satisfactory agreement with measurements for the presented cases of a monodisperse packed bed. This proves that even unresolved flow can predict the flow field accurate enough to describe the entire process within a monodisperse packed bed. This statement is valid for packed beds in which the particle size distribution is narrow and if the ratio between the particle size to the reactor size is small enough. Otherwise unresolved flow is not able to capture local flow conditions inside such an inhomogeneous packed bed.

In order to achieve a more precise description of the flow field some authors have successfully presented fully resolved models where the entire void space accessible by the gas phase is resolved in space [110, 111, 112, 113, 114, 115] . Atmakidis and Kenig [110] have used a fully resolved model in the gas phase and focused on mass transfer phenomena in the reactor. In order to avoid low-quality mesh elements at the contact points (particle-particle or particle-wall), all particles were shrunk by 2% of their diameter after the bed generation. Behnam et al. [113] have also used a similar method for modeling of heat transfer in a fixed bed.

Eventhough shrinking of particles is a commonly used technique for meshing around particle's contact points and it is used by several authors [110, 113, 114], it has some disadvantages: Shrinking of the particles increases the void space of the bed which directly influences flow rate and mass transport in the reactor. Furthermore, this technique removes the physical contact between particles which results in two problems: First, conduction between particles cannot be considered immediately by contact detection schemes. Second, in case of particles moving in the bed (either due to external forces or due to shrinking of particles as a result of a chemical reaction) prediction of force interaction between particles and re-meshing the bed is a complicated and computationally expensive task.

Kriebitzsch et al. [115] used Immersed Boundary method combined with a CFD approach to simulate fully resolved gas flow in a fluidized bed. They found that average DEM gas-solid force is about 33% smaller than the value calculated from a fully resolved model.

A fully resolved gas phase model predicts more precisely the flow field inside a packed bed than an unresolved gas phase approach (average model). Nevertheless, a fully resolved model requires a very fine mesh to properly account for the shape of the void space between particles. This fact considerably increases CPU time and decreases the efficiency of the model especially in case of beds large in scale. Furthermore, during mesh generation of state-of-the-art fully resolved models particles are slightly reduced in size and flattened at the point of particle neighbour contact in order to avoid problems with distorted cells. The objective of this chapter is to propose an approach for which the solid phase is fully resolved while the gas phase is semi-resolved. This method is based on a volume averaging model implemented in the XDEM framework in which the fluid phase is a continuous phase and individual particles are tracked with a Lagrangian approach [116, 117, 14]. For such a semi-resolved model, the gas phase is described on a length scale smaller than the particles' size.

The main difference between the presented model and a fully resolved model is that for the proposed semi-resolved model, regardless the shape of particles and morphology of the void space in the bed, the grid is generated for the entire bed. The static grid does not need to be regenerated in case the solid particles of the bed move in space, only cell properties have to be updated. This implies the following advantages: Mesh generation is facilitated even for complex geometries. Furthermore, a coarser grid to solve gas flow through the void space can be used which improves calculation efficiency. The numerical model is compared with measurements and the simulation results are discussed in details.

8.2 Mathematical model

In XDEM particles may be of different shapes such as sphere, block or cylinder. Such a discrete particle may be considered to consist of different phases: Solid, liquid, gas or inert material. For the particle scale modeling it is assumed that particles are isotropic and properties change along the radius. The distribution of temperature and species within a single particle is accounted for by a system of one-dimensional and transient conservation equations for energy and species. Transport of gaseous species within the pore space of the particle is considered to obey Darcy's law. Subject to the boundary conditions specified by its surrounding gas, a particle is allowed to exchange heat and mass with its environment. The particle model has been described in full detail in chapters 2 and 3.

Particles forming a packed bed are exchanging energy, species and mass by means of convective transfer with the surrounding gas phase. Such packed beds may be treated as a porous media in which fluid flow behaves like an external flow. Gas phase is modeled in an Eulerian approach. For the addressed multiphase systems of a packed bed of particles

within a streaming gas an exact and detailed microscopic treatment of fluid flow and transport processes in individual channels of the tortuous void space between the particles (fully resolved method) is generally undesirable because such detailed solutions are presumed to be of little practical relevance [118] and computationally expensive. Thus, a valid approach is to describe the gas flow as one through a porous medium by averaging relevant variables on a coarser level. As extensively described by Hoffmann [14] the set of governing equations for the gas phase in such a multiphase system are obtained from volume averaging theory. Macroscopic governing equations for mass, momentum, energy and species conservation are obtained from the corresponding microscopic equations through an averaging process over a representative elementary volume (REV) [119, 47, 48]. For a given system three characteristic length scales are introduced: For the global system under study there exists a macroscopic length scale L. The choice of a REV introduces a length scale l_{REV} related to the dimension of this volume and the third one is a microscopic scale l_g representative of the void space. For any real porous flow it holds $l_g \ll l_{\mathrm{REV}} \ll L$ and in that case the medium is considered homogeneous within one REV [119, 47]. The formulation of the macroscopic equations for multiphase systems can further be classified into two groups depending on the number of phases included into the averaging process [120]:
Performing spatial averaging for each phase individually leads to the *multi-fluid model*. For each phase a set of conservation equations (mass, species, momentum and energy) is obtained and appropriate source terms account for any transfer between phases.
If spatial averaging is performed over all phases present in a multiphase control volume, a single set of equations is obtained. This is called *homogeneous model* and it is equivalent to the summation of the individual phase equations of the multi-fluid model.
Current state-of-the-art numerical models can be distinguished by their choice of REV. Previously presented models by Hoffmann [14] and Mahmoudi [117, 116] used REV being of an order larger in size than particle sizes (unresolved). For the approach proposed in this contribution a semi-resolved model is chosen. The idea is to combine the advantages of treating the flow as a continuous flow through a porous medium but attenuate the disadvantage that the REV must be of an order larger than the particle size.
Fig. 8.2.1 compares the REV of the unresolved and semi-resolved approach. In the proposed semi-resolved model the homogeneous approach is chosen to account for the flow of the continuous phase in all cells which are not fully occupied by the solid phase.

For the proposed model the spatially volume averaged conservation equations of the continuous phase are listed in table 8.2.1. It should be noted that for the momentum equation the homogeneous model is applied, whereas for conservation of energy and species solid and fluid phases are individually accounted for by a respective multi-fluid model.

Intrinsic properties of the packed bed may be evaluated directly from the particles' prop-

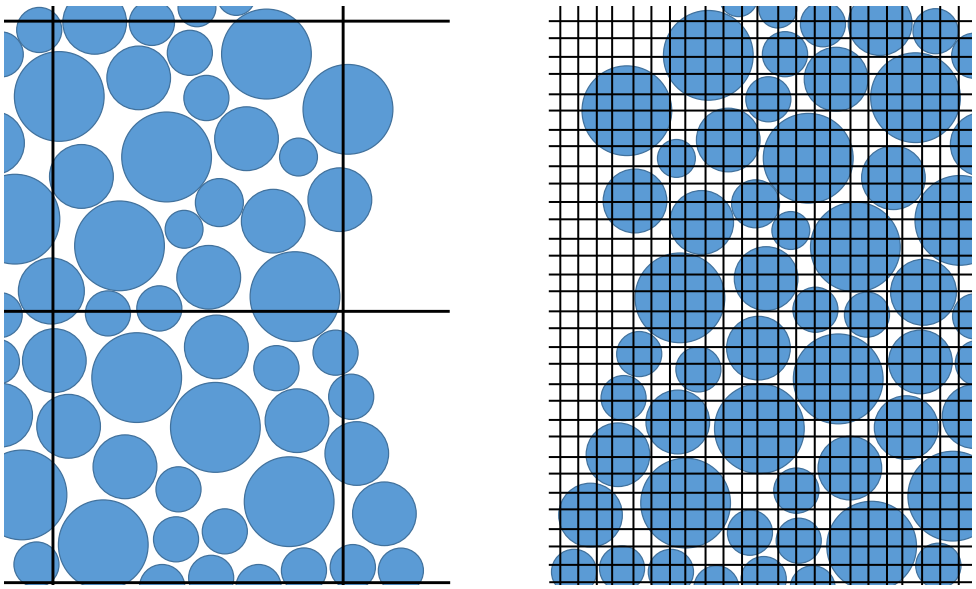

Figure 8.2.1: Comparison of REV for continuous phase for unresolved (left) and semi-resolved approach (right).

erties. Volume fraction of the fluid ϵ_f (equivalent to the bed voidage) is evaluated using the position and the volume of the particles. In the proposed model a hexaeder grid is used in the discretisation of the fluid phase. Grid cells have to be smaller in size than the smallest particle dimension. Particles contribute their volume to cells it overlaps with. More precisely, grid cells are distinguished into the following three categories:

- Fluid cells: Cells entirely filled with fluid and no solid particles near. These cells have a fluid volume fraction of unity. They do not take part in momentum, heat and mass exchange between the solid and fluid phase.
- Solid cells: Cells entirely contained within a solid particle's volume. These cells are excluded from the evaluation of the fluid flow since they are entirely occupied by the solid phase.
- Boundary cells: Cells partially located within one or more particles. These cells have a fluid volume fraction between zero and one and represent the locations where momentum, heat and mass transfer between the solid and the fluid phase take place.

This is schematically illustrated in fig. 8.2.2 and fig. 8.2.3 for three touching spherical particles. In fig. 8.2.2a solid cells are highlighted, whereas in fig. 8.2.2b boundary cells are marked. For a given particle i the contribution coefficient to one of its boundary cells j is calculated based on an inverse distance weighting approach as follows:

$$\omega_{i,j} = \frac{\frac{1}{d_{i,j}}}{\sum_k^N \frac{1}{d_{i,k}}} \tag{8.2.7}$$

Table 8.2.1: Coupling equations

- Continuity equation

$$\frac{\partial}{\partial t}\left(\epsilon_f \langle\rho_f\rangle^f\right) + \vec{\nabla}\cdot\left(\epsilon_f \langle\rho_f\rangle^f \langle\vec{v}_f\rangle^f\right) = \dot{m}'''_{s,f} \tag{8.2.1}$$

- Momentum Equation

$$\frac{\partial}{\partial t}\left(\epsilon_f \langle\rho_f\rangle^f \langle\vec{v}_f\rangle^f\right) + \vec{\nabla}\cdot\left(\epsilon_f \langle\rho_f\rangle^f \langle\vec{v}_f\vec{v}_f\rangle^f\right) = \vec{\nabla}\cdot\left(\epsilon_f \langle\vec{\tau}'_f\rangle^f\right) - \frac{\mu_f}{K}\epsilon_f^2 \langle\vec{v}_f\rangle^f - C\langle\rho_f\rangle^f \epsilon_f^3 |\langle\vec{v}_f\rangle^f| \langle\vec{v}_f\rangle^f \tag{8.2.2}$$

$$K = \frac{D_P^2\epsilon_f^3}{150(1-\epsilon_f)^2} \tag{8.2.3}$$

$$C = \frac{1.75(1-\epsilon_f)}{D_P\epsilon_f^3} \tag{8.2.4}$$

- Energy equation

$$\frac{\partial}{\partial t}\left(\epsilon_f \langle\rho_f\rangle^f \langle h_f\rangle^f\right) + \left(\epsilon_f \langle\rho_f\rangle^f \langle\vec{v}_f h_f\rangle^f\right) = \frac{\partial\langle p_f\rangle}{\partial t} + \epsilon_f \cdot \langle\vec{v}_f\rangle^f \cdot \vec{\nabla}\langle p_f\rangle + q'''_{s,f} \tag{8.2.5}$$

- Species equation

$$\frac{\partial}{\partial t}\left(\epsilon_f \langle\rho_{f,i}\rangle^f\right) + \nabla\cdot\left(\epsilon_f \langle\rho_{f,i}\rangle^f \cdot \langle V_f\rangle^f\right) = \sum_{i=1}^{M} m'''_{s,f,i} \tag{8.2.6}$$

where $d_{i,j} = |\vec{x}_i - \vec{x}_j|$ is the distance between the particle's centre and the centre of the cell as shown in fig. 8.2.4. Thus, a given particle contributes a fraction of its solid volume to its boundary cell according to the corresponding weight. Weights for a given particle with all its boundary cells N are designed in such a way that they sum up to unity. The fluid volume fraction $\epsilon_{f,j}$ of a cell j is then evaluated to:

$$\epsilon_{f,j} = 1 - \frac{1}{V_j}\cdot\sum_{i}^{M}\omega_{i,j}V'_i \tag{8.2.8}$$

where V'_i is the volume of the particle i remaining after the sum of the volumes of the solid cells (cells entirely contained inside particle i) have been subtracted.

Conservation equations for the continuous phase presented in table 8.2.1 contain volumetric source or sink terms that mathematically allow the coupling between the particulate

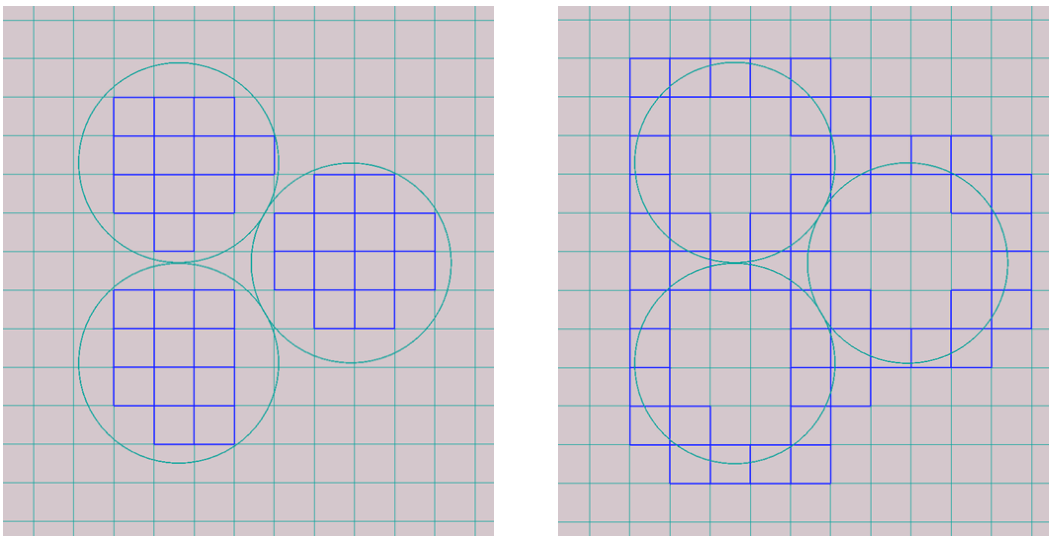

(a) Solid cells. **(b)** Boundary cells.

Figure 8.2.2: Schematic drawing highlighting the grid used for the semi-resolved method for three touching spherical particles immersed in a fluid

and the continuous phase. For heat and mass transfer between the two phases the following terms have to be evaluated:

$$\text{Species mass source terms: } \dot{m}'''_{s,f,i} \tag{8.2.9}$$

$$\text{Gas mass source term: } \dot{m}'''_{s,f} = \sum_i \dot{m}'''_{s,f,i} \tag{8.2.10}$$

$$\text{Heat source term: } q'''_{s,f} \tag{8.2.11}$$

As already mentioned the so-called boundary cells represent the location where heat and mass is exchanged between the fluid and the solid phase. Thus, a boundary cell receives source or sink terms for energy and species from all the particles contributing to it based on the above mentioned weights. In order to account for the temperature and composition gradients between a particle i and a boundary cell j modified weights $\omega^*_{i,j}$ are calculated as follows:

$$\omega^*_{i,j} = \frac{\omega_{i,j}(\theta_j - \theta_i)}{\sum_k^N \omega_{i,k}(\theta_k - \theta_i)} \tag{8.2.12}$$

where θ stands for temperature in the case of heat exchange and for partial density of species in the case of mass exchange, respectively. For a boundary cell j the total sink or source term is calculated by summing up the contributions of all contributing particles M. Thus, the volumetric heat source term from equation (8.2.5) in table 8.2.1 for a cell

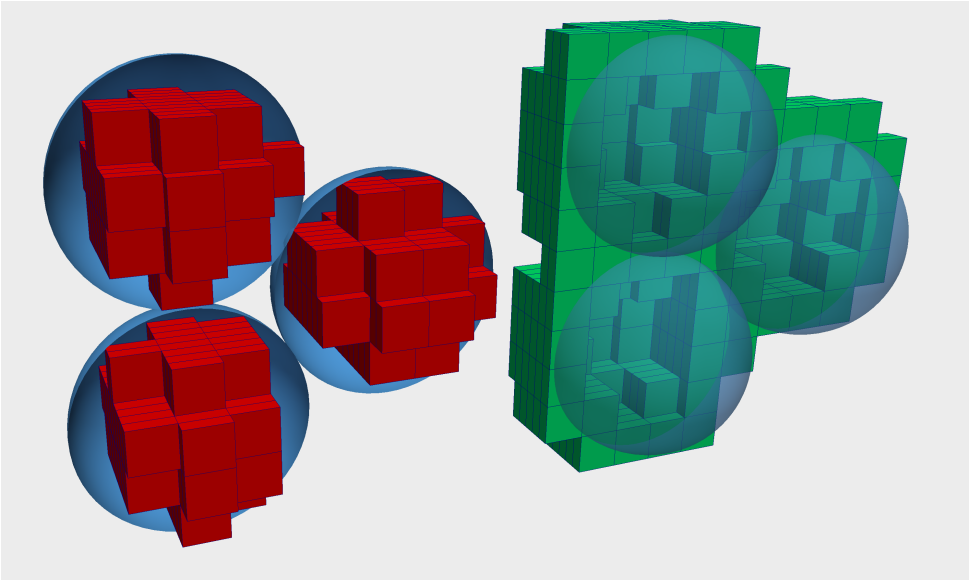

Figure 8.2.3: 3D visualisation of inner cells (red) and boundary cells (green) for three touching spheres.

j writes as:

$$q'''_{s,f} = \frac{1}{V_j} \cdot \sum_{i}^{M} \omega^*_{i,j} q_i \tag{8.2.13}$$

where q_i is the heat rate of particle i.

8.3 Validation

In order to validate the numerical model, the predicted results are compared with several experimental data for both single particle and packed bed. Yang et al. [8] studied experimentally the macroscopic hydrodynamic and heat transfer characteristics in some structured packed beds. The packed bed was formed by spherical steel particles with diameter of 12 mm with SC (simple cube packing) packing structure, fig 8.3.1. The solid particles are initially at the temperature of $60 - 65$ ℃. Cold air is injected to the channel to cool down particles to ambient temperature ($25 - 28$ ℃). Fig 8.3.2 and 8.3.3 illustrate that the numerical results are in a good agreements with measurements of outlet gas temperature over time and pressure drop over bed height at different Reynolds numbers. This proves that the proposed model predicts precisely hydrodynamic and heat transfer characteristics of a packed bed.

In a next validation step, it is concentrated more on the thermal degradation (pyrolysis) of solid fuel. Lu et al. [6] used near-sphere particle ($D = 9.5\ mm$) to study devolatilization

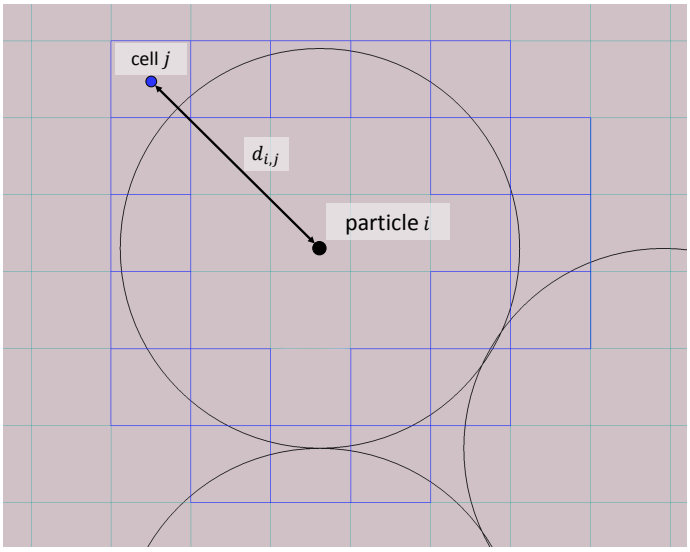

Figure 8.2.4: Weights for boundary cells (blue) use distance between particle centre and cell centre.

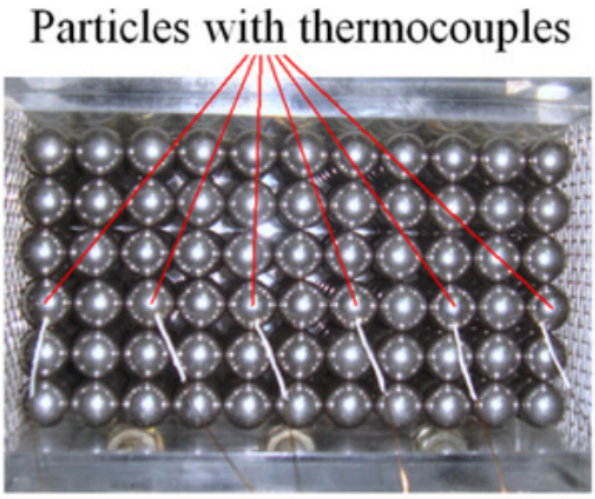

Figure 8.3.1: Real photos for SC (simple cube) packing structure [8].

of poplar wood. Gas temperature around the particle and average wall temperature of the reactor were measured 1050 K and 1276 K respectively and they were assumed to be constant during the experiment. The experiments have been conducted for two initial moisture contents (6.0 wt% and 40.0 wt%). Temperature distribution and gas flow pattern around the particle is illustrated in fig 8.3.4.

As it can be seen in fig 8.3.5 and 8.3.6, predicted surface temperature and mass loss of the particle (due to drying and pyrolysis) show good agreement with experimental data in both cases. During the conversion of wood particle, volatiles and tar leave the solid particle while char yield remains in the particle. The value of mass loss at the end of experiment indicates the percentage of the char yield.

Fig 8.3.7 shows mass fraction of tar around the particle at different times in case of 6.0

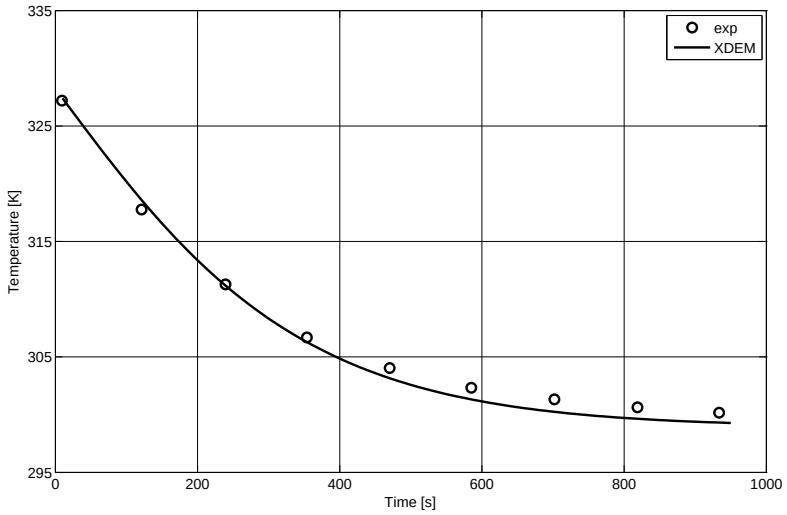

Figure 8.3.2: Temporal evolution of gas temperature at outlet - validation with experiments by Yang [8].

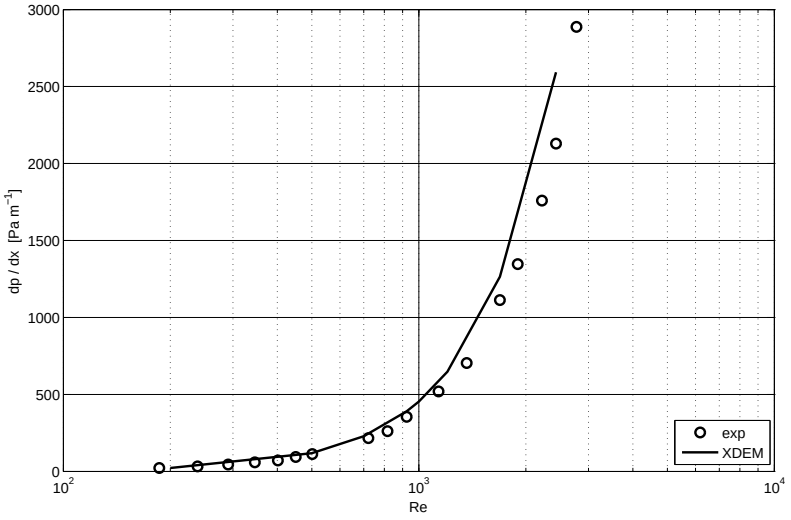

Figure 8.3.3: Pressure gradient over bed height at different Reynold numbers - validation with experiments by Yang [8].

wt%. At the earlier stage of the conversion ($t = 5\ s$ and $t = 10\ s$), considerable amount of tar is observed around the particle that propagates in the channel either by convection or diffusion. Towards the end of the conversion process ($t = 20\ s$ and $t = 30\ s$) tar production decreases and consequently mass fraction of tar in the gas phase decreases, due to less available raw wood inside the particle.

The numerical model was also tested with experiments conducted by Petek [7]. In his work, a spherical beech wood particle with diameter of 20 mm was used and it was sub-

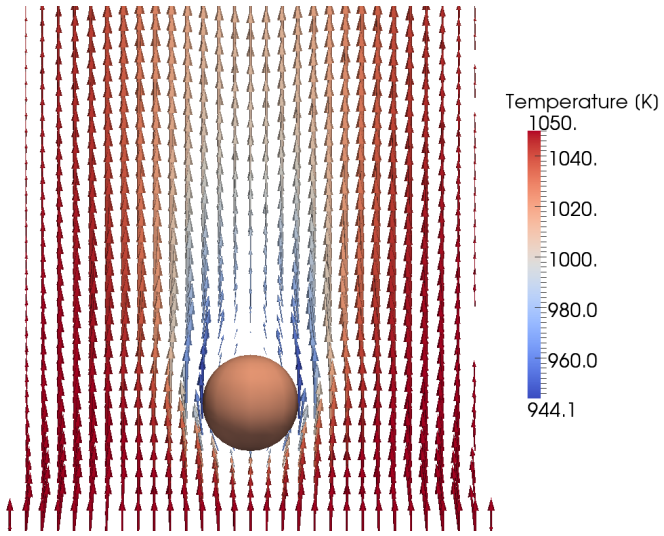

Figure 8.3.4: Velocity vectors for the flow field and gas phase temperature.

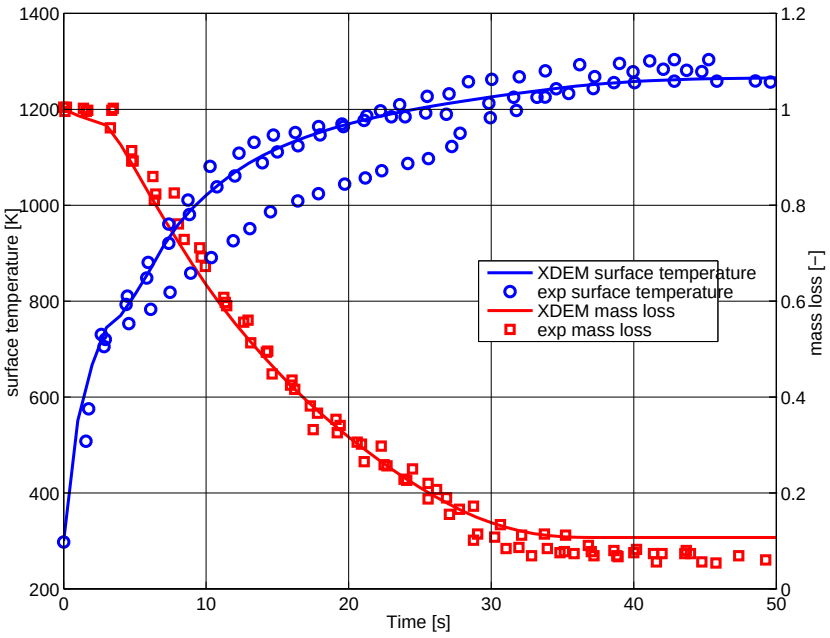

Figure 8.3.5: Validation with single particle experiments by Lu et al. [6]: Comparison of temporal evolution of mass loss and surface temperature for 6% initial water content.

jected by hot inlet gas with temperature of 1123 K. Predicted results for mass loss, center and surface temperature were compared with the measurements and good agreements was achieved, fig 8.3.8.

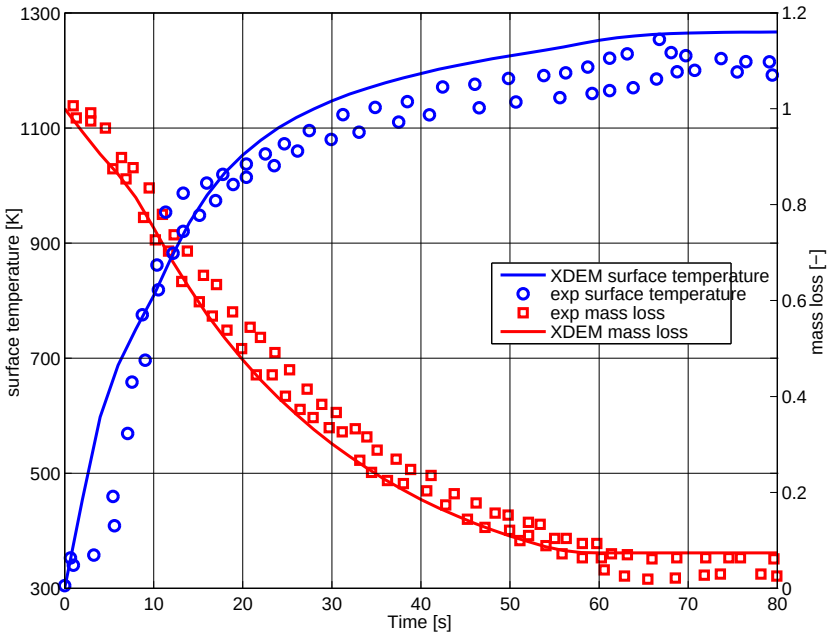

Figure 8.3.6: Validation with single particle experiments by Lu et al. [6]: Comparison of temporal evolution of mass loss and surface temperature for 40% initial water content.

8.4 Results and Discussion

In the last section, the numerical model was validated by comparing the predictions with several different measurements. The presented results proved that the current model is a reliable tool for prediction of devolatilisation of biomass. In this section XDEM is used to calculate drying and pyrolysis of wood particles in an heterogeneous bed formed by spherical particles of three different sizes (diameter of 5, 20 and 100 mm), fig. 8.4.1. Nitrogen with temperature of 1400 K is injected from the bottom and leaves the reactor from the top. Solid particles are initially at temperature of 300 K and contain 10% db moisture.

Different particle sizes and heterogeneous distribution of the particles in the reactor form a non-uniform porosity distribution inside the packed bed. This causes a non-uniform and complex flow field in the reactor. Figure 8.4.2 illustrates the gas flow in the void space between particles.

To understand better the gas flow in the reactor, porosity distribution and gas velocity at different cross sections of the reactor are shown in fig. 8.4.3. Void space values of zero correspond to the area inside the particles whereas void space equal to one indicates that there is no solid particle in that area. Accordingly, zero velocity is associated with

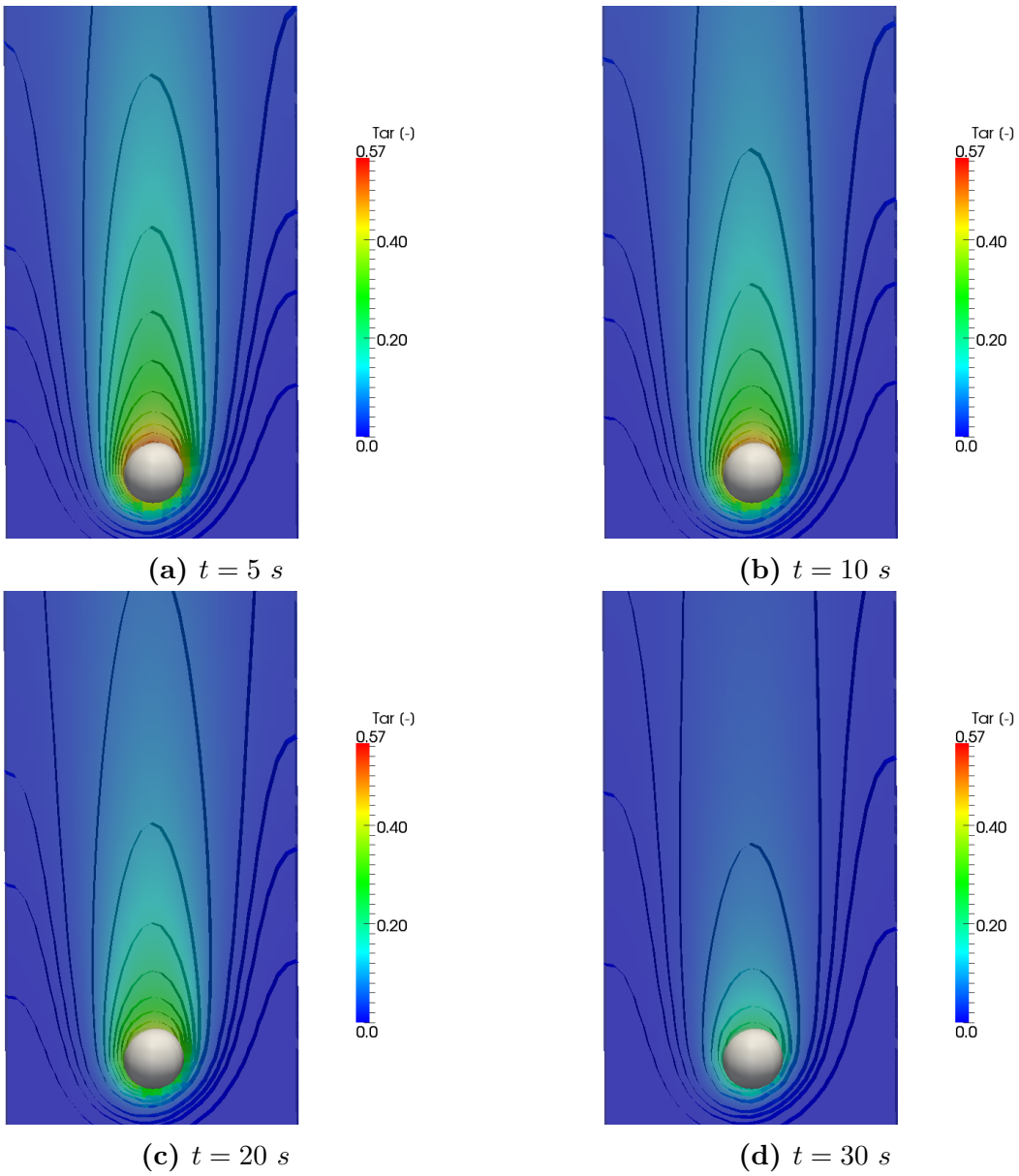

(a) $t = 5\ s$ **(b)** $t = 10\ s$

(c) $t = 20\ s$ **(d)** $t = 30\ s$

Figure 8.3.7: Spatial distribution of tar at different times.

the area inside the particle. Due to the wall effect, there are larger void space near the wall, hence higher mass flow rate is observed close to the wall. As can be seen later, this influences heat transfer between solid and gas phases and consequently the drying and pyrolysis front in the bed.

Figure 8.4.4 depicts temperature distribution in the gas and the solid phase. In order to present better the temperature distribution in the bed, an axial cut through the gas phase is shown in this figure. Hot gas is injected into the reactor from the bottom and exchanges heat with the cold particles while traveling through the packed bed, thus leaving the reactor at the top at a lower temperature. The results indicate that due to the high rate of heat exchange between the two phases, the gas temperature reaches to the cold particle temperature at the top of the bed.

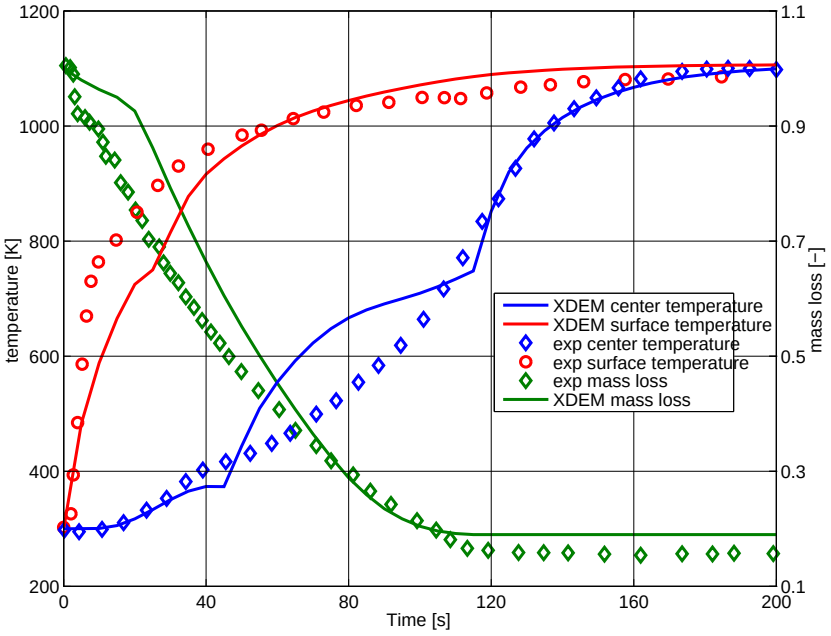

Figure 8.3.8: Validation with single particle experiments by Petek [7]: Comparison of temporal evolution of mass loss and surface temperature.

Higher void space near the wall causes higher flow rate passing around particles located near the wall, hence heat exchange between the gas and the solid is more pronounced there. This is the reason why particles close to the wall have a bit higher temperatures compared to particles at the center of the packed-bed.

Here, the interesting point is that some of small particles have higher temperature compared to the bigger particles bellow them. This is due to the fact that the hot inlet gas still has considerable thermal energy and high temperature after passing the lower large particles. Furthermore, the small particles located above them have larger ratio of surface to volume. Therefore gas loses considerable amount of its thermal energy while passing between the small particles. Hence, the temperature of small particles may rise above the big particles located below them. Larger temperature difference between big particles and gas phase and smaller difference between small particles and gas phase that located at the same height, confirms this explanation.

Figure 8.4.5 illustrates moisture content in the solid particles and vapor mass fraction in the gas phase at different times. In order to show clearly vapor distribution in the gas phase and also the drying in the bed, an axial cut through the gas domain and through the packed bed of particles are shown in this figure. Moisture distribution in the particles shows the 'drying front' in the bed, which starts from the bottom and moves upward. Due to the wall effect, heat exchange between solid and gas phases is higher near the wall. Therefore drying in particles close to the wall is more intense than particles at the middle

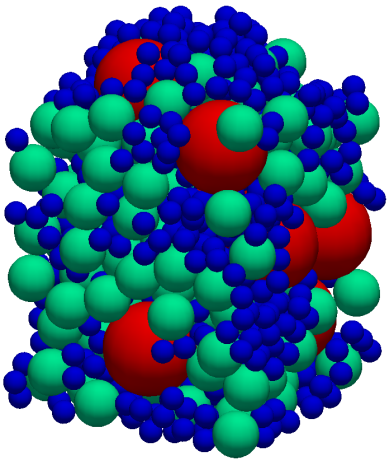

Figure 8.4.1: Heterogeneous bed formed by spherical particles of three different sizes (diameter of 5, 20 and 100 mm).

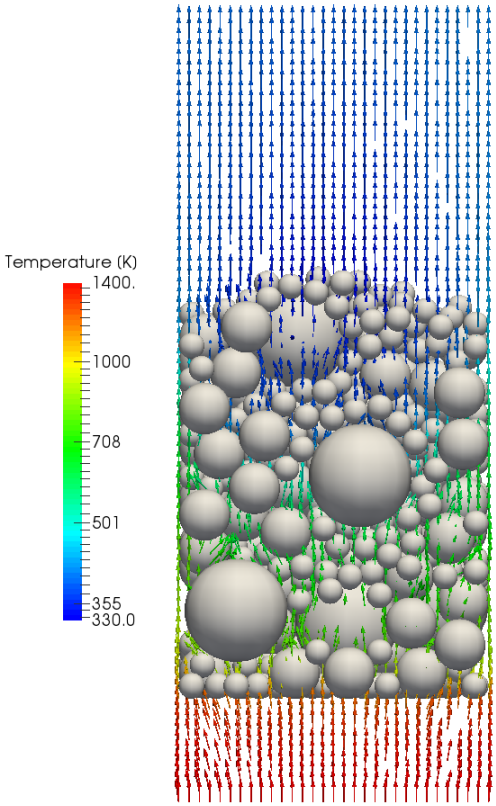

Figure 8.4.2: Velocity vector field and spatial temperature distribution for the gas phase.

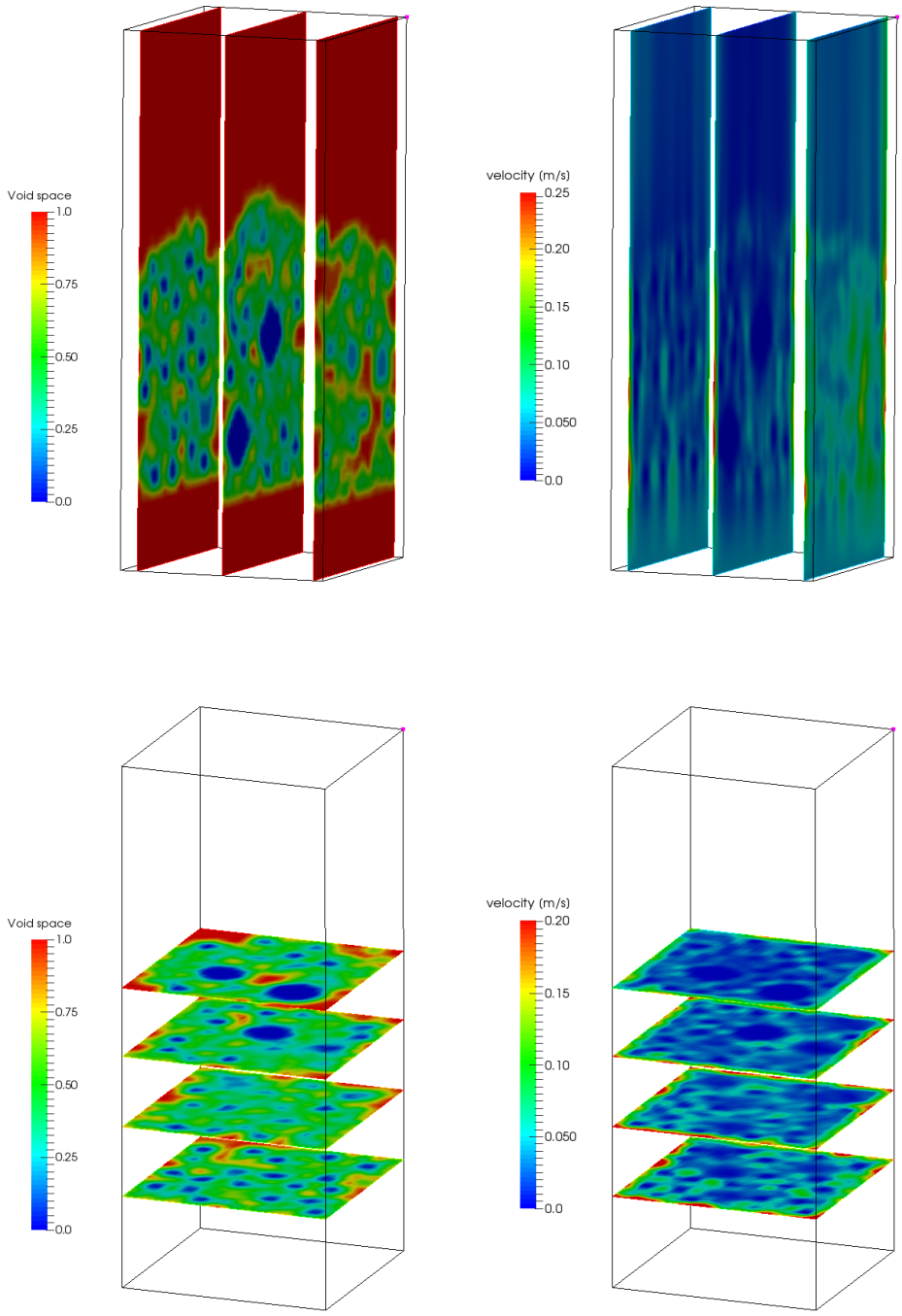

Figure 8.4.3: Void space and gas velocity at different cross sections.

of the bed. So that, at $t = 2000\ s$ particles close to the wall have already dried while particles further at the center of the bed are still wet. It should be noted that their is no simple two dimensional drying front since local drying rates highly depend on particle size as well as location inside the reactor (wall effect).

Vapor in the gas phase can have two origins; one due to the evaporation of the moisture

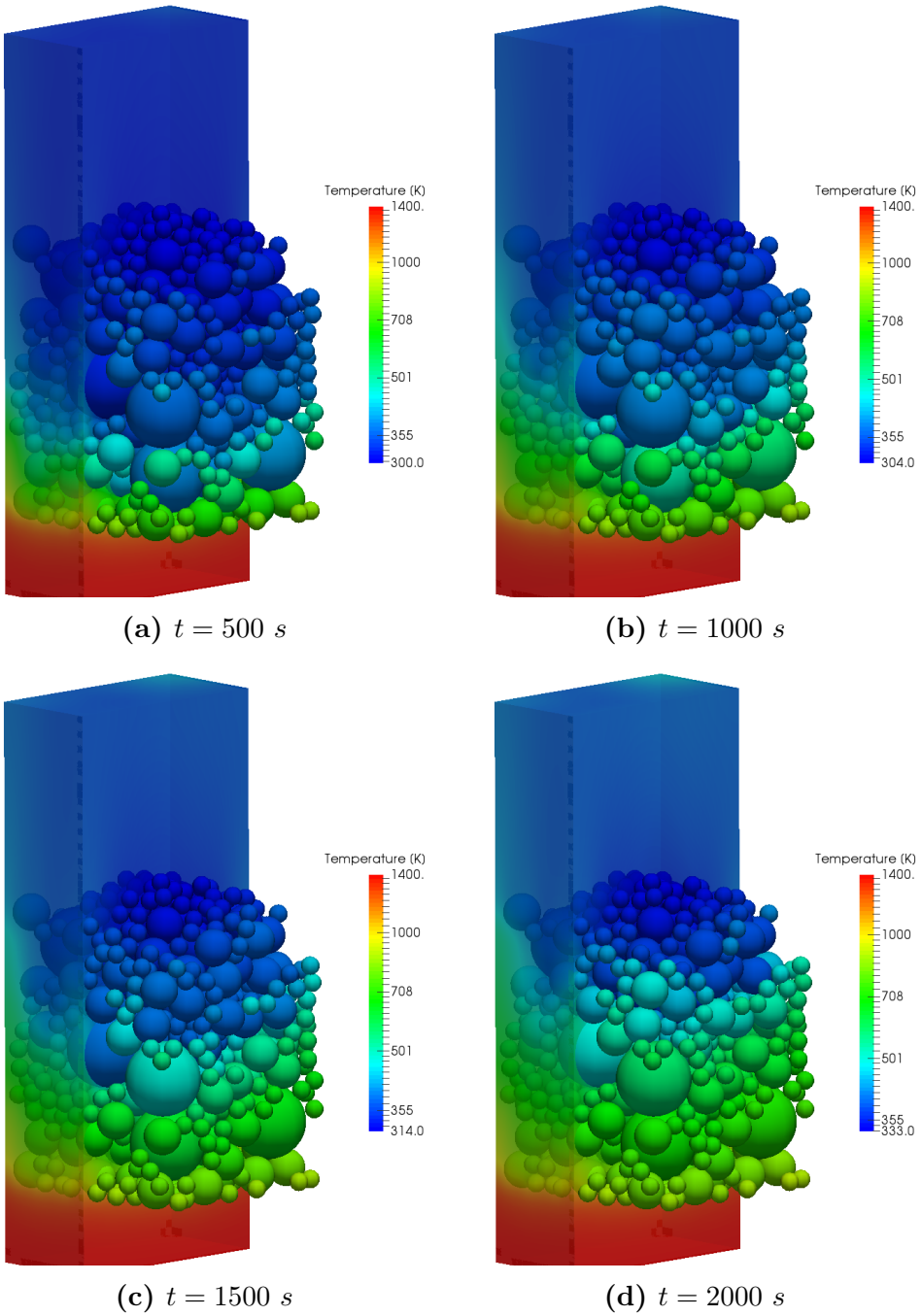

(a) $t = 500\ s$ **(b)** $t = 1000\ s$

(c) $t = 1500\ s$ **(d)** $t = 2000\ s$

Figure 8.4.4: Particle surface temperature and gas phase temperature at different times.

content in the bed and the other one is due to the pyrolysis of wood particles. By comparing the position of particles that are in the drying period with the mass fraction of vapor in the gas phase, it can be concluded that the high mass fraction of vapor is due to the intense drying of particles in that area.

Similar to fig 8.4.5, an axial cut of the bed is used in fig 8.4.6 to show conversion of biomass and mass fraction of tar in the gas phase at different times. Zero value of conversion refers

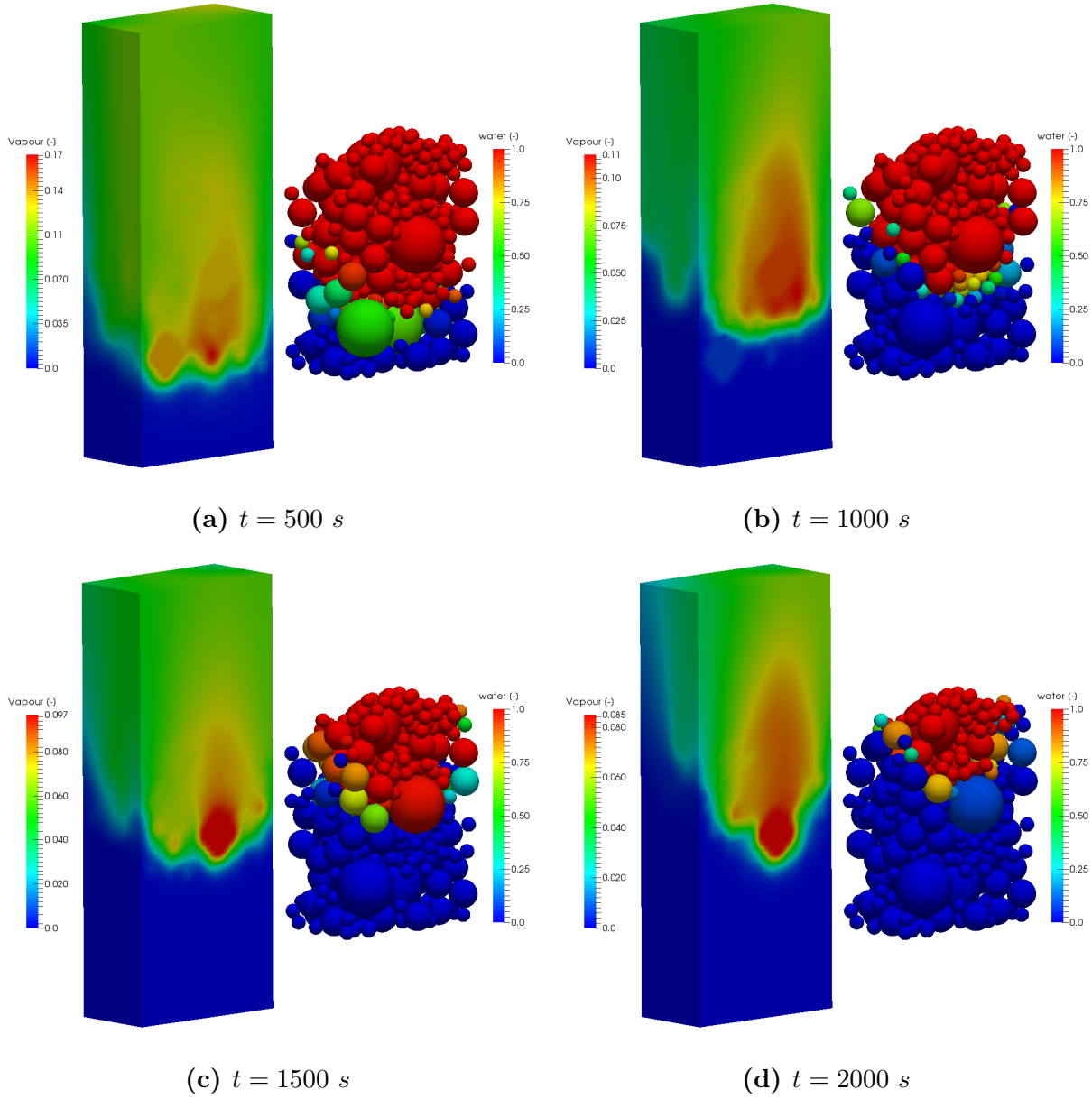

(a) $t = 500\ s$ **(b)** $t = 1000\ s$

(c) $t = 1500\ s$ **(d)** $t = 2000\ s$

Figure 8.4.5: Moisture content in the solid particles and vapor mass fraction in the gas phase at different times.

to 100% raw wood and conversion equal to one indicates that wood has been converted completely to its products and only char as a solid product remains in the particle. The results show that about 40% raw biomass in the bed is converted after 2000 s.

Although the bed is formed heterogeneously with three different particle sizes, there are more small particles at the bottom of the bed. Small particles have larger ratio of surface to volume, hence convective heat transfer with the hot gas (which is the dominant mode of heat transfer in this case) is more intense for them. Therefore conversion of smaller particles is faster. This leads to a situation of high tar content in the gas phase at $t = 500\ s$ when smaller particles at the bottom of the bed are in their main devolatilisation phase.

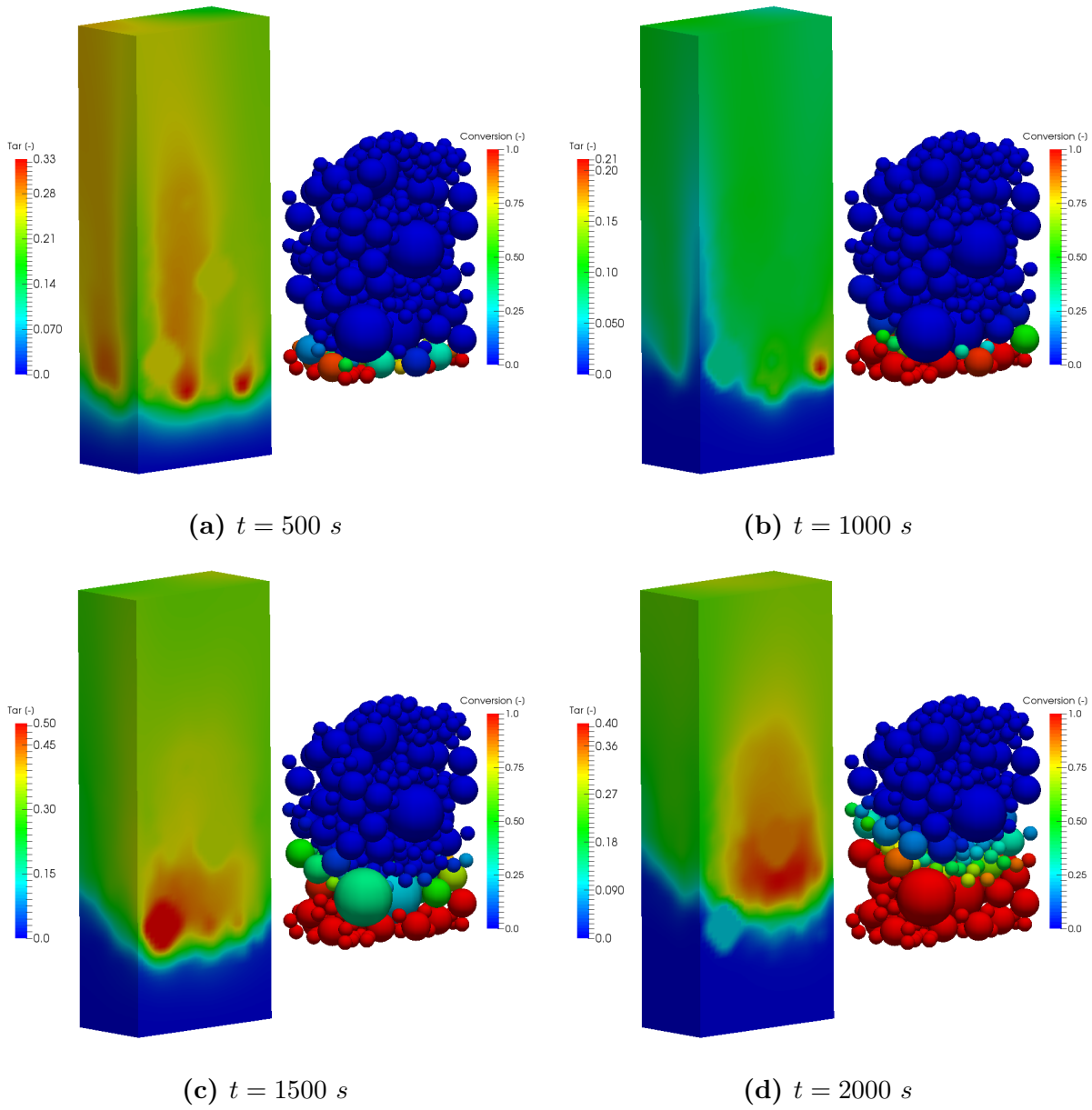

(a) $t = 500\ s$ **(b)** $t = 1000\ s$

(c) $t = 1500\ s$ **(d)** $t = 2000\ s$

Figure 8.4.6: Conversion extent of wood particles and tar mass fraction in the gas phase at different times.

At $t = 1000\ s$ when mostly bigger particles are being devolatilized, tar mass fraction decreases by about 30%.

8.5 Conclusions

A comprehensive numerical model for heat and mass transfer within a packed bed formed by a granular material was presented. It allows for prediction of processes such as heat-up, drying and pyrolysis of biomass materials in packed beds. A packed bed was considered as an ensemble of a finite number of particles. For the presented model the solid phase

is fully resolved while the gas phase is semi-resolved. This method is based on a volume averaging model implemented in the XDEM framework in which the fluid phase is a continuous phase treated by an Eulerian approach whereas individual solid particles are tracked with a Lagrangian approach. However for the presented semi-resolved model, the gas phase is described on a length scale smaller than the particles size.

An appropriate resolution of the fluid's flow field in a bed becomes more important as in two situations: Firstly, if involved particles differ significantly in size. Secondly, whenever the particle size is in the order of reactor size. Fully resolved methods (for both solid and gas phase) can be a solution, however semi-resolved (fully resolve for solid phase and semi-resolved for gas phase) have some considerable advantages:

- It facilitates mesh generation for complex geometries.
- No special treatment of solid-solid contact points is necessary during grid generation.
- It allows for usage of a coarser grid to solve gas flow through the void space which improves calculation efficiency.
- The static grid does not need expensive regeneration in case solid particles move in space; only cell properties are updated.

The proposed model has been validated by comparing the predicted results with measurements for several cases. Presented results illustrate in detail the gas flow in the bed, heat and mass transfer between the two phases as well as drying and conversion within the wood particles.

Chapter 9

Conclusion and Outlook

During the last decades, an interest has grown to substitute fossil fuels by an alternative energy source. This is due to many reasons including environmental and technical issues as well as uncertainties over longevity of fossil fuels. These reasons lead to the conclusion that the dependency on fossil fuels will have serious consequences in the near future. Therefore it should be looked for alternative, renewable and environmental friendly fuels. Biomass as a renewable source of energy is almost accessible everywhere and it is possible to either convert it to other forms of fuel or burn it directly for generation of heat. Moreover biomass is considered as a CO_2 neutral source of energy. These advantages have attracted many attention in studying biomass conversion during the last decades in both academia and industry.

A better understanding of the processes in biomass furnaces will help designers to improve reactor efficiency and better control the reactor. However, the entire process is of very complex nature due to many involved physical and chemical phenomena. Hence the main objective of this thesis was to study the process of biomass conversion in a furnace in large detail and analyse the highly interconnected phenomena.

For this purpose a numerical model with an Euler-Lagrange approach was developed to capture the solid motion, conversion, gas flow through the void space, heat and mass transfer between two phases, heterogeneous and homogeneous reactions. In the proposed model the fluid phase is a continuous phase while each biomass particle is tracked with a Lagrangian approach. A packed bed is considered as an ensemble of a finite number of particles. Heat-up, drying, pyrolysis, gasification and combustion process of each particle is described by one-dimensional and transient conservation equations for mass and energy. Applying this model to all particles of a packed bed forms the entire packed bed process as the sum of the individual particle processes. The flow through the void space in the bed was modeled as a flow passing through a porous media by three-dimensional and transient conservation equations.

The proposed numerical model has been compared with measurements for each main process of biomass conversion (drying, pyrolysis, combustion) separately. However, validation of combustion/gasification of biomass in the fixed-bed contained all the involved phenomena in biomass conversion. Several validation studies with experimental data from independent research groups, prove the reliability of the model in predicting the entire process of biomass conversion in the furnace types under study.

The presented results of biomass combustion on a forward acting grate highlight the fact that the moving bed is of heterogeneous nature due to intensive heating of surface particles by wall radiation and mixing of particles. Mixing of particles takes place but is not able to entirely homogenize conditions that an individual particle is experiencing. Shrinking of particles during char consumption was another important parameter studied. On the one

hand it influences the kinematics of particles. On the other hand shrinkage of particles forming the surface of the moving bed allows particles below the surface to receive heat input from the furnace walls by radiation. Thus, shrinking of surface particles alters the region of intensive heat input into the bed.

Knowing that low heating rates are favorable for char formation and high heating rates are favorable for tar formation, led to investigate the effect of different packing mode on pyrolysis products. For this purpose, three packed beds were generated consisting of the same mass but differing in particle sizes and packing of particles. Predicted results showed, when a layer of small particles was located between a layer of larger particles, the average char yield from small particles increased by 31% compared to a packed bed consisting of only small particles.

Understanding the characteristics of self-ignition is important either as a favorable or unfavorable phenomena. Self ignition was studied in ch. 7 and the details of the phenomenon has been explained. Moreover, the effect of different key parameters such as gas velocity, gas temperature, particle size and moisture content on self-ignition has been studied. Results show that ignition delay increases with increasing moisture content and increasing particle size, while it decreases with increasing inlet gas velocity and temperature. Moisture content and particle size have lower impact on ignition delay compared to gas temperature and velocity. Higher inlet gas velocity causes occurring ignition at further position from inlet port while higher gas temperature and moisture content move the location of ignition closer to the inlet.

In the model that is presented in chapter 2-5, the solid phase is fully resolved while fluid phase is resolved with low degree. However, there are two situations where a more appropriate resolution of the flow field in a bed is required: First, if involved particles differ significantly in size. Second, whenever the particle size is in the order of the reactor size. A semi-resolved approach (fully resolve for the solid phase and semi-resolved for the gas phase) offered a better resolution of the fluid field. This method has been explained in details in chapter 8. Advantages of the proposed semi-resolved approach are:

- Higher resolution in the gas phase.
- It facilitates mesh generation for complex geometries.
- No special treatment of solid-solid contact points is necessary during mesh generation.
- It allows to use a coarser grid (compared to fully resolved method) to solve the gas flow through the void space which improves calculation efficiency.

- The static grid does not need an expensive regeneration in case solid particles move in space; only cell properties are updated.

In the following some improvements in order to account more accurately for some phenomena in a furnace will be proposed. Future work should include heat transfer to the reactor walls. This will help to find the wall temperature distribution (specially in the case of forward acting grate). This will influence heat transfer with solid particles both by conduction and radiation. Considering the heat transfer inside the wall will allow to take into account the bed's heat loss to the wall. This is essential for modeling of those boilers where the insulation is not very well applied for outer walls.

Accounting for radiation between the gas phase and solid particles adds further complexity to the model, however it will improve the gas-solid interaction to a higher degree of accuracy.

During combustion of char particle porosity increases due to mass removal. Thus, it is likely that at some point particles disintegrate into smaller particles. From one side, this will increase the total surface of solid particles and consequently heat and mass transfer with the surrounding gas phase. Form the other side, it influences the motion of particles in the bed. Accounting for particle disintegration is of higher importance in large scale beds where higher mechanical loads act on particles.

In the presented model, conduction between particles which are in contact is taken into account. However, the surface contact does not change by the existing pressure due to the weight of the bed above it. This effect is negligible in small beds, but it might play a considerable role in large scale beds.

Appendix A

Appendix

A.1 Heat and mass transfer coefficient

Heat transfer between the solid particle and surrounding gas phase is calculated as following

$$q_i = h_i A_i (T_i - T_{ambient}) \tag{A.1.1}$$

where h_i, A_i, T_i and $T_{ambient}$, are convective heat transfer coefficient, particle surface area, particle surface temperature and ambient gas temperature, respectively. Heat transfer coefficient (the same for mass transfer coefficient) is calculated using relevant available correlations in literature [121]. This correlation is valid for calculation of heat transfer coefficient between particle and gas in a packed bed.

$$Nu = 2 + 1.1(Pr^{1/3} Re^{0.6}) \tag{A.1.2}$$

Where $Re = d.u.\rho/\mu$.

Similar correlation is used for calculation of mass transfer coefficient.

$$Sh = 2 + 1.1(Sc^{1/3} Re^{0.6}) \tag{A.1.3}$$

A.2 mechanical contact model

The interaction between particle-particle and particle-wall was modeled using Hook's law. The equation for Hooke's impact model can be written as

$$F_n = m_{ij}\ddot{\delta} = -(k_n\delta + c_n\dot{\delta}) \tag{A.2.1}$$

Where δ is the overlap depth between the contacting pair, m_{ij}, k_n, and c_n are reduced mass, the normal spring stiffness and normal damping coefficients, respectively. Reduced mass is calculated as following:

$$\frac{1}{m_{ij}} = \frac{1}{m_i} + \frac{1}{m_j} \tag{A.2.2}$$

The spring stiffness constant is Hookes model is calculated from the material properties and geometry $k_n = \frac{4}{3}E_{ij}R_{ij}$. Where R_{ij}, E_{ij} and ν are reduced radius, effective young modules and Poisson ratio.

$$\frac{1}{R_{ij}} = \frac{1}{R_i} + \frac{1}{R_j} \tag{A.2.3}$$

$$\frac{1}{E_{ij}} = \frac{1-\vartheta_i^2}{E_i} + \frac{1-\vartheta_j^2}{E_j} \tag{A.2.4}$$

Table of Symbols

Latin Symbols

Symbol	Meaning
A	pre exponential factor
C	concentration
c_p	specific heat capacity at constant pressure, J/kgK
d	diameter, m
D	diffusion coefficient, m^2/s
E	activation energy, J/mol
h	Enthalpy, J/kg
H_{evap}	heat of evaporation, $\frac{J}{kg}$
H_k	heat of reaction, evaporation, J/kg
K^*	permeability, m^2
K	reaction rate
m	mass
$\dot{m}$	mass flow rate, kg/s
$\dot{m}'''$	mass source, kg/m^3s
p	pressure, Pa
$\dot{q}''$	heat flux, W/m^2
$\dot{q}'''$	heat source, W/m^3
r	radius; radial coordinate, m
R	radius, m
$\mathcal{R}$	universal gas constant, J/molK
R_v	specific gas constant, J/kgK
S	surface, m^2
S_a	specific surface area, m^{-1}
t	time, s
T	temperature, K
v	velocity, m/s
$\dot{\omega}$	mass source, kg/m^3s

Greek Symbols

Symbol	Meaning
α	heat transfer coefficient, W/m^2K
β	mass transfer coefficient, m/s
ϵ	porosity, -
λ	heat conductivity, W/mK
μ	dynamic viscosity, kg/ms
ρ	density, kg/m^3
ν	mass fraction, -
ξ	mass fraction, -
Subscripts	
f	fluid
g	gas
p	particle
in	inlet
s	solid
∞	ambient
t	tar
c	char

Bibliography

[1] B. Peters, E. Schröder, C. Bruch, T. Nussbaumer, Measurements and particle resolved modeling of heat-up and drying of paked bed, Biomass and Bioenergy 23 (2002) 291 – 306.

[2] C. D. Blasi, Modeling wood gasication in a countercurrent fixed-bed reactor, AICHE Journal 50 (2004) 2306–2319.

[3] B. Peters, E. Schröder, C. Brunch, Measurements and particle resolved modeling of the thermo and fluid dynamics of a packed bed, Analytical and Applied Pyrolysis 70 (2003) 211–231.

[4] P. Basu, Biomass gasification and pyrolysis, Elsevier, 2010.

[5] M. G. Gronli, M. C. Melaaen, Mathematical model for wood pyrolysisscomparison of experimental measurements with model predictions, Energy & Fuels 14 (2000) 791–800.

[6] H. Lu, W. Robert, G. Peirce, B. Ripa, L. L. Baxter, Comprehensive study of biomass particle combustion, Energy & Fuels 22 (2008) 2826 – 2839.

[7] J.Petek, Experimentelle untersuchung der pyrolyse in inerter und reaktiver atmosphäre unter den bedingungen der wurfbeschickung, Ph.D. thesis, Graz University of Technology (1998).

[8] J. Yang, J. Wang, S. Bu, M. Zeng, Q. Wang, A. Nakayama, Experimental analysis of forced convective heat transfer in novel structured packed beds of particles, Chemical Engineering Science 71 (2012) 126 – 137.

[9] E. I. Administration, http://www.eia.gov, accessed on 8 March 2012.

[10] C. Yin, L. A. Rosendahl, S. K. Kr, Grate-firing of biomass for heat and power production, Progress in Energy and Combustion Science 34 (2008) 725–754.

[11] J. Wurzenberger, S. Wallner, H. Raupenstrauch, Thermal conversion of biomass: comprehensive reactor and particle modelling, AIChE Journal 48 (2002) 23982411.

[12] A. Anca-Couce, N. Zobel, H. A. Jakobsen, Multi-scale modeling of fixed-bed thermochemical processes of biomass with the representative particle model: Application to pyrolysis, Fuel 103 (2012) 773782.

[13] J. Collazo, J. Porteiro, D. Patino, E. Granada, Numerical modeling of the combustion of densified wood under fixed-bed conditions, Fuel 93 (2012) 149–159.

[14] F. Hoffmann, Modelling heterogeneous reactions in packed beds and its application to the upper shaft of a blast furnace, Ph.D. thesis, University of Luxembourg (2014).

[15] B. Peters, Thermal Conversion of Solid Fuels, WIT press, 2003.

[16] Y. Yang, Y. Goh, R. Zakaria, V. Nasserzadeh, J. Swithenbank, Mathematical modelling of MSW incineration on a travelling bed, Waste Management 22 (2002) 369 – 380.

[17] D. Shin, S. Choi, The combustion of simulated waste particles in a fixed bed, Combustion and Flame 121 (2000) 167 – 180.

[18] M. Markovic, E. A. Bramer, G. Brem, Experimental investigation of wood combustion in a fixed bed with hot air, Waste Management 34 (2014) 49 – 62.

[19] J. Martinez-Garcia, T. Nussbaumer, A one-dimensional transient solid fuel conversion model for grate combustion optimisation, Combustion Science and Technology 187 (2015) 1208 – 1228.

[20] L. van Kessel, A. Arendsen, P. de Boer-Meulman, G. Brem, The effect of air preheating on the combustion of solid fuels on a grate, Fuel 83 (2004) 1123 – 1131.

[21] D. Kurz, U. Schnell, G. Scheffknecht, CFD simulation of wood chip combustion on a grate using an eulereuler approach, Combustion Theory and Modelling 16 (2012) 251 – 273.

[22] E. Simsek, B. Brosch, S. Wirtz, V. Scherer, F. Krll, Numerical simulation of grate firing systems using a coupled cfd/discrete element method (dem), Powder Technology 193 (2009) 266 – 273.

[23] B. Brosch, V. Scherer, S. Wirtz, Simulation of municipal solid waste incineration in grate firing systems with a particle based novel discrete element method, in: VGB PowerTech, 2014.

[24] L. Liang, R. Sun, J. Fei, S. Wu, X. Liu, K. Dai, N. Yao, Experimental study on effects of moisture content on combustion characteristics of simulated municipal solid wastes in a fixed bed, Bioresource Technology 99 (2008) 7238–7246.

[25] J. Brammer, A. Bridgwater, The influence of feedstock drying on the performance and economics of a biomass gasifierengine chp system, Biomass and Bioenergy 22 (2002) 271–281.

[26] K. Svoboda, J. Martinec, M. Pohorely, D. Baxter, Integration of biomass drying with combustion/gasification technologies and minimization of emissions of organic compounds, Chemical Papers 63 (2009) 15–25.

[27] B. Peters, A. D. iugys, R. Navakas, Simulation of thermal conversion of solid fuel by discrete particle method, Lithuanian Journal of Physics 51 (2011) 91–105.

[28] M. Bellais, Modelling of the pyrolysis of large wood particles, Ph.D. thesis, KTH - Royal Institute of Technology (2007).

[29] M. Izadifar, O. D. Baik, C. J. Simonson, Modeling of the packed bed drying of paddy rice using the local volume averaging (lva) approach, Food Research International 39 (2006) 712–720.

[30] M. Assari, H. B. Tabrizi, M. Saffar-Avval, Numerical simulation of fluid bed drying based on two-fluid model and experimental validation, Applied Thermal Engineering 27 (2007) 422–429.

[31] S. B. Mabrouk, B. Khiari, M. Sassi, Modelling of heat and mass transfer in a tunnel dryer, Applied Thermal Engineering 26 (2006) 2110–2118.

[32] J. J. Saastamoinen, Comparison of moving bed dryers of solids operating in parallel and counterflow modes, Drying Technology 23 (2005) 1003–1025.

[33] A. Picado, J. Martinez, Mathematical modeling of a continuous vibrating fluidized bed dryer for grain, Drying Technology 30 (2012) 1469–1481.

[34] W. Yang, A. Ponzio, C. Lucas, W. Blasiak, Performance analysis of a fixed-bed biomass gasifier using high-temperature air, Fuel Processing Technology 87 (2006) 235–245.

[35] J. Bruchmuller, B. van Wachem, S. Gu, K. , Luo, R. Brown, Modeling the thermochemical degradation of biomass inside a fast pyrolysis fluidized bed reactor, AIChE Journal 58 (2012) 3030–3042.

[36] C. Mandl, I. Obernberger, F. Biedermann, Modelling of an updraft fixed-bed gasifier operated with softwood pellets, Fuel 89 (2010) 37953806.

[37] W. Chan, M. Kelbon, B. Krieger, Modelling and experimental verification of physical and chemical processes during pyrolysis of a large biomass particle, Fuel 64 (1985) 15051513.

[38] P. A. Cundall, O. D. L. Strack, A discrete numerical method for granular assemblies, Geotechnique 29 (1979) 47–65.

[39] M. P. Allen, D. J. Tildesley, Computer Simulation of Liquids, Claredon Press Oxford, 1990.

[40] B. Peters, A. Dziugys, R. Navakas, A discrete approach to thermal conversion of solid fuel by the discrete particle method (dpm), in: Modern building materials, structures and techniques, 2010.

[41] K. Samiei, B. Peters, The discrete particle method (dpm). an advanced numerical simulation tool for particulate applications., in: ECCM 2010 IV European Conference on Computational Mechanics, Paris, France, 2010.

[42] Y. H. Man, R. C. Byeong, A numerical study on the combustion of a single carbon particle entrained in a steady flow, Combustion and Flame 97 (1994) 1–16.

[43] A. Faghri, Y. Zhang, Transport Phenomena in Multiphase Systems, Elsevier Academic Press, 2006.

[44] E. Specht, Kinetik der Abbaureaktionen, Cuvillier Verlag Göttingen, 1993.

[45] R. B. Bird, W. E. Stewart, E. N. Lightfoot, Transport Phenomena, John Wiley & Sons, 1960.

[46] S. Whitaker, Transport Processes with Heterogeneous Reaction, Gordon and Breach,New York, 1986, Ch. Concepts and Design of Chemical Reactors, Ch.1.

[47] H. Teng, T. S. Zhao, An extension of darcy's law to non-stokes flow in porous media, Chemical Engineering Science 55 (2000) 2727–2735.

[48] J. L. Lage, M. D. Lemos, D. Nield, Transport Phenomena in porous media II, chapter 8 Modelling Turbulence in Porous Media, Pergamon, 2002, pp. 198–230.

[49] C. D. Blasi, Modeling chemical and physical processes of wood and biomass pyrolysis, Progress in Energy and Combustion Science 34 (2008) 4790.

[50] B. Peters, C. Bruch, A flexible and stable numerical method for simulating the thermal decomposition of wood particles, Chemosphere 42 (2001) 481–490.

[51] C. D. Blasi, C. Branca, Modeling a stratified downdraft wood gasifier with primary and secondary air entry, Fuel 104 (2013) 847–860.

[52] F. Thurner, U. Mann, Kinetic investigation of wood pyrolysis, Industrial and Engineering Chemistry Process Design and Development 20 (1981) 482–488.

[53] C. D. Blasi, C. Branca, Kinetics of primary product formation from wood pyrolysis, Industrial & Engineering Chemistry Research 40 (2001) 5547– 5556.

[54] E. Ranzi, A. Cuoci, T. Faravelli, A. Frassoldati, G. Migliavacca, S. Pierucci, S. Sommariva, Chemical kinetics of biomass pyrolysis, Energy & Fuels 22 (2008) 42924300.

[55] B. Peters, Validation of a numerical approach to model pyrolysis of biomass and assessment of kinetic data, Fuel 90 (2011) 2301–2314.

[56] J. Rath, M. Wolfinger, G. Steiner, G. Krammer, F. Barontini, V. Cozzani, Heat of wood pyrolysis, Fuel 82 (2003) 8191.

[57] Y. Haseli, J. van Oijen, L. de Goey, Modeling biomass particle pyrolysis with temperature-dependent heat of reactions, Journal of Analytical and Applied Pyrolysis 90 (2011) 140–154.

[58] H. Ström, H. Thunman, CFD simulations of biofuel bed conversion: A submodel for the drying and devolatilization of thermally thick wood particles, Combustion and Flame 160 (2013) 417431.

[59] Y. Haseli, J. van Oijen, L. de Goey, Numerical study of the conversion time of single pyrolyzing biomass particles at high heating conditions, Chemical Engineering Journal 169 (2011) 299–312.

[60] C. Blasi, Kinetic and heat transfer control in the slow and flash pyrolysis of solids, Industrial & Engineering Chemistry Research 35 (1196) 37–46.

[61] C. Koufopanos, N. Papayannakos, G. Maschio, A. Lucchesi, Modelling of the pyrolysis of biomass particles. studies on kinetics, thermal and heat transfer effects, Canadian Journal of Chemical Engineering 69 (1991) 907–915.

[62] H. Lu, E. Ip, J. Scott, P. Foster, M. Vickers, L. L. Baxter, Effects of particle shape and size on devolatilization of biomass particle, Fuel 89 (2010) 11561168.

[63] K. Umeki, T. Namioka, K. Yoshikawa, Analysis of an updraft biomass gasifier with high temperature steam using a numerical model, Applied Energy 90 (2012) 3845.

[64] S. Balci, T.Dogu, H. Yucel, Pyrolysis kinetics of lignocellulosic materials, Industrial & Engineering Chemistry Research 32 (1993) 2573–2579.

[65] C. D. Blasi, Dynamic behaviour of stratified downdraft gasifiers, Chemical Engineering Science 55 (2000) 2931– 2944.

[66] I. Milosavljevic, V. Oja, E. M. Suuberg, Thermal effects in cellulose pyrolysis: relationship to char formation processes, Industrial & Engineering Chemistry Research 35 (1996) 653–662.

[67] W. S.-L. Mok, M. J. A. Jr., Effects of pressure on biomass pyrolysis. ii. heats of reaction of cellulose pyrolysis, Thermochimica Acta 68 (1983) 165 – 186.

[68] R. Mehrabian, S. Zahirovic, R. Scharler, I. Obernberger, S. Kleditzsch, S. Wirtz, V. Scherer, H. Lu, L. L. B. and, A CFD model for thermal conversion of thermally thick biomass particles, Fuel Processing Technology 95 (2012) 96 – 108.

[69] M. Fatehi, M. Kaviany, Adiabatic reverse combustion in a packed bed, Combustion and Flame 99 (1994) 1 – 17.

[70] R. Gort, On the propagation of a reaction front in a packed bed: thermal conversion of municipal solid waste and biomass, Ph.D. thesis, Twente University (1995).

[71] M. van Blijderveen, E. M. Gucho, E. A. Bramer, G. Brem, Spontaneous ignition of wood, char and rdf in a lab scale packed bed, Fuel 89 (2010) 2393 – 2404.

[72] L. van Kessel, A. Arendsen, P. de Boer-Meulman, G. Brem, The effect of air preheating on the combustion of solid fuels on a grate, Fuel 83 (2004) 1123 – 1131.

[73] Y. Yang, H. Yamauchi, V. Nasserzadeh, J. Swithenbank, Effects of fuel devolatilisation on the combustion of wood chips and incineration of simulated municipal solid wastes in a packed bed, Fuel 82 (2003) 2205 – 2221.

[74] van Kuijk. H, Grate furnace combustion: a model for the solid fuel layer, Ph.D. thesis, Eindhoven University (2008).

[75] Y. Haseli, J. van Oijen, L. de Goey, A detailed one-dimensional model of combustion of a woody biomass particle, Bioresource Technology 102 (2011) 9772 – 9782.

[76] S. L. Singer, A. F. Ghoniem, Comprehensive gasification modeling of char particles with multi-modal pore structures, Combustion and Flame 160 (2013) 120 – 137.

[77] M. Momeni, C. Yin, S. K. K. aer, S. L. Hvid, Comprehensive study of ignition and combustion of single wooden particles, Energy & Fuels 27 (2013) 1061– 1072.

[78] H. Tolvanen, R. Raiko, An experimental study and numerical modeling of combusting two coal chars in a drop-tube reactor: A comparison between N_2/O_2, CO_2/O_2, and $N_2/CO_2/O_2$ atmospheres, Fuel 124 (2014) 190 – 201.

[79] C. Bruch, B. Peters, T. Nussbaumer, Modelling wood combustion under fixed bed conditions, Fuel 82 (2003) 729–738.

[80] G. Groppi, E. Tronconi, P. Forzatti, M. Berg, Mathematical modelling of catalytic combustors fuelled by gasified biomasses, Catalysis Today 59 (2000) 151 – 162.

[81] K. M. Bryden, K. W. Ragland, Numerical modeling of a deep, fixed bed combustor, Energy & Fuels 10 (1996) 269 – 275.

[82] D. D. EVANS, H. W. EMMONS, Combustion of wood charcoal, Fire Research 1 (1977) 57– 66.

[83] R. Johansson, H. Thunman, B. Leckner, Influence of intraparticle gradients in modeling of fixed bed combustion, Combustion and Flame 149 (2007) 49 – 62.

[84] L. Sun, S. Wang, H. Lu, G. Liu, H. Lu, Y. Liu, F. Zhao, Prediction of configurational and granular temperatures of particles using DEM in reciprocating grates, Powder Technology 269 (2015) 495 – 504.

[85] K. Samiei, B. Peters, Experimental and numerical investigation into the residence time distribution of granular particles on forward and reverse acting grates, Chemical Engineering Science 87 (2013) 234 – 245.

[86] B. Peters, A. Dziugys, H. Hunsinger, L. Krebs, An approach to qualify the intensity of mixing on a forward acting grate, Chemical Engineering Science 60 (2005) 1649 – 1659.

[87] F. Sudbrock, E. Simsek, S. Wirtz, V. Scherer, An experimental analysis on mixing and stoking of monodisperse spheres on a grate, Powder Technology 198 (2010) 29 – 37.

[88] F. Sudbrock, E. Simsek, S. Rickelt, S. Wirtz, V. Scherer, Discrete element analysis of experiments on mixing and stoking of monodisperse spheres on a grate, Powder Technology 208 (2011) 111 – 120.

[89] E. Simsek, F. Sudbrock, S. Wirtz, V. Scherer, Influence of particle diameter and material properties on mixing of monodisperse spheres on a grate: Experiments and discrete element simulation, Powder Technology 221 (2012) 144 – 154.

[90] S. Rickelt, F. Sudbrock, S. Wirtz, V. Scherer, Coupled DEM/CFD simulation of heat transfer in a generic grate system agitated by bars, Powder Technology 249 (2013) 360 – 372.

[91] B. Peters, A. Dziugys, Influence of bar motion on heat-up and temperature dispersion of a wooden bed on a forward acting grate, Chemical Engineering transactions 24 (2011) 637 – 642.

[92] B. Peters, A. Dziugys, Comparison of the heat-up of a moving bed on forward and backward acting grates, Numerical Heat Transfer, Part A: Applications 62 (2012) 547–564.

[93] H.-H. Frey, B. Peters, H. Hunsinger, J. Vehlow, Characterization of municipal solid waste combustion in a grate furnace, Waste Management 23 (2003) 689 – 701.

[94] T. Nussbaumer, M. Kiener, P. Horat, Fluid dynamic optimization of grate boilers with scaled model flow experiments, CFD modeling, and measurements in practice, Biomass and Bioenergy 76 (2015) 11 – 23.

[95] P. A. Cundall, O. D. L. Strack, A discrete numerical model for granular assemblies, Gotechnique 29 (1979) 47 – 65.

[96] K. Samiei, B. Peters, M. Bolten, A. Frommer, Assessment of the potentials of implicit integration method in discrete element modelling of granular matter, Computers & Chemical Engineering 49 (2013) 183 – 193.

[97] K. Samiei, Assessment of implicit and explicit algorithms in numerical simulation of granular matter, Ph.D. thesis, University of Luxembourg (2012).

[98] D. Neves, H. Thunman, A. Matos, L. Tarelho, A. Gmez-Barea, Characterization and prediction of biomass pyrolysis products, Progress in Energy and Combustion Science 37 (5) (2011) 611 – 630.

[99] M. Nik-Azar, M. Hajaligol, M. Sohrabi, B. Dabir, Effects of heating rate and particle size on the products yields from rapid pyrolysis of beech-wood, Fuel Science and Technology International 14 (1996) 479–502.

[100] J. Zhu, N. He, D. Li, The relationship between oxygen consumption rate and temperature during coal spontaneous combustion, Safety Sci. 50 (2012) 842–845, first International Symposium on Mine Safety Science and Engineering 2011.

[101] A. Yasuhara, Y. Amano, T. Shibamoto, Investigation of the self-heating and spontaneous ignition of refuse-derived fuel (RDF) during storage, Waste Manage. 30 (2010) 1161–1164, {IWWG} Task Group on Thermal Treatments Special Thematic Issue Thermal Treatment of Solid Waste.

[102] L. M. Pejic, N. F. Anez, J. G. Torrent, lvaro Ramrez-Gmez, Determination of spontaneous combustion of thermally dried sewage sludge, J. Loss. Prevent. Proc. 36 (0) (2015) 352–357.

[103] L. Shi, M. Y. L. Chew, Experimental study of woods under external heat uxby autoignition, J. Therm. Anal. Calorim. 17 (2012) 1399–1407.

[104] N. F. Anez, J. G. Torrent, L. M. Pejic, C. G. Olmedo, Detection of incipient self-ignition process in solid fuels through gas emissions methodology, J. Loss. Prevent. Proc. 36 (2015) 343–351.

[105] J. G. Torrent, N. F. Anez, L. M. Pejic, L. M. Mateos, Assessment of self-ignition risks of solid biofuels by thermal analysis, Fuel 143 (2015) 484–491.

[106] W. Yafei, Y. Lizhong, Z. Xiaodong, D. Jiakun, Z. Yupeng, D. Zhihua, Experiment study of the altitude effects on spontaneous ignition characteristics of wood, Fuel 89 (5) (2010) 1029–1034.

[107] A. Ejlali, D. Mee, K. Hooman, B. Beamish, Numerical modelling of the self-heating process of a wet porous medium, Int. J. Heat Mass Transfer 54 (2526) (2011) 5200–5206.

[108] X. Gao, C. Man, S. Hu, X. Xu, D. Che, Theoretical and experimental study on spontaneous ignition of lignite during the drying process in a packed bed, Energy Fuels 26 (2012) 6876–6887.

[109] M. van Blijderveen, E. A. Bramer, G. Brem, Modelling spontaneous ignition of wood, char and RDF in a lab-scale packed bed, Fuel 108 (0) (2013) 190–196.

[110] T. Atmakidis, E. Y. Kenig, Numerical analysis of mass transfer in packed-bed reactors with irregular particle arrangements, Chemical Engineering Science 81 (0) (2012) 77 – 83.

[111] A. Guardo, M. Coussirat, F. Recasens, M. Larrayoz, X. Escaler, CFD study on particle-to-fluid heat transfer in fixed bed reactors: Convective heat transfer at low and high pressure, Chemical Engineering Science 61 (2006) 4341 – 4353.

[112] H. Tavassoli, S. Kriebitzsch, M. van der Hoef, E. Peters, J. Kuipers, Direct numerical simulation of particulate flow with heat transfer, International Journal of Multiphase Flow 57 (0) (2013) 29 – 37.

[113] M. Behnam, A. G. Dixon, M. Nijemeisland, E. H. Stitt, A new approach to fixed bed radial heat transfer modeling using velocity fields from computational fluid dynamics simulations, Industrial & Engineering Chemistry Research 52 (2013) 15244–15261.

[114] F. Augier, F. Idoux, J. Delenne, Numerical simulations of transfer and transport properties inside packed beds of spherical particles, Chemical Engineering Science 65 (2010) 1055 – 1064.

[115] S. Kriebitzsch, M. van der Hoef, J. Kuipers, Fully resolved simulation of a gas-fluidized bed: A critical test of {DEM} models, Chemical Engineering Science 91 (2013) 1 – 4.

[116] A. H. Mahmoudi, F. Hoffmann, B. Peters, Detailed numerical modeling of pyrolysis in a heterogeneous packed bed using XDEM, J. Anal. Appl. Pyrolysis 106 (2014) 9–20.

[117] A. H. Mahmoudi, F. Hoffmann, B. Peters, Application of xdem as a novel approach to predict drying of a packed bed, Int. J. Therm. Sci. 75 (2013) 65–75.

[118] A. K. Datta, Porous media approaches to studying simultaneous heat and mass transfer in food processes. I: Problem formulations, Journal of Food Engineering 80 (2007) 80–95.

[119] S. Whitaker, Flow in Porous Media I: (A) Theoretical Derivation of Darcy's law, D. Reidel Publishing Company, 1986, pp. 3–25.

[120] A. Faghri, Y. Zhang, Transport Phenomena in Multiphase Systems, Elsevier, 2006.

[121] N. Wakao, S. Kaguei, Heat and Mass Transfer in Packed Beds, McGraw-Hill, New York, 1982, pp. 138–158, 264–295.